THE UNIVERSITY OF MANITOBA

A COMPARISON OF TURBULENT FLOW PREDICTIONS FOR SQUARE DUCTS USING THREE VORTICITY SOURCE MODELS

BY

SATISH KUMAR YADAVA

A Thesis

Submitted to the Faculty of Graduate Studies in

Partial Fulfillment of the Requirements for the Degree of

Master of Science

Department of Mechanical Engineering

Winnipeg, Manitoba

September 1983

A COMPARISON OF TURBULENT FLOW PREDICTIONS FOR SQUARE DUCTS USING THREE VORTICITY SOURCE MODELS

BY

SATISH KUMAR YADAVA

A thesis submitted to the Faculty of Graduate Studies of the University of Manitoba in partial fulfillment of the requirements of the degree of

MASTER OF SCIENCE

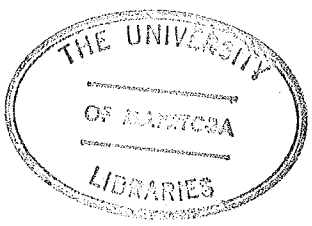

ACKNOWLEDGEMENTS

The author is privileged to acknowledge his indebtedness to Dr. A. C. Trupp (Thesis Supervisor), Department of Mechanical Engineering who not only took pains in guiding but also has been a source of inspiration throughout the work.

Thanks are also due to colleagues A. Lau and K. S. Bhatia for the fruitful discussions held at times.

The author held both Teaching and Research Assistantships with the Department of Mechanical Engineering during the course of this work and this support is acknowledged.

ABSTRACT

A two-equation turbulence model ($k - \varepsilon$) was applied to predict fluid flow characteristics under fully developed turbulent flow conditions through a square duct. The five coupled, non-linear, elliptic equations for axial vorticity, stream function, turbulent kinetic energy, turbulence kinetic energy dissipation rate and mean axial velocity were solved by means of the general elliptic finite difference procedure of Gosman et al [1969] with a cartesian coordinate grid. Three different vorticity source term models were employed for the vorticity equation. The first model is based on the Reynolds stress model proposed by Launder and Ying [1973]. In the second model, the vorticity source term is calculated based upon the relationships between turbulent intensities as proposed by Alshamani [1979]. In the third model, a synthetic distribution of turbulent kinetic energy (k) is specified and combined with the vorticity equation to produce a simple algebraic term for the source of vorticity as suggested by Seale [1982]. The vorticity source term model constants (C', C'' and C''' for models I, II and III respectively) were tuned to yield best overall agreement with the experimental measurements, which incidentally occur when the maximum resultant secondary velocity is about 1.5% of the centreline velocity in all three models. The predicted results of all three models were compared with the

experimental data of Hoagland [1960], Leutheusser [1963], Brundrett and Baines [1964], Gessner and Jones [1965] and Launder and Ying [1972].

Predictions are presented over a Reynolds number range of 60×10^3 to 300×10^3. The predicted characteristics of the flow are shown to be in reasonable agreement with the available experimental data. The effects of secondary flow were evident in the cross-sectional distributions of mean axial velocity, wall shear stress and very prominent in the turbulent kinetic energy distributions.

Finally, the performances of the three models were compared with each other and it was observed that the predicted characteristics of all three models were very close. The predictions of model II were judged to be best overall compared to the experimental data, although, admittedly, the differences between models were small. Model II, subsequently, was employed to compare predicted wall shear stress at different Reynolds numbers and model III was used to show the variation of friction factor with Reynolds number in smooth square ducts.

The success of model II and especially model III, promises good prospects for their application to multi-cell geometries.

TABLE OF CONTENTS

ABSTRACT.....(i)
TABLE OF CONTENTS.....(iii)
LIST OF TABLES.....(vi)
LIST OF FIGURES.....(vii)
NOMENCLATURE.....(x)

1.0 INTRODUCTION
1.1 Motivation..... 1
1.2 Objectives and Scope..... 2

2.0 LITERATURE REVIEW
2.1 General..... 6
2.2 Review of Experimental Work..... 7
2.3 Turbulence Models.....14
2.3.1 General.....14
2.3.2 Classification of Turbulence Models.....15
2.3.3 The k-ε Turbulence Models (Two Equation Models).....18
2.4 Review of Analytical Work.....20

3.0 GOVERNING EQUATIONS
3.1 Continuity and Reynolds Equations.....24
3.2 Axial Vorticity and Stream Function Equations.....27
3.3 Turbulent Kinetic Energy Equation.....29
3.4 Turbulence Energy Dissipation Rate Equation.....30

4.0 THE ANALYTICAL MODELS
4.1 Closure of $\bar{U}$, k and ε Equations.....32
4.2 Boundary Conditions.....35

4.3 Vorticity Source Term Modelling..... 38
4.3.1 Model I: Launder and Ying's Model.....39
4.3.2 Model II: Turbulent Properties Correlations Model.....41
4.3.3 Model III: Seale's Model.....44
4.4 Summary of Equations to be Solved.....46
4.4.1 Transport Equations.....46
4.4.2 Algebraic Equations.....47
4.4.3 Boundary conditions.....48
4.5 Various Constants of the Models.....49

5.0 THE NUMERICAL PROCEDURE
5.1 Introduction.....50
5.2 The Finite-Difference Equations.....50
5.2.1 Convection Terms.....52
5.2.2 Diffusion Terms.....54
5.2.3 Source Term.....56
5.2.4 The Complete Finite Difference Equation.....57
5.2.5 Boundary Conditions.....58
5.3 Stability Analysis of the Successive Substitution Formula.....60
5.4 Iterative Technique.....61
5.5 Convergence Criterion.....61
5.6 Initial Conditions.....62
5.7 The Employed Grid Spacings.....62

6.0 NUMERICAL RESULTS AND DISCUSSION
6.1 General.....64
6.2 Secondary Velocity Profiles..... 65
6.3 Mean Axial Velocity Distributions.....68
6.4 Vorticity and Stream Function Distributions.....70

6.5 Mean Turbulent Kinetic Energy Distributions.....71
6.6 Local Wall Shear Stress Distribution.....73
6.7 Effect of Reynolds Number.....74
6.8 Comparison of Three models.....75

7.0 CONCLUSIONS AND RECOMMENDATIONS FOR FUTURE WORK..79

8.0 REFERENCES.....83

APPENDIX A - Derivation of Turbulent Kinetic Energy Equation.....90
APPENDIX B - Derivation of Turbulence Energy Dissipation Rate Equation.....97
APPENDIX C - Derivation of Equation for Source of Vorticity for Model II.....101
APPENDIX D - Derivation of Equation for Source of Vorticity for Model III.....104
APPENDIX E - Computer Program.....107
Appendix E-1 Main Program.....112
Appendix E-2 Vorticity Source - Model II.....131
Appendix E-3 Vorticity Source - Model III.....133

TABLES
FIGURES

LIST OF TABLES

Table		Page
1.	Summary of the constants of Models I, II and III	134
2.	Comparison of the k-ε model constants of the present work with others	135
3.	The functions involved in the general elliptic equations for square ducts	136

LIST OF FIGURES

Figure		Page
1.	The domain and coordinate system considered for the analytical models I, II and III	137
2.	Finite difference grid and grid notation for the analytical models I, II and III	138
3.	Portion of the finite difference cartesian grid and the area of integration	139
4.	Comparison of contour plots of predicted secondary velocity, $\bar{V}$ by model I, II and III, Re = 75,000	140
5.	Comparison of contour plots of predicted secondary velocity, $\bar{W}$ by model I, II and III, Re = 75,000	141
6.	Comparison of contour plots of predicted resultant secondary velocity, V_{sec} (model II) and measured V_{sec} [9], Re = 75,000	142
7.	Comparison of predicted secondary velocity $\bar{V}$ profiles (model II) and measured $\bar{V}$ profiles [14], Re = 215,000	143
8.	Comparison of predicted secondary velocity ($\bar{V}$) profiles (model II) and measured $\bar{V}$ profiles [15], Re = 100,000 , y/L= 0.4	144
9.	Comparison of predicted secondary velocity ($\bar{V}$) profiles (model I) and measured $\bar{V}$ profiles [14], Re = 215,000	145
10.	Predicted secondary velocity ($\bar{V}$) profiles (model I), Re = 83,000	146
11.	Comparison of predicted secondary velocity ($\bar{V}$) profiles (model III) and measured $\bar{V}$ profiles [14], Re = 215,000	147
12.	Predicted secondary velocity ($\bar{V}$) profiles (model III), Re = 83,000	148

13. Comparison of secondary velocity($\bar{V}$) profiles predicted by model I, II and III, Re = 83,000 149
14. Comparison of contour plots of predicted $\bar{U}$ (model I, II and III) and measured $\bar{U}$ [10], Re = 83,000 150
15. Comparison of predicted $\bar{U}$ (model I) and measured $\bar{U}$ [14] profiles, Re = 215,000 151
16. Comparison of predicted $\bar{U}$ (model II) and measured $\bar{U}$ [14] profiles, Re = 215,000 152
17. Comparison of predicted $\bar{U}$ (model III) and measured $\bar{U}$ [14] profiles, Re = 215,000 153
18. Comparison of contour plots of predicted $\bar{U}$ (model II) at Re = 75,000 and Re = 300,000 . 154
19. Comparison of contour plots of predicted $\bar{U}$ (model II) (with and without secondary flow) Re = 83,000 155
20. Comparison of contour plots of predicted Ψ (model I, II and III) and measured Ψ [9], Re = 75,000 156
21. Comparison of contour plots of predicted ω (model II) and measured ω [9], Re = 60,000 . 157
22. Comparison of contour plots of predicted k (model I, II and III) and measured k [11], Re = 83,000 158
23. Distribution of $k/(\bar{u}^*)^2$ (model I, II and III), Re = 83,000 159
24. Distribution of $k/(\bar{u}^*)^2$ (model I, II and III), Re - 83,000 160
25. Comparison of contour plots of predicted k (model I, with C' = 0.0035 and 0.006) and measured k [11], Re = 83,000 161
26. Comparison of contour plots of predicted $\bar{U}$ (model I, with C'= 0.0035 and 0.0060) and measured k 11 , Re = 83,000 162

27. Comparison of shear stress (τ) distribution (model I, with C' = 0.0035 and 0.006) and measured τ [10], Re = 83,000 163
28. Comparison of contour plots of predicted k (model II) at Re = 75,000 and Re = 300,000 .
29. Wall shear stress distribution (model I, II and III), with and without secondary flow, Re = 83,000 165
30. Comparison of wall shear stress (τ) distribution (model I, II and III) and measured τ [19], Re = 75,000 166
31. Friction factor (f) (model III) vs. Reynolds number in square ducts 167
32. Comparison of Predicted wall shear stress (model II) at different Reynolds numbers ... 168
33. Comparison of contour plots of predicted (model I) and measured [11] production of vorticity, Re = 83,000 169
34. Comparison of contour plots of predicted (model II) and measured [11] production of vorticity, Re = 83,000 170
35. Comparison of contour plots of predicted (model III) and measured [11] production of vorticity, Re = 83,000 171
36. Variation of k^+ with $\tilde{u}^+$ for turbulent flow in square duct 172

NOMENCLATURE

a_ϕ, b_ϕ	Finite difference equations coefficients, equation (5.1).
A, B	Universal law of the wall constants, equation (4.11).
C_1, C_2, C_μ, C_D	Turbulence model constants (Refer Table 1).
C', C'', C''', m	Vorticity source term models constants.
c_p	Constant pressure specific heat.
D_h	Equivalent hydraulic diameter.
f	Friction factor, equation (4.41).
k	Mean turbulent kinetic energy, $\frac{1}{2}(\bar{u}^2 + \bar{v}^2 + \bar{w}^2)$.
k'	Fluctuating component of turbulent kinetic energy.
k^+	$k/(u^*)^2$.
$k_{c,+}$	Value at centre of duct (model III); taken as 1.
$k_{w,+}$	Value at the wall (model III); taken as 4.
$k_{i,+}$	$k_{c,+}\{1 - m(1 - \hat{y}/\hat{y}_{max})^2\}$.
KE^+	Non dimensional turbulent kinetic energy, $\frac{1}{2}(\bar{u}^{+2} + \bar{v}^{+2} + \bar{w}^{+2})$.
L	Half duct width.
L*	Length of test section from inlet to measuring station.
$\dot{m}$	Mass flow rate.
M	Grid parameter.
n	Direction normal to corner bisector.
P	Pressure.
Re	Reynolds number based on U_b and D_h.
S	Source term, equation (5.1).
t	Time.

u^*	Local friction velocity, $(\tau/\rho)^{1/2}$.
$\bar{u}^*$	Average friction velocity, $(\tau_w/\rho)^{1/2}$.
U	Instantaneous axial velocity.
$\bar{U}$	Axial mean velocity (time-average).
U_b	Average mean velocity over primary flow cell cross-section (bulk velocity).
V_{sec}	Resultant of $\bar{V}$ and $\bar{W}$, $(\bar{V}^2 + \bar{W}^2)^{1/2}$.
u, v, w	Fluctuating components of the velocities in the axial, lateral and bi-normal directions respectively.
$\bar{u}, \bar{v}, \bar{w}$	Root mean square values of u, v and w respectively.
V, W	Instantaneous velocities in the lateral and bi-normal directions respectively.
$\bar{V}, \bar{W}$	Lateral and bi-normal mean velocities (secondary velocities).
x	Axial coordinate.
y, z	Lateral and bi-normal coordinate.
$\hat{y}$	Normal distance from the wall to the surface of no-shear (model III).
Y_P	$1 - \hat{y}/\hat{y}_{max}$
Y_L	$1 - y/\hat{y}_{max}$
Y_M	$k_{c,+} (1 - m Y_P^2))$
Y_N	$\{2 + Y_M + (k_{w,+} - Y_M) Y_L^2\} - \{(1 - Y_L)^2 (k_{w,+} - Y_M)\}$.
α	Thermal diffusivity.
α_R	Relaxation factor, equation (5.30)
ε	Dissipation rate of turbulence kinetic energy.
ξ	Convergence criterion, equation (5.31).
μ	Laminar dynamic viscosity (fluid).
μ_t	Eddy viscosity (isotropic).
ν	Kinematic viscosity.
ρ	Fluid density.

σ_k, σ_ε	Turbulence model constants (Refer Table 1).
τ	Local wall shear stress.
τ_t	Turbulent shear stress, $-\overline{uv}.\rho$.
τ_w	Average wall shear stress.
ϕ	Parameter in the general elliptic equation (5.1).
Ψ	Stream function defined by equations (3.7),(3.8).
ω	Axial vorticity defined by equation (3.9).
∇^2	Laplacian Operator.

Subscripts

b	Bulk.
h	Hydraulic.
i,j	Finite difference indices (directions).
max	Maximum.
-	Overbar designates time-averaging.
C/L	Duct center-line.
c/p	Duct wall center-point.

Superscript

+	Non dimensionalized.

A COMPARISON OF TURBULENT FLOW PREDICTIONS FOR SQUARE DUCTS USING THREE VORTICITY SOURCE MODELS

1.0 INTRODUCTION

1.1 Motivation

Many turbulent flows in engineering practice occur in ducts of non-circular cross-section, e.g. compact heat-exchangers, nuclear reactor channels, air conditioning systems and rotary machinery. During the past two decades, a number of turbulence models and numerical procedures have been developed to enable prediction of turbulent flow and heat transfer in ducts of non-circular cross-section. Much of this work, however, has been directed at nuclear reactors where the fuel bundles form a matrix of rods arranged mainly in triangular and/or square arrays along which the coolant flows axially.

One of the simplest geometries, in which secondary flows arise, is a straight duct of square or rectangular cross-section. The square duct was chosen here for the purpose of analysis because extensive experimental data are available for the primary quantities i.e. axial velocity, secondary velocities, turbulent kinetic energy and wall shear stress. These parameters can all be predicted numerically through a turbulence model. In

turn, a key ingredient in a successful and versatile computation scheme, concerns modelling of the vorticity source term.

The present work was motivated by a desire to test a few models for vorticity source in order to predict the primary quantities in a smooth square duct and thereafter compare them with the available experimental data. This represents a first step towards determining their suitabilities for a simple geometry where a single cell is observed in each primary flow cell. However, the possible application of these vorticity source term models to complicated geometries involving two or more cells (i.e. multicells)[e.g. eccentric annuli (Kacker [1]), non-equilateral isosceles triangles, rectangular ducts and rod-bundles] are discussed briefly and further study is recommended.

1.2 Objectives and Scope

The present work was concerned essentially with developing an analytical model to predict fully developed turbulent flows in square ducts using, in turn three different vorticity source term models, viz., Launder and Ying's [2] Model - Model I; a model based upon turbulent properties correlation - Model II and Seale's [3] Model - Model III.

A two-equation turbulence model was applied which used turbulent kinetic energy (k) and its dissipation rate (ε) as its two additional variables. The five

coupled, non-linear, elliptic equations for axial vorticity, stream function, turbulent kinetic energy, turbulence kinetic energy dissipation rate and mean axial velocity were solved using the method of Gosman et al [4]. This general elliptic finite-difference procedure was used with a uniform cartesian coordinate grid.

Regarding the models for vorticity source term, the first prediction scheme is based on the Reynolds stresses gradients model proposed by Launder and Ying [2]. The second prediction strategy rests upon the relationships between turbulent intensities in turbulent flows as suggested by Alshamani [5]. However, Launder and Singham [6] were probably one of the first of several investigators to suggest the possibility of relating Reynolds normal stresses to the turbulent kinetic energy. They postulated a relationship in the following form:

$$(\bar{v}^2 - \bar{w}^2) = k.g,$$

where k is the turbulent kinetic energy, $(\bar{u}^2 + \bar{v}^2 + \bar{w}^2)/2$ and g is a geometric function of position prescribed in terms of half-widths of the investigated rectangular duct. In the third prediction technique, a synthetic distribution of turbulent kinetic energy (k) is specified and combined with the vorticity equation to produce a simple algebraic term for the source of vorticity as proposed by Seale [3]. The respective model constants

(C'in model I, C'' in model II and C''' in model III) were appropriately tuned to yield the best overall agreement with the experimental data. The eddy viscosity was assumed to be isotropic and was expressed in terms of turbulent kinetic energy and its dissipation rate as per the Prandtl-Kolmogorov formula.

Turbulent predictions were undertaken for both with and (in some cases) without secondary flow. The predictions are shown to be in fairly reasonable agreement with the experimental results of various investigators. However, the main focus of the study concerned the testing of the three models for vorticity source term and assessment of predicted results based on each model with respect to the experimental ones.

Predictions are presented for smooth ducts of width 2L = 7.62, 10.16, 12.70 and 20.32 cm (3,4,5 and 8 in. respectively) for Reynolds number (based on hydraulic diameter) in the range 60×10^3 to 300×10^3. Air at standard temperature and pressure was taken as working fluid in the analysis and the air properties were assumed to be uniform and homogeneous throughout.

In Section 2.0 the experimental and analytical work (with particular emphasis on k-ε turbulence models) on square ducts is reviewed. Section 3.0 deals with the development of the governing equations for the k-ε model whereas the three employed analytical models are treated

in section 4.0. A numerical procedure for solving the governing equations is presented in section 5.0. The predicted results are presented and discussed in detail in section 6.0. Lastly, the chief findings of the present work are itemized in section 7.0.

2.0 LITERATURE REVIEW

2.1 General

There is abundant evidence that turbulent flow in a straight duct of non-circular cross-section is accompanied by lateral spiral motions. The secondary flow of this type, termed by Prandtl [7] as secondary flow of the second kind, is due to the differences in gradients of normal Reynolds stresses across the cross-sectional plane. Secondary flows are experienced in turbulent flows through non-circular ducts of arbitrary cross-sections. It has been discovered that it was differences in gradients of normal Reynolds stresses in the plane of the cross-section that gave rise to a source of streamwise vorticity. This secondary flow convects main flow momentum and energy towards the wall in some regions (typically corners) and away from the wall in other regions. Thus, mean flow streamlines must be helical and not the straight lines as found in circular pipes.

Although the secondary velocities are usually small (within typically 1.5% of the centreline axial velocity), their existence displaces the isovels (i.e. lines of constant axial velocity) significantly toward the corners of the duct, resulting in a relatively high velocity field there. They also act to distribute the shear stresses equally over the wall of the duct. Thus the

effects of secondary flow motion must be included in the simulation of turbulence to avoid any unrealistic interpretation of the phenomenon. Any attempt to deal with this class of flow must pay special attention to the simulation of this secondary flow motion.

The following is a brief review of the published experimental work on rectangular (and especially square) ducts.

2.2 Review of Experimental Work

More than 50 years have passed since Nikuradse [8] delineated the discrepancies between flow in circular pipes and square ducts by discovering that the axial velocity contours in turbulent flow through straight rectangular* ducts were displaced towards the corners of the duct. The cause of these displacements was traced by dye injection to the presence of secondary flows in the plane of the duct cross-section which convected high velocity fluid from the centre of the duct towards the corners. Prandtl [7] suggested that these were the result of secondary flows toward the corners which, to satisfy continuity, required a return flow at the mid-point of the walls. It was also postulated that these were the result of turbulent fluctuations along the isovels giving a net flow normal to the isovel wherever a

---

* The reader is reminded that a square duct is a rectangular duct with unity aspect ratio.

variation in curvature occured. The magnitude of the secondary velocities could not be determined at that time due to error introduced by the presence of the yaw-meter, when used in regions possessing mean velocity gradients.

After the advent of hot-wire anemometer, these velocities were measured and found to be smaller than the root-mean-square turbulent velocity. Hoagland [9] noticed that the flow pattern was exactly the same as predicted by Prandtl, but did not pursue the study of their origins. He selected a 12.7 cm (5 in.) square duct as a compromise between a large cross-section to minimize probe interference and a large velocity to facilitate measurements. A duct length of 9.754 m (32 ft)(L^*/D_h= 75) was employed to insure fully developed flow. The experiment was performed with air as the working fluid. In his experimentation, two methods were considered and employed for velocity measurements; 1) the hot wire anemometer and 2) the pitot tube. The pitot tube generally provides much more accurate velocity measurements but its use for this application was considered to involve two major drawbacks; 1) at velocities below about 3.05 m/sec (10 ft/sec)the velocity pressure is too small to be measured accurately by available means [0.56 mm (.022 in.) H_2O] and 2) it is difficult to obtain pitot tube readings close to a solid boundary due to the size of the pitot tube and the

presence of a steep velocity gradient. Therefore, he decided to use a pitot tube for velocity measurements at the higher Reynolds number and a hot wire for the measurements at the lower Reynolds numbers where the velocities were below 3.05 m/sec (10 ft/sec) and where it was desired to obtain measurements in the viscous sublayer. He considered the measurement of the flow direction to be the best way to determine the secondary velocities and employed only the hot wire for flow direction measurements, principally because of the need to avoid velocity gradient errors. He measured mean axial velocities for rectangular ducts of aspect ratio 1:1 (square duct), 2:1 and 3:1, and the secondary velocities. He also used a Preston tube to measure wall shear stress distribution at a Reynolds number of 78,500. The average wall shear stress was determined by measuring the axial pressure drop and equating the pressure force to the wall shear force.

Leutheusser [10] reported the turbulent mean flow distributions in smooth rectangular duct of aspect ratio 1:1 and 3:1 over a range of Reynolds number between 10^4 and 10^5. In his investigation, atmospheric air was drawn through ducts of 7.62 cm x 7.62 cm (3 in. x 3 in.) and 22.86 cm x 7.62 cm (9 in. x 3 in.) nominal cross-section. In longitudinal development, the ducts comprised a 6.1 m (20 ft) long flow development section, followed by the actual test section, 15.85 m (52 ft) long. He used round

total-head (Pitot) tubes to measure velocity and static pressure distribution whereas round, square-tipped stagnation tubes were used to measure local wall shear stress. He observed that the flow in the neighbourhood of the wall could be properly described by the inner law of the wall whereas in the centre of the duct the velocity distribution did not follow the outer law formulation.

The most substantial description of the phenomena was probably given first by Brundrett and Baines [11]. Their experimental data was obtained from a 7.62 cm (3 in.) square, 21.34 m (70 ft) long horizontal duct using air at room temperature as the working fluid. They discovered that imbalance in the Reynolds turbulence stresses in the plane of the cross-section gave rise to a source of stream-wise vorticity. They used a constant-current hot wire anemometer to measure all six components of the Reynolds stress tensor as well as the three mean velocity components. They were able to conclude from their data that it was predominantly the normal stress gradients which generated the velocities in the plane of the cross-section of rectangular sectioned ducts with axes chosen parallel to the sides. Gessner [12] used a hot wire anemometer to show that a transverse flow is initiated and directed towards the corner as a direct result of turbulent shear stress gradients normal to the bisector. He also indicated that anisotropy of the

turbulent normal stress was not crucial in the generation of secondary flow. His findings do not necessarily contradict that of Brundrett and Baines [11] since they used different coordinate system for their investigations.

Brundrett and Baines [11], like Hoagland [9], established that at any point in the duct the Reynolds number does not affect the ratio of primary to secondary velocity. In contrast to this, the measurements of Gessner and Jones [13] indicated that secondary velocities, when non-dimensionalized by either the bulk velocity or the axial centreline velocity, decreased with increasing Reynolds number. Their experiment used room air through channel cross-sections of 20.32 cm (8 in.) square with L^*/D_h ratio of 40 and 20.32 cm x 10.16 cm (8 in. x 4 in.)(i.e. aspect ratio 2) with L^*/D_h ratio of 60. In their investigation, the axial mean-flow velocity measurements were made with a total head tube in conjunction with a wall static-pressure tap in the same transverse plane on the opposite wall. A probing of the flow field with a Pitot static tube indicated that the error involved in the use of a wall tap for these measurements was negligible over the Reynolds number range of the investigation (i.e. 60,000 to 300,000). In order to measure secondary-flow velocity components quantitatively, they used the method of single-wire rotation described by Hoagland [9].

Launder and Ying [14] used two 10.16 cm (4 in.) square ducts (one duct smooth and the other rough) 7.01 m (23 ft) in length and room air as the working fluid. They found that secondary velocities normalized with average friction velocity yielded similar secondary velocity profiles for smooth and rough surfaces. However, for rough walls, secondary velocities were a substantially larger proportion of the axial bulk velocity than for the case of smooth-walled ducts. They also revealed that secondary velocities normalized with friction velocity are unaffected by Reynolds number variation. A hot-wire anemometer was used to measure axial velocity whereas the technique of measuring the secondary flow was similar to Brundrett and Baines [11].

Kokorev et al [15] measured one of the two components of secondary velocities by using a five-tap tube out of which four taps were oriented at approximately 45° angle to the probe axis. The probe was used for secondary flow measurements in a square channel. The channel had a 7 cm x 7 cm cross-section and was 3.3 m long (L^*/D_h ratio of 47).

Ahmed and Brundrett [16] performed experimental investigation of developing flow in a wind-tunnel of 9.21 cm (3 5/8 in.) square cross-section. They examined generalized mean properties of turbulent flow for the developing region and presented experimental data for

mean velocity profiles and peripheral wall shear distributions at various axial locations as well as the longitudinal static pressure distribution. In the investigation, the mean velocities were taken by traversing a Pitot-static tube connected to a Betz manometer. The peripheral wall shear readings were taken with a Preston tube at each location.

The developing turbulent flow in a rectangular (almost square) duct was studied recently by Melling and Whitelaw [17] using laser Doppler anemometer. They used a straight duct of rectangular cross-section 40 mm wide by 41 mm deep. In their work, water was chosen as the working fluid because it allowed almost continuous Doppler signals from the anemometer to operate with a frequency-tracking demodulator without the addition of particles. Laser Doppler anemometer enabled them to measure mean axial velocity and turbulent intensities in the developing flow whereas all three mean velocity components and five of the six Reynolds stresses were measured in almost fully developed flow.

Gessner et al [18] also measured developing turbulent flow in a square duct at L^*/D_h ratio of 1 to 26 at 1 D_h intervals and then 26 to 84 at 2 D_h intervals. They used a duct of 2.54 cm x 2.54 cm (1 in. x 1 in.) cross-section and air was taken as working fluid. They

measured axial mean velocities by means of a miniature probe in conjunction with a wall static pressure tap. Turbulence measurements were made with hot wire probes similar in design to configurations recommended by Comte-Bellot [19], for minimal prong interference effects. They revealed that at the location where peaking of the axial centreline velocity occurs, certain Reynolds stress components and mean rates of strain are elevated above their counterparts for fully developed flow. They also suggested that the turbulence kinetic energy dissipation rate can be modelled in terms of a suitably defined length scale and either the resultant primary shear stress or the turbulent kinetic energy.

2.3 Turbulence Models

2.3.1 General

Since exact solutions of turbulent flows are not possible due to the closure problem, a turbulence model is employed. It is a set of differential equations (controlling the distributions of turbulence properties under consideration), associated algebraic equations and constants which, when solved, closely simulate the characteristics of the turbulent flow through the configuration in question.

These models can be broadly classified into two categories, viz., algebraic models and differential

models. The algebraic models find their base on the assumption that turbulence stresses are solely dependent on the velocity field. The turbulence parameters in differential models, however, are controlled by differential transport equations and hence are subjected to convective and diffusive processes on top of the local processes. Therefore the differential models are more accurate for all flows where convection or turbulent diffusion, or both, have a significant influence on the turbulent stresses.

In the literature, turbulence models have received considerable attention but investigators continue to strive to achieve a better and more successful model. Reynolds [20][21], Wolfshtein [22] Launder and Spalding [23], Bradshaw [24][25] and Spalding [26] have contributed significantly to this subject.

2.3.2 Classification of Turbulence Models

Depending upon the number of turbulence parameters used as the dependent variables in the differential transport equations, Reynolds [20] classified turbulence models as follows:

(i) Zero-equation Models (or Mean Velocity Field (MVF) Closure)

These models call for a partial differential equation (PDE) for only the mean velocity field.

The examples include Prandtl mixing length hypothesis (1925) and Von Karman mixing length model (1930).

(ii) One-equation models (or Mean Turbulent Energy (MTE) Closure)

These models incorporate an additional PDE relating to the turbulent kinetic energy (k); e.g., k-ℓ model where ℓ is represented by an algebraic expression such as Buleev's [27] model. Zero-equation and one-equation models are typically algebraic models.

(iii) Two-equation Models

These models incorporate an additional PDE linked to a turbulence length scale (ℓ); e.g., k-ℓ, k-ε, k-kℓ models.

(iv) Stress-equation Models (Five-equation model)

PDE's are employed for all terms of the turbulent stress tensor; i.e Reynolds stress models. These models provide a new approach to the turbulent flow modelling [28][29].

All these models have their own usefulness and limitations. Zero-equation models can predict integral properties of the flow much better than the local details. However, they are not suitable for surfaces with strong curvature and for free stream turbulent flows. One-

equation model avoids assumptions of zero-equation model such as the quick adjustment of turbulence with the changes in mean condition and the existence of universal relationship between the turbulent stresses and the mean strain rates. One-equation models have been employed by several investigators in various applications including equilateral triangular duct [30], rod bundle [31][32] as well as square duct (2). The turbulence length scale (ℓ) in one-equation model which appears in the respective turbulence transport equation for the turbulent kinetic energy in conjunction with constitutive equations relating the Reynolds stresses to the turbulent kinetic energy, is not a particular well-conditioned variable to employ. Rather variables of the form $k^x \ell^y$ (where x and y are mathematical constants) have been favoured by several investigators, e.g. ℓ, $k\ell$, k/ℓ^2 and $k^{3/2}/\ell$ which paved the way for many two-equation models, e.g., k-ℓ, k-kℓ, k-W and k-ε. Here k is the turbulent kinetic energy,

$$k = \frac{1}{2} \overline{u_i u_i} \quad ; \qquad (2.1)$$

ε is the turbulence energy dissipation rate,

$$\varepsilon = \nu \overline{\left(\frac{\partial u_i}{\partial x_j} \cdot \frac{\partial u_i}{\partial x_j}\right)} \qquad (2.2)$$

The turbulence length scale can be defined by k, ε and C_D as:

$$\ell = C_D k^{3/2}/\varepsilon, \qquad (2.3)$$

where C_D is a constant.

Similarly, W is a quantity having the dimension of $(\text{time})^{-2}$ which Bradshaw [24] figured as representing the mean square vorticity or frequency of the energy containing eddies. W can be expressed as:

$$W = \varepsilon^2/(C_D k)^2 . \qquad (2.4)$$

Tennankore and Steward [33] presented a comparison between three models (viz. mixing length model, k-ℓ turbulence model and k-ε turbulence model) for predicting flow characteristics within confined jets. They concluded that the mixing length model provided the best results for the isothermal case. Whereas, for non-isothermal jets, the k-ε model gave better predictions than the other two models. Launder and Spalding [34] noted the interchangeability of k-kℓ, k-W and k-ε models and indicated that they differ merely in mathematical form and, not in content. They also advocated that the k-ε model is the simplest to use for the prediction of both near-wall and free-shear flows without adjusting the constants or functions.

2.3.3 The k-ε Turbulence Models (Two Equation Models)

There are two types of k-ε turbulence models, viz. the low-Reynolds number and the high Reynolds number model.

Low-Reynolds Number k-ε Turbulence Model

This model type is particularly useful in handling regions near the wall where viscosity exerts an influence on the turbulence structure. This type was developed originally by Jones and Launder [35][36] where k and ε were determined as following (in cartesian coordinates):

$$\rho \frac{Dk}{Dt} = \frac{\partial}{\partial x_j}\left[\left(\mu + \frac{\mu_t}{\sigma_k}\right)\frac{\partial k}{\partial x_j}\right] + \mu_t\left[\frac{\partial \bar{U}_i}{\partial x_j} + \frac{\partial \bar{U}_j}{\partial x_i}\right]\frac{\partial \bar{U}_i}{\partial x_j} - \rho\varepsilon - 2\mu\left(\frac{\partial k^{1/2}}{\partial x}\right)^2, \qquad (2.5)$$

$$\rho \frac{D\varepsilon}{Dt} = \frac{\partial}{\partial x_j}\left[\left(\mu + \frac{\mu_t}{\sigma_\varepsilon}\right)\frac{\partial \varepsilon}{\partial x_j}\right] + C_1 \mu_t \frac{\varepsilon}{k}\left[\frac{\partial \bar{U}_i}{\partial x_j} + \frac{\partial \bar{U}_j}{\partial x_i}\right] \frac{\partial \bar{U}_i}{\partial x_j} - C_2 \rho \frac{\varepsilon^2}{k} + 2\nu \mu_t \left(\frac{\partial^2 \bar{U}_i}{\partial x_j \partial x_\ell}\right)^2 . \quad (2.6)$$

The isotropic eddy viscosity (μ_t) is formulated by Prandtl-Kolmogorov in terms of kinetic energy and its dissipation rate,

$$\mu_t = C_\mu \rho k^2/\varepsilon . \quad (2.7)$$

Both k and ε were found from the solution of the appropriate conservation equations.

C_1, C_2, C_μ, σ_ε and σ_κ are model constants to be determined by reference to some special cases (e.g. the constant-stress layer adjacent to the wall, decay of turbulence behind a grid etc.) and/or experimental data C_2 and C_μ are designed to vary with turbulence Reynolds number as follows:

$$C_2 = C_{2\infty}\left[1 - 0.3 \exp\left(-Re_t^2\right)\right] \quad (2.8)$$

and,

$$C_\mu = C_{\mu\infty} \exp\left[-2.5/(1 + Re_t/50)\right], \quad (2.9)$$

where $Re_t = \rho k^2/\mu\varepsilon$ is the turbulence Reynolds number and $C_{2\infty}$ and $C_{\mu\infty}$ are the values assumed by C_μ and C_2 at high Reynolds numbers.

High-Reynolds Number k-ε Turbulence Model

Launder and Spalding [34] expressed the approximate model equations for k and ε (in cartesian-coordinates) as follows:

$$\rho \frac{Dk}{Dt} = \frac{\partial}{\partial x_j}\left[\frac{\mu_t}{\partial_k}\frac{\partial k}{\partial x_j}\right] + \mu_t \left[\frac{\partial \bar{U}_i}{\partial x_j} + \frac{\partial \bar{U}_j}{\partial x_i}\right] \frac{\partial \bar{U}_i}{\partial x_j} - \rho\varepsilon , \quad (2.10)$$

$$\rho \frac{D\varepsilon}{Dt} = \frac{\partial}{\partial x_j}\left[\frac{\mu_t}{\sigma_\varepsilon}\frac{\partial \varepsilon}{\partial x_j}\right] + C_1 \mu_t \frac{\varepsilon}{k}\left[\frac{\partial \bar{U}_i}{\partial x_j} + \frac{\partial \bar{U}_j}{\partial x_i}\right] \frac{\partial \bar{U}_i}{\partial x_j} - C_2 \rho \frac{\varepsilon^2}{k} \qquad (2.11)$$

In equations (2.10) and (2.11), μ_t is given by equation (2.9).

The present work employs the high Reynolds number k-ε turbulence model.

2.4 Review of Analytical Work

Closed form analytical solutions of turbulent flow in circular and non-circular ducts are still not possible. However, various attempts for approximate solutions have been made by several investigators in order to predict the flow anlytically and achieve reasonable agreement with the available experimental data.

Theoretical treatments of the flow in non-circular ducts show considerable variation both in the style of approach and in the predictions produced. Deissler and Taylor (37) advocated the applicability of the well-known semi-logarithmic law, which holds good in pipes or one-dimensional plane channels, for the arbitrary ducts along 'velocity gradient' lines (the set of lines orthogonal with the axial isovels). The findings, however, substantially deviated from the experimental data of Leutheusser [10] and Gessner and Jones [13].

Krajewski [38] suggested that the non-dimensionalized effective viscosity in a square duct would be the same as in a pipe and Buleev [39] discussed the application of mixing length to the prediction of flow in arbitrarily shaped conduits. Their assumption of isotropic effective diffusion coefficient for momentum transport resulted in no display of secondary flow and hence in a serious discrepancy in the prediction of such flows. Ibragimov et al [40][41] modified this approach by making the effective transport coefficients direction dependent. The predictions showed correct qualitative trends such as displacements of velocity and temperature contours towards the corners, however, the approach weighed too heavily on direct experimental input to be utilized for generalizing to arbitrary geometries.

Wilson et al [42] employed two models for effective viscosity. The one was based on Van Driest's modification* to the Prandtl mixing length concept, and the other was a modification to Reichardt's model for fully developed pipe flow. The solution method required the input of two types of empirical data - the effective viscosity model and the experimental data for vorticity source. This, of course, limited the versatility of the method.

---

* Hornby et al [46] also studied the damping influence of the wall on turbulent fluid flow and extended Von Driest's original hypothesis to find a damping factor in conjunction with mixing length expressions to obtain the velocity field.

Launder and Ying [2] noted the inadequacy of the notion of an isotropic turbulent viscosity and proposed the direct modelling of turbulent Reynolds stress inducing the streamwise vorticity. In their earlier work, Ying [43] and Launder and Singham [6] modelled the vorticity generating stress gradients in a rectangular duct by reference to experimental data in a one-dimensional channel involving a simple hypothesis which was too particularized to permit its application to other complex geometries. Hanjalic and Launder [28] proposed a form which predicted accurately a wide range of boundary layer flows. However it was a major task to solve simultaneously the seven strongly coupled highly non-linear differential equations for turbulence quantities together with others for the mean flow.

In 1973, Launder and Ying [2] devised a much simpler derivative of Hanjalic and Launder's [28] model which, while retaining the essential vorticity-generating features, required the solution of only one turbulence property to be found from a differential equation. Tatchell [44] adopted the model proposed by Launder and Ying [2] to allow the prediction of the turbulence induced lateral motions for both developing and fully developed flow in a square duct. He was probably the first investigator to use the two-equations (k-ε) model for fully developed turbulent flow through a non-circular duct.

Wolfshtein et al [45] presented a five-equations model involving the Reynolds stress equations and proposed a special linearized implicit representation of the source terms to ensure numerical stability of the solution. He used a special procedure near the wall by which the Reynolds stress equations were assumed to be in local equilibrium.

Based on the work of Alshamani [5], [47], Seale [3] tackled complex geometries and came up with an algebraic vorticity source term in the vorticity equation, which is calculated directly and without iteration. He illustrated the model to reproduce secondary velocities in square and triangular cross-section ducts, and in a duct consisting of two inter-connected subchannels.

Recently, Nakayama et al [48] employed Launder and Ying's [2] basic model to predict secondary flow, but, with a strong emphasis on the local structures of turbulence. In their investigation, the anisotropy of normal stresses and the secondary shear stress acting in the cross-sectional plane (the gradients of which are major causes of the secondary-flow motions) were reported to be under-estimated to one order of magnitude less than the experimental data.

3.0 GOVERNING EQUATIONS:

The following governing equations are presented for the square duct configuration where geometrical symmetry permits only one octant of the flow cross-section to be considered (other octants being the mirror-image of the adjacent ones). Subsequently, we get eight primary flow cells which are identical when viewed with respect to rotated and reversed coordinate system (except for handedness of secondary flow circulation) and no net mass, momentum or energy is transferred across any boundary. The turbulent flow predictions in one cell is sufficient to predict the entire flow field. Figures 1 and 2 show the primary flow cells together with the octant and cartesian coordinate system under consideration in this work.

The following sections outline the governing equations for continuity of the flow, $\bar{U}$, ω, Ψ, k and ε. The equations hold good for fully developed, steady and incompressible turbulent flow of a constant property fluid with negligible body forces.

3.1 Continuity and Reynolds Equations

The continuity equation for the mean flow for a flow cell can be expressed as:

$$\frac{\partial \bar{V}}{\partial y} + \frac{\partial \bar{W}}{\partial z} = 0, \qquad (3.1)$$

whereas for the fluctuating flow it is given as

$$\frac{\partial u}{\partial x} + \frac{\partial v}{\partial y} + \frac{\partial w}{\partial z} = 0 \qquad (3.2)$$

The Reynolds Equations for a turbulent flow are expressed as:

For the axial direction (x):

$$\rho \left(\bar{V} \frac{\partial \bar{U}}{\partial y} + \bar{W} \frac{\partial \bar{U}}{\partial z}\right) = - \frac{\partial \bar{P}}{\partial x} + \mu \left(\frac{\partial^2 \bar{U}}{\partial y^2} + \frac{\partial^2 \bar{U}}{\partial z^2}\right)$$

$$- \rho \left(\frac{\partial \overline{uv}}{\partial y} + \frac{\partial \overline{uw}}{\partial z}\right) . \qquad (3.3)$$

For the lateral horizontal direction (y):

$$\rho \left(\bar{V} \frac{\partial \bar{V}}{\partial y} + \bar{W} \frac{\partial \bar{V}}{\partial z}\right) = - \frac{\partial \bar{P}}{\partial y} + \mu \left(\frac{\partial^2 \bar{V}}{\partial y^2} + \frac{\partial^2 \bar{V}}{\partial z^2}\right)$$

$$- \rho \left(\frac{\partial \overline{v^2}}{\partial y} + \frac{\partial \overline{vw}}{\partial z}\right) . \qquad (3.4)$$

For the lateral vertical direction (z):

$$\rho \left(\bar{V} \frac{\partial \bar{W}}{\partial y} + \bar{W} \frac{\partial \bar{W}}{\partial z}\right) = - \frac{\partial P}{\partial z} + \mu \left(\frac{\partial^2 \bar{W}}{\partial y^2} + \frac{\partial^2 \bar{W}}{\partial z^2}\right)$$

$$- \rho \left(\frac{\partial \overline{vw}}{\partial y} + \frac{\partial \overline{w^2}}{\partial z}\right) . \qquad (3.5)$$

In the above expressions the over-bar designates time-averaged quantities.

The axial momentum equation (i.e. equation 3.3) can be rearranged in the following form:

$$- \frac{1}{\rho} \frac{\partial \bar{P}}{\partial x} = \left[\frac{\partial \overline{uv}}{\partial y} + \frac{\partial \overline{uw}}{\partial z}\right] - \nu \left[\frac{\partial^2 \bar{U}}{\partial y^2} + \frac{\partial^2 \bar{U}}{\partial z^2}\right] + \bar{V} \frac{\partial \bar{U}}{\partial y}$$

$$+ \bar{W} \frac{\partial \bar{U}}{\partial z} \qquad (3.6)$$

The term on the left hand side of the equation (i.e. source term) indicates the variation in x-direction momentum due to the pressure gradient in the same direction. If equations (3.3), (3.4) and (3.5) are differentiated with respect to x, it is easy to show that

the magnitude of $\frac{\partial \bar{P}}{\partial x}$ is constant over the cross-section of the flow.

On the right hand side of equation (3.6) the first two bracketed terms represent the variation in axial momentum as a result of viscous effects and Reynolds shear stresses. The remaining two terms represent the change in the axial momentum of a small fluid particle due to convection by secondary flows. These two terms are absent in a flow through circular conduit.

The boundary conditions for the Reynolds equations are as follows:

i) Along the y-axis (i.e. solid wall boundary) the convective terms and gradients in the direction parallel to the wall (i.e. $\frac{\partial}{\partial y}$) vanish from the Reynolds equations as a result of the no-slip condition at the wall.

ii) Along the corner bisector, no net flow is crossing the boundary, therefore,

$\bar{V} \cos 45° + \bar{W} \cos 45° = 0$

or, $\bar{V} = -\bar{W}$

iii) Along the mid-wall bisector, equation (3.4) vanishes since there can be no net momentum transfer across this symmetry line. Thus,

$\bar{V} = 0$ and therefore,

$\frac{\partial \bar{V}}{\partial z} = 0 = \frac{\partial^2 V}{\partial z^2}$, and

since $\bar{V}$ has opposite signs on each side of z-axis, therefore,

$$\frac{\partial^2 \bar{V}}{\partial y^2} = 0.$$

Similarly, due to symmetry

$$\frac{\partial \bar{P}}{\partial y} = 0 = \frac{\partial \overline{v^2}}{\partial y}, \quad \text{and}$$

hence it can be readily shown that

$\overline{vw} = 0$, along the mid-wall bisector.

However, $\frac{\partial \overline{uv}}{\partial y}$(as well as $\frac{\partial \bar{V}}{\partial y}$) may have finite values along the mid-wall bisector since $\overline{uv}$ (as well as $\bar{V}$) is antisymmetrically distributed about the z-axis. Since $\bar{W}$ may have finite values along the z-axis except at the wall and duct centreline, it is impossible to achieve a simple theoretical distribution for $\overline{uw}$ at the mid-wall bisector from equation (3.3).

(iv) At the duct centreline, due to symmetry

$$\frac{\partial \bar{U}}{\partial y} = 0 = \frac{\partial \bar{U}}{\partial z}, \quad \text{and}$$

$$\bar{V} = 0 = \bar{W}.$$

3.2. Axial Vorticity and Stream Function Equations

The following definition for the stream function (Ψ) and the axial vorticity (ω) forms the basis for the calculation procedure:

$$\rho \bar{V} = \frac{\partial \Psi}{\partial z} \qquad (3.7)$$

$$\rho \bar{W} = -\frac{\partial \Psi}{\partial y}, \qquad (3.8)$$

and $$\omega = \frac{\partial \bar{W}}{\partial y} - \frac{\partial \bar{V}}{\partial z}. \qquad (3.9)$$

The pressure gradients in equations (3.4) and (3.5) may be eliminated by cross-differentiation and then subtraction. By making use of the continuity equation (3.1) as well as the definition of ω, the transport equation for the axial vorticity may be written as following:

$$\bar{V} \frac{\partial \omega}{\partial y} + \bar{W} \frac{\partial \omega}{\partial z} = \frac{\partial^2}{\partial y \partial z} \left(\overline{v^2} - \overline{w^2} \right) - \left(\frac{\partial^2 \overline{vw}}{\partial y^2} - \frac{\partial^2 \overline{vw}}{\partial z^2} \right) + \nu \left(\frac{\partial^2 \omega}{\partial y^2} + \frac{\partial^2 \omega}{\partial z^2} \right) \qquad (3.10)$$

This equation as well as the expression for ω include only velocities and gradients in the y and z directions and obviously exists only if the secondary velocities exist and vice versa. The terms on the left hand side of equation (3.10) indicate the convection of axial vorticity due to secondary velocities. This process tends to make vorticity constant along the secondary flow streamlines. The last term on the right produces a similar effect and represents the diffusion of the axial vorticity by viscous effects. It tends to spread out vorticity uniformly over the flow cross-section by diffusing it from regions of high momentum to regions of low momentum. The other remaining terms may represent either production or dissipation of the axial vorticity depending upon the local turbulence field.

Substitution of equations (3.7) and (3.8) into (3.9) results in the stream function equation:

$$\frac{\partial}{\partial y} \left(\frac{\partial \Psi}{\partial y} \right) + \frac{\partial}{\partial z} \left(\frac{\partial \Psi}{\partial z} \right) + \rho \omega = 0, \qquad (3.11)$$

where $\rho\omega$ represents the source term in this equation.

3.3 Turbulent Kinetic Energy Equation

The approximate (simulated) transport equation for the turbulent kinetic energy for high Reynolds numbers, is expressed as;

$$\left[\bar{V}\frac{\partial k}{\partial y} + \bar{W}\frac{\partial k}{\partial z}\right] + \frac{\partial}{\partial y}\left(\nu\frac{\partial k}{\partial y} - \overline{vk'}\right) + \frac{\partial}{\partial z}\left(\nu\frac{\partial k}{\partial z} - \overline{wk'}\right)\Big] - \left[\overline{uv}\frac{\partial \bar{U}}{\partial y} + \overline{wu}\frac{\partial \bar{U}}{\partial z}\right] - \varepsilon. \qquad (3.12)$$

Equation (3.12) has been derived in detail in Appendix A.

For the sake of discussion, the same equation can be rewritten as:

$$I + II + III + IV = 0$$

where,

(a) Term $I = \bar{V}\frac{\partial k}{\partial y} + \bar{W}\frac{\partial k}{\partial z}$ or convection term represents convection of the mean turbulent kinetic energy due to secondary velocities.

(b) Term $II = -\left[\frac{\partial}{\partial y}\left(\nu\frac{\partial k}{\partial y} - v\overline{k'}\right) + \frac{\partial}{\partial z}\left(\nu\frac{\partial k}{\partial z} - \overline{wk'}\right)\right]$, a diffusion term, represents energy diffusion by viscous and turbulence effects.

(3) Term $III = \left[\overline{uv}\frac{\partial \bar{U}}{\partial y} + \overline{uw}\frac{\partial \bar{U}}{\partial z}\right]$, a production term, represents the rate of production of turbulence energy. The physical meaning of this term is that the mean flow performs work on the turbulent eddies and thus the energy is

transferred from the mean motion to the fluctuating motion; this process constitutes the so-called "energy-cascade".

(d) Term IV = ε, a dissipation term represents the rate of dissipation of kinetic energy by molecular viscosity. In the energy cascade, energy is transferred from the mean motion to the large eddies and then to smaller eddies. At the end of the cascade, viscous resistance counteracts the turbulent fluctuations and all the turbulent energy is eventually dissipated into thermal energy.

3.4. Turbulence Energy Dissipation Rate Equation

The approximate (simulated) transport equation for the turbulence energy dissipation rate (ε), for high Reynolds number, is derived in Appendix B and is expressed as:

$$\left[\bar{V}\frac{\partial \varepsilon}{\partial y} + \bar{W}\frac{\partial \varepsilon}{\partial z}\right] = \left[\frac{\partial}{\partial y}\left(\nu\frac{\partial \varepsilon}{\partial y} - \overline{v\varepsilon'}\right) + \frac{\partial}{\partial z}\left(\nu\frac{\partial \varepsilon}{\partial w} - \overline{w\varepsilon'}\right)\right]$$

$$- C_1\frac{\varepsilon}{k}\left[\overline{uv}\frac{\partial \bar{U}}{\partial y} + \overline{wu}\frac{\partial \bar{U}}{\partial z}\right] - C_2\frac{\varepsilon^2}{k}, \qquad (3.13)$$

where C_1 and C_2 are empirical constants. Previous investigations [34] [49] [50] have suggested a value of $C_1 = 1.44$ based on computer optimization to yield the best agreement with experimental data. Similarly a number of workers [34] [44] [49] [50] have determined a value of $C_2 = 1.92$ with reference to the limited case of decay of turbulence behind a grid. The above values of C_1 and C_2 were used in the present work.

The effects of the various terms in equation (3.13) on dissipation rate are parallel to those terms in equation (3.12) on kinetic energy.

The convection terms in equations (3.6)(3.10) (3.12) and (3.13) may be expressed in terms of stream functions (Ψ) in the following forms:

Axial momentum (Reynolds equation):

$$\frac{\partial}{\partial y}\left(\bar{U}\,\frac{\partial \Psi}{\partial z}\right) - \frac{\partial}{\partial z}\left(\bar{U}\,\frac{\partial \Psi}{\partial y}\right) - \mu\left[\frac{\partial^2 \bar{U}}{\partial y^2} + \frac{\partial^2 \bar{U}}{\partial z^2}\right]$$

$$+ \rho\left[\frac{\partial}{\partial y}\,\overline{uv} + \frac{\partial\,\overline{uw}}{\partial z}\right] + \frac{\partial P}{\partial x} = 0. \qquad (3.14)$$

Axial vorticity equation:

$$\frac{\partial}{\partial y}\left(\omega\,\frac{\partial \Psi}{\partial z}\right) - \frac{\partial}{\partial z}\left(\omega\,\frac{\partial \Psi}{\partial y}\right) - \frac{\partial}{\partial y}\left[\frac{\partial}{\partial y}\,(\mu\omega)\right] - \frac{\partial}{\partial z}\left[\frac{\partial}{\partial z}\,(\mu\omega)\right]$$

$$- \rho\,\frac{\partial^2\,(\overline{v^2} - \overline{w^2})}{\partial y\,\partial z} + \rho\left(\frac{\partial^2 \overline{vw}}{\partial y^2} - \frac{\partial^2 \overline{vw}}{\partial z^2}\right) = 0\ . \qquad (3.15)$$

Stream function equation:

$$-\left[\frac{\partial}{\partial y}\,\frac{\partial \Psi}{\partial y} + \frac{\partial}{\partial z}\,\frac{\partial \Psi}{\partial z}\right] - \rho\omega = 0\ . \qquad (3.16)$$

Tubulent kinetic energy equation:

$$\left[\frac{\partial}{\partial y}\left(k\,\frac{\partial \Psi}{\partial z}\right) - \frac{\partial}{\partial z}\left(k\,\frac{\partial \Psi}{\partial y}\right)\right] - \left[\frac{\partial}{\partial y}\left(\mu\,\frac{\partial k}{\partial y} - \rho\,\overline{vk'}\right] + \frac{\partial}{\partial z}\right.$$

$$\left.\left(\mu\frac{\partial k}{\partial z} - \rho\,\overline{wk'}\right)\right] + \rho\left[\overline{uv}\,\frac{\partial \bar{U}}{\partial y} + \overline{wu}\,\frac{\partial \bar{U}}{\partial z}\right] + \rho\varepsilon = 0. \qquad (3.17)$$

Turbulence energy dissipation rate equation:

$$\left[\frac{\partial}{\partial y}\left(\varepsilon\,\frac{\partial \Psi}{\partial z}\right) - \frac{\partial}{\partial z}\left(\varepsilon\,\frac{\partial \Psi}{\partial y}\right)\right] - \left[\frac{\partial}{\partial y}\left(\mu\,\frac{\partial \varepsilon}{\partial y} - \rho\,\overline{v\varepsilon'}\right) + \frac{\partial}{\partial z}\right.$$

$$\left.\left(\mu\,\frac{\partial \varepsilon}{\partial w} - \rho\,\overline{w\varepsilon'}\right)\right] + C_1\,\rho\,\frac{\varepsilon}{k}\left[\overline{uv}\,\frac{\partial \bar{U}}{\partial y} + \overline{wu}\,\frac{\partial \bar{U}}{\partial z}\right]$$

$$+ C_2\,\rho\,\frac{\varepsilon^2}{k} = 0. \qquad (3.18)$$

The boundary conditions for the above equations [(3.14) to (3.18)] are discussed in detail in section 4.2.

4.0 THE ANALYTICAL MODELS

In the present work, fully-developed turbulent flow of a constant properties fluid with negligible body forces was considered. Under the above assumptions, the continuity and momentum equations (equations 3.1 to 3.5) in section 3.1 were reduced to a set of three transport equations (equations 3.14 to 3.16) for the axial momentum, axial vorticity and stream function respectively. Predictions of the flow characteristics in a square duct may now be possible provided closure is prescribed.

4.1 Closure of $\bar{U}$, k and ε Equations:

It is obvious from the axial vorticity equation (3.15) that its complete closure requires of gradients of the difference in Reynolds normal stresses (i.e. $\overline{v}^2 - \overline{w}^2$) as well as Reynolds shear stress (i.e. $\overline{v\,w}$) in the axial vorticity source term i.e. the last two terms of equation (3.15). Also, other Reynolds shear streses i.e. $\overline{u\,v}$ and $\overline{w\,u}$ have appeared in the diffusion term of the axial momentum equation (3.14) and in the source terms of the turbulent kinetic energy equation (3.17) and the turbulence energy dissipation rate equation (3.18). These latter shear stress components lie in planes parallel to the direction of the primary velocity and therefore, the conventional turbulent-viscosity concept serves well enough for their simulation. These

shear stress components are approximated as:

$$\overline{u\,v} = -\frac{1}{\rho}\,\mu_t\,\frac{\partial \bar{U}}{\partial y}\,, \text{ and} \qquad (4.1)$$

$$\overline{w\,u} = -\frac{1}{\rho}\,\mu_t\,\frac{\partial \bar{U}}{\partial z} \qquad (4.2)$$

where μ_t is isotropic turbulent (eddy) viscosity and is given by Prandtl-Kolmogorov formula [equation (2.7)] which is repeated here;

$$\mu_t = C_\mu\,\rho\,k^2/\varepsilon \qquad (2.7)$$

where C_μ is an empirical constant and was assigned a value of 0.09 in all three models considered in this work. The value was determined with reference to the properties of the 'constant-stress' wall region. In this particular region, the convective transport is negligible and the dissipation and production rates of turbulent energy are equal.

The complete closure of the turbulent kinetic energy equation (3.17) and the turbulence energy dissipation rate equation (3.18) requires the specification of the turbulent diffusion terms i.e. $\overline{vk'}$, $\overline{wk'}$, $\overline{v\varepsilon'}$ and $\overline{w\varepsilon'}$. Hinze [51] represented the turbulent diffusion of a scalar quantity by its flux approximation as follows:

$$\overline{vk'} = -\frac{1}{\rho}\,\frac{\mu_t}{\sigma_k}\cdot\frac{\partial k}{\partial y}\,,\quad \overline{wk'} = -\frac{1}{\rho}\,\frac{\mu_t}{\sigma_k}\,\frac{\partial k}{\partial z}\,, \text{ and} \qquad (4.3)$$

$$\overline{v\varepsilon'} = -\frac{1}{\rho}\,\frac{\mu_t}{\sigma_\varepsilon}\cdot\frac{\partial \varepsilon}{\partial y}\,,\quad \overline{w\varepsilon'} = -\frac{1}{\rho}\,\frac{\mu_t}{\sigma_\varepsilon}\,\frac{\partial \varepsilon}{\partial z}\,: \qquad (4.4)$$

In the above equations, σ_k and σ_ε are empirical constants. σ_k is a well-established constant and has been given a value of 1.0 by several workers e.g. Launder and Spalding [34], Jones and Launder [36], Tatchell [44], Gosman et al. [50], Gosman and Rapley [52], Date [53] etc. The other turbulence model constant, σ_ε is determined by reference to the properties of the "constant-stress" wall region as follows:

$$\sigma_\varepsilon = (\kappa^2 / c_\mu^{1/2}) \; / \; (C_2 - C_1), \qquad (4.5)$$

where κ is the universal Von-Karman constant, C_1 and C_2 are the other turbulence model constants and have somewhat well-established values of 1.44 and 1.92 respectively due to Launder and Spalding [34], Tatchell [44] and Gosman et al [50].

The Reynolds shear stress components $\overline{uv}$ and $\overline{wu}$ are given by equations (4.1) and (4.2). The gradients of $\bar{U}$ appearing in equations (4.1) and (4.2) were calculated at the solid boundaries by differentiating the universal law of the wall whereas central-difference was employed elsewhere. The central-difference technique was also used in determining the first and second derivatives of the Reynolds stresses appearing in the vorticity source terms of the axial vorticity equation (3.15).

4.2. Boundary Conditions

(i) Stream Function (Ψ)

Since no net mass is transferring across the three boundaries (i.e. solid wall, mid-wall bisector and corner bisector), the stream function is constant along these boundaries of the primary flow cell (Fig. 1). This constant was conveniently chosen to be zero.

(ii) Axial Vorticity (ω)

The vorticity is taken to be zero at the two symmetry line boundaries (i.e. mid-wall bisector and corner bisector). Near the wall, it was assumed that the vorticity varies linearly with the normal distance from the wall.

(iii) $\bar{U}$, k and ε

Along the corner and mid-wall bisectors, the symmetry demands the normal-to-boundary gradients of $\bar{U}$, k and ε to be set equal to zero. Mathematically, it is given as:

a) At the mid-wall bisector

$$\frac{\partial \bar{U}}{\partial y} = 0 = \frac{\partial k}{\partial y} = \frac{\partial \varepsilon}{\partial y}. \qquad (4.6)$$

Taylor's expansion was used to satisfy equation (4.6) near these symmetry lines and is expressed as:

$$\phi_p \approx [(y_n - y_p)^2 \phi_m - (y_m - y_p)^2 \phi_n]/[(y_n - y_p)^2 - (y_m - y_p)^2] \quad , \qquad (4.7)$$

where ϕ represents $\bar{U}$, k and ε whereas p is the node on the boundary, n is the node next to the boundary and m is the node twice removed from the boundary in the y-direction.

b) <u>At the corner bisector</u>

$$\frac{\partial \bar{U}}{\partial n} = 0 = \frac{\partial k}{\partial n} = \frac{\partial \varepsilon}{\partial n}, \qquad (4.8)$$

where n is distance in the direction normal to the corner bisector.

c) <u>At the duct centreline</u> (a symmetry point)

$$\frac{\partial \bar{U}}{\partial y} = 0 = \frac{\partial \bar{U}}{\partial z},$$

$$\frac{\partial k}{\partial y} = 0 = \frac{\partial k}{\partial z}, \quad \text{and} \qquad (4.9)$$

$$\frac{\partial \varepsilon}{\partial y} = 0 = \frac{\partial \varepsilon}{\partial z}.$$

The finite-difference form via backward linear extrapolation along the mid-wall bisector (i.e. symmetry line) was used to represent equations (4.9). The substituting equation may be expressed as:

$$\phi_{C/L} = \phi_n + \frac{\frac{1}{4}\left(z_n - z_{C/L}\right)}{\left(z_m - z_n\right)} \left(\phi_n - \phi_m\right), \qquad (4.10)$$

where ϕ, stands for $\bar{U}$, k and ε and the suffix C/L denotes the centreline node whereas n indicates the node next to the centreline and m is the node twice removed from the centreline in the negative z-direction.

d) $\bar{U}$, k and ε near the solid wall:

It is assumed that the universal law of the wall holds good in secondary flow problems and can be used to represent accurately the velocity profile in the region close to the wall. Therefore, a boundary condition was imposed on the nodes next to the wall. However care was taken in designing the grid such that these first string of nodes are located beyond the viscous sublayer for the Reynolds number involved. The boundary condition is expressed as

$$\bar{U} = u^* \left[A \, \ell n \left(\frac{\rho u^* | z_n - z_p |}{\mu} \right) + B \right], \qquad (4.11)$$

where u* represents the local friction velocity and A and B are constants. The suffix p denotes the wall node whereas n and m stands, as before, for the node next to the wall and the node twice removed from the wall respectively, in the direction normal to the wall.

The local friction velocity (u*) is given by:

$$u^* = \sqrt{\tau / \rho} \, , \qquad (4.12)$$

where the local shear stress (τ) is calculated from the turbulence field data at the second string of nodes (m) in the fluid as follows:

$$\tau = \rho \, C_\mu^{1/4} \, k_m^{1/2} \, \bar{U}_m / \left[A \, \ell n \left(\frac{\rho \, C_\mu^{1/4} \, k_m^{1/2} | z_m - z_p |}{\mu} \right) \right] + B \Big]. \qquad (4.13)$$

Launder and Ying [2] used a value of 2.44 and 5.0 for A and B respectively in their analysis for the turbulent core region of a square duct having smooth surface. Since the present work also deals with square duct with smooth surface hence the above values were adopted for A and B.

By reference to the properties of the "constant-stress" wall region, the boundary conditions for the turbulent kinetic energy (k) and its dissipation rate (ε) were prescribed. They were also imposed at the first string of nodes (n), adjacent to the wall and given by the conventional form:

$$k_n = u^{*2}/C_\mu^{1/2}, \qquad (4.14)$$

and $$\varepsilon_n = u^{*3}/(\kappa \cdot z), \qquad (4.15)$$

where κ is universal Von-Karman constant and z is the distance normal to the wall.

4.3 Vorticity Source Term Modelling:

As is obvious from the axial vorticity equation (3.15), the vorticity source term consists of the difference in the gradients of Reynolds normal stresses and gradients of Reynolds shear stress. In the present work, three models have been prescribed to determine the vorticity production.

A number of investigators have shown that the shear stress terms in equation (3.15) are negligibly small compared with normal stress terms, e.g. the measurements of Brundrett and Baines [11] in a square duct, and those of Aly et al. [30] in a triangular duct. Trupp and Aly [31] found that the normal stress vorticity production predominated everywhere in the subchannels of a rod bundle.

Vorticity production, therefore, was considered to be solely due to the inbalance in the normal stresses, for model II and model III. However, to demonstrate this fact, both normal and shear terms were considered for vorticity production in model I.

4.3.1 Model I: Launder and Ying's Model

Launder and Ying [2] proposed an approximation for determination of Reynolds turbulence stresses as following:

$$(\overline{v}^2 - \overline{w}^2) = C' \frac{k}{\varepsilon} \left[\overline{uv} \frac{\partial \bar{U}}{\partial y} - \overline{wu} \frac{\partial \bar{U}}{\partial z} \right], \qquad (4.16)$$

and

$$\overline{vw} = \frac{C'}{2} \frac{k}{\varepsilon} \left[\overline{wu} \frac{\partial \bar{U}}{\partial y} + \overline{uv} \frac{\partial \bar{U}}{\partial z} \right], \qquad (4.17)$$

which relates the vorticity-generating Reynolds stresses to axial gradients of mean velocity. This formula was derived from simplifying a more elaborate, tensor-

invariant simulation of the Reynolds stresses. They claimed the model to give reasonably good predictions in ducts of more complicated cross-section such as commonly arise in nuclear fuel-rod bundles and certain other heat-exchanger types.

C', in the equations (4.16) and (4.17), is an empirical constant and denotes a group of constants i.e.

$$C' = 2\,(6C_2 - 2)/\,11(C_1 - 2\,C_2), \qquad (4.18)$$

where Launder and Ying [2] suggested C_1 and C_2 having values approximately 2.5 and 0.40 respectively.

The approximation indicates that the stress field in the lateral plane of the duct is a result of mean rates of strain in planes orthogonal to it. Their approximation for turbulent flow through straight ducts was based on the fact that "the implied cross-planar influence is solely responsible for causing the secondary motions".

Substituting equations (4.1) and (4.2) into equations (4.16) and (4.17) gives:

$$(\overline{v}^2 - \overline{w}^2) = C' \frac{1}{\rho}\frac{k}{\varepsilon} \left[\left(\frac{\partial \bar{U}}{\partial z}\right)^2 - \left(\frac{\partial \bar{U}}{\partial y}\right)^2\right], \qquad (4.19)$$

and

$$\overline{vw} = C' \frac{k}{\rho\varepsilon}\, \mu_t \left[\frac{\partial \bar{U}}{\partial y} \cdot \frac{\partial \bar{U}}{\partial z}\right]. \qquad (4.20)$$

In the present work, C' was tuned to suit the best overall agreement between predicted and experimental results. A value of 0.0035 for C' produced compatible prediction overall.

Thus equations (4.19) and (4.20) complete the closure of axial vorticity equation (3.15) and equations (4.1) and (4.2) complete the closure of the axial momentum equation (3.14) straightforwardly.

4.3.2 Model II - Turbulent Properties Correlations Model

Alshamani [5] examined carefully the axial, normal (radial) and tangential turbulence intensity measurements carried out by several investigators and observed a similarity in the distribution of these turbulence intensities. He noted that "they are all minimum at the centreline, increasing steadily as the wall is approached, until they reach some maximum value close to the wall, then they start to decrease as the wall is approached further". He also noted that the three components of turbulence intensity vary in a similar way with the Reynolds number. But as per Prandtl mixing length theory, the turbulent fluctuations are proportional to the product of a local mixing length and a velocity gradient which implied that the turbulence fluctuations are directly proportional to each other. His examination included turbulent flow in the inlet and in the fully developed regions of smooth pipes and channels and he concluded that "any two components of turbulence intensity are very nearly linearly related".

Harsha and Lee [54] were probably the first to study the relationship between Reynolds stresses and the turbulent kinetic energy. They studied a relationship between the turbulent shear stress and the turbulent kinetic energy and suggested a linear relationship between them as follows:

$$\tau_t = A\ 1/2\ (\overline{u}^{-2} + \overline{v}^{-2} + \overline{w}^{-2}), \text{ or} \qquad (4.21)$$

$$-\overline{uv}^{+} = A\ (KE^{+}),$$

where A is a constant and is given a value of 0.3. It is obvious that the equation (4.21) does not hold good at the pipe centreline where the turbulent shear stress is zero but the turbulent kinetic energy is not. Alshamani [47] further checked the validity of equation (4.21) and revealed that the linear relationship between turbulent shear stress and turbulent kinetic energy is, in general, not accurate when applied to pipe and channel flows. He also studied the relationship between the turbulent kinetic energy (KE^{+}) and the axial component of turbulence intensity (u^{+}). He used the data of Sandborn [55], Laufer (56)(57) Lawn (58), (59), Clark (60)(61) and Comte-Bellot (62) to carry out the investigation and found that for such flows, however, "the turbulent kinetic energy varies linearly with the axial component of turbulence intensity. The linearity holds for rough and smooth ducts, for the inner and outer layers and over a range of Reynolds numbers".

Based upon the correlations among turbulent shear stress, turbulent kinetic energy and axial turbulence intensity as presented by Alshamani (47), it was possible to develop an expression for Reynolds normal stress in terms of turbulent kinetic energy as follows:

$$\overline{v^{+2}} - \overline{w^{+2}} = (0.2708 - 0.1245\, k^{+} - 0.0286\, k^{+2}) \qquad (4.22)$$

The derivation of equation (4.22) is given in Appendix C. However, finally, a constant (C'') was introduced in equation (4.22) to make the predictions more agreeable with the experimental data. With the newly introduced constant, the equation (4.22) is rewritten as:

$$\overline{v^{+2}} - \overline{w^{+2}} = C''(0.2708 - 0.1245\, k^{+} - 0.0286\, k^{+2}) \qquad (4.23)$$

This equation provides a closure to the axial vorticity equation (3.15). It must be remembered that the Reynolds shear stress term in the vorticity source term i.e. the last term of axial vorticity equation (3.15) is considered negligible as compared to the Reynolds normal stresses and hence has been ignored. The gradient (i.e. second derivative) of the difference in coplanar Reynolds normal stresses have been derived in Appendix C and have been used directly for the calculation of vorticity source term in the axial vorticity equation (3.15).

4.3.3 Model III - Seale's Model

Seale [3] presented a method for calculating the source of axial vorticity without the need for the precise calculation of the normal stresses. As stated earlier, the Reynolds shear stress was neglected altogether for this model.

Based upon Alshamani's [5][47] investigations, he developed an expression for the difference in the normal stresses in terms of the turbulence kinetic energy (basically, the same exercise which was followed for model II). For a square duct, it can be given as:

$$\overline{v}^{+2} - \overline{w}^{+2} = (0.2708 - 0.1245\ k^{+} - 0.0286\ k^{+2}) \qquad (4.24)$$

which was substituted in the expression for source of axial vorticity i.e.

$$\rho \frac{\partial^2}{\partial y\ \partial z} (\overline{v}^{+2} - \overline{w}^{+2}) = S\omega = \rho\ u^{*2} \frac{\partial^2}{\partial y\ \partial z}$$

$$(0.2708 - 0.1245\ k^{+} - 0.0286\ k^{+2}), \qquad (4.25)$$

or,

$$S\omega = 0.0286\ \rho\ u^{*2} \frac{\partial^2}{\partial y\ \partial z} (k^{+2} + 4.0\ k^{+}), \qquad (4.26)$$

by recognizing that the numerical values of the coefficients are not precise and taking advantage of the fact that the coefficient of k^{+} is about 4.0 times larger than that of k^{+2}.

He went on to propose an alternative technique, in which a synthetic distribution of turbulent kinetic

energy is specified and combined with equation (4.26) to produce a simple algebraic term for the source of vorticity.

He carefully examined the measurements of Laufer [63] in a circular pipe and of Aly et al [30] along the mid-wall plane of the triangular duct and found that k^+ varies parabolically with normalized distance from about one in the core to an extrapolated figure of about four at the wall. His study for ducts of non-circular cross-section revealed a similar parabolic relationship describing the variation of k^+ with $y/\hat{y}$ but the two-dimensional effects modify the value of k^+ in the 'core' region. He presented an expression to describe the distribution of turbulent kinetic energy, normalized by the mean shear velocity, in ducts with a well defined surface of no shear,

$$k^+ = k_{i,+}^+ (k_{w,+} - k_{i,+})(1 - y/\hat{y}_{max})^2 \qquad (4.27)$$

The surface of no-shear is assumed to be coincident with the position of the maximum axial velocity on the normal from the wall.

The substitution of equation (4.27) into equation (4.26) yields the following algebraic equation for the source of axial vorticity:

$$S\omega = 8\, C'''\rho\, u^{*2}\, k_{c,+}/(\hat{y}_{max}) \quad m\, Y_P\, Y_L\, Y_N \frac{\partial y}{\partial z} . \qquad (4.28)$$

where C''' = 0.0286 [comes from equation (4.26)]. A detailed derivation of equation (4.28) is presented in Appendix D.

The constant m was determined by matching the computed and measured secondary velocities and was given a value of 2.4. Subsequently C''' was turned to suit best overall agreement between predicted and measured results. A value of 0.0110 for C''' yielded best results and hence was adopted.

4.4 Summary of Equations to be Solved:

4.4.1 Transport Equations

a) Axial Momentum Equations:

$$\frac{\partial}{\partial y}\left(\bar{U}\frac{\partial \Psi}{\partial z}\right) - \frac{\partial}{\partial z}\left(\bar{U}\frac{\partial \Psi}{\partial y}\right) - \left\{\left[\frac{\partial}{\partial y}(\mu + \mu_t)\frac{\partial \bar{U}}{\partial y}\right] + \left[\frac{\partial}{\partial z}(\mu + \mu_t)\frac{\partial \bar{U}}{\partial z}\right\} + \frac{\partial P}{\partial x} = 0 \qquad (4.29)$$

b) Axial Vorticity Equation:

$$\frac{\partial}{\partial y}\left(\omega\frac{\partial \Psi}{\partial z}\right) - \frac{\partial}{\partial z}\left(\omega\frac{\partial \Psi}{\partial y}\right) - \frac{\partial}{\partial y}\left[\frac{\partial}{\partial y}(\mu\omega)\right] - \frac{\partial}{\partial z}\left[\frac{\partial}{\partial z}(\mu\omega)\right] - \rho\frac{\partial^2(\bar{v}^2 - \bar{w}^2)}{\partial y\,\partial z} + \rho\left(\frac{\partial^2 \overline{vw}}{\partial y^2} - \frac{\partial^2 \overline{vw}}{\partial z^2}\right) = 0. \qquad (4.30)$$

It should be recalled that the last term of equation (4.30) (i.e. gradients of Reynolds shear stress) has been neglected in Model II as well as Model III and axial vorticity takes the form as follows:

$$\frac{\partial}{\partial y}\left(\omega \frac{\partial \Psi}{\partial z}\right) - \frac{\partial}{\partial z}\left(\omega \frac{\partial \Psi}{\partial y}\right) - \frac{\partial}{\partial y}\left[\frac{\partial}{\partial y}(\mu\omega)\right] - \frac{\partial}{\partial z}\left[\frac{\partial}{\partial z}(\mu\omega)\right]$$

$$- \rho \frac{\partial^2(\bar{v}^2 - \bar{w}^2)}{\partial y\, \partial z} = 0. \qquad (4.31)$$

c) Stream Function Equation:

$$-\left[\frac{\partial}{\partial y}\frac{\partial \Psi}{\partial y} + \frac{\partial}{\partial z}\frac{\partial \Psi}{\partial z}\right] - \rho\omega = 0. \qquad (4.32)$$

d) Turbulent kinetic energy equation:

$$\left[\frac{\partial}{\partial y}\left(k \frac{\partial \Psi}{\partial z}\right) - \frac{\partial}{\partial z}\left(k \frac{\partial \Psi}{\partial y}\right)\right] - \frac{\partial}{\partial y}\left[\left(\mu + \frac{\mu_t}{\sigma_k}\right)\frac{\partial k}{\partial y}\right]$$

$$- \frac{\partial}{\partial z}\left[\left(\mu + \frac{\mu_t}{\sigma_k}\right)\frac{\partial k}{\partial z}\right] - \mu_t\left[\left(\frac{\partial \bar{U}}{\partial y}\right)^2 + \left(\frac{\partial \bar{U}}{\partial z}\right)^2\right] + \rho\varepsilon = 0. \qquad (4.33)$$

e) Turbulence Energy Dissipation Rate Equation:

$$\left[\frac{\partial}{\partial y}\left(\varepsilon \frac{\partial \Psi}{\partial z}\right) - \frac{\partial}{\partial z}\left(\varepsilon \frac{\partial \Psi}{\partial y}\right)\right] - \frac{\partial}{\partial y}\left[\left(\mu + \frac{\mu_t}{\sigma_\varepsilon}\right)\frac{\partial \varepsilon}{\partial y}\right] - \frac{\partial}{\partial z}$$

$$\left[\left(\mu + \frac{\mu_t}{\sigma_\varepsilon}\right)\frac{\partial \varepsilon}{\partial z} - C_1 \frac{\mu_t \varepsilon}{k}\left[\left(\frac{\partial \bar{U}}{\partial y}\right)^2 + \left(\frac{\partial \bar{U}}{\partial z}\right)^2\right] + C_2 \rho \frac{\varepsilon^2}{k} = 0. \qquad (4.34)\right.$$

4.4.2 Algebraic Equations

a) Turbulent (Eddy) Viscosity

$$\mu_t = C_\mu \rho\, k^2/\varepsilon \,. \qquad (4.35)$$

b) Reynold Stresses:

b.1) Model I:

b.1.1) Normal Stress:

$$(\bar{v}^2 - \bar{w}^2) = C' \frac{1}{\rho} \mu_t \frac{k}{\varepsilon}\left[\left(\frac{\partial \bar{U}}{\partial z}\right)^2 - \left(\frac{\partial \bar{U}}{\partial y}\right)^2\right]. \qquad (4.36)$$

b.1.2) Shear Stress

$$\overline{vw} = -C' \frac{1}{\rho} \frac{k}{\varepsilon} \mu_t \frac{\partial \bar{U}}{\partial y} \frac{\partial \bar{U}}{\partial z} \,. \qquad (4.37)$$

b.2) Model II:

b.2.1) Normal Stress:

$$(\bar{v}^2 - \bar{w}^2) = u^{*2}.$$

$$C'' (0.2708 - 0.1245\ k^{+} - 0.0286\ k^{+2}) \quad (4.38)$$

b.3) Model III:

b.3.1) Normal Stress:

$$(\bar{v}^2 - \bar{w}^2) = 8\ C'''\ \rho u^{*2}\ k_{c,+}/(\hat{y}_{max})^2$$

$$m\ Y_P\ Y_L\ Y_N \frac{\partial y}{\partial Z}\ . \quad (4.39)$$

c) Source Term for Axial Momentum Equation:

$$\frac{\partial P}{\partial x} = -\ 4\ \tau_w / D_h \quad (4.40)$$

d) Friction Factor

$$f = 8\ \tau_w / (\rho U_b^2). \quad (4.41)$$

e) Average Wall Shear Stress:

$$\tau_w = \frac{1}{L} \int_o^L \tau\ dy \quad (4.42)$$

4.4.3 Boundary Conditions

a) Mid-wall bisector:

$$\Psi = \omega = 0, \quad (4.43)$$

$$\frac{\partial \bar{U}}{\partial y} = \frac{\partial k}{\partial y} = \frac{\partial \varepsilon}{\partial y} = 0. \quad (4.44)$$

b) Corner bisector:

$$\Psi = \omega = 0, \quad (4.45)$$

$$\frac{\partial \bar{U}}{\partial n} = \frac{\partial k}{\partial n} = \frac{\partial \varepsilon}{\partial n} = 0\ . \quad (4.46)$$

c) Duct centreline:

$$\Psi = \omega = 0 \tag{4.47}$$

$$\bar{V} = \bar{W} = 0, \tag{4.48}$$

$$\frac{\partial \bar{U}}{\partial y} = \frac{\partial \bar{U}}{\partial z} = 0, \tag{4.49}$$

$$\frac{\partial k}{\partial y} = \frac{\partial k}{\partial z} = 0, \tag{4.50}$$

$$\frac{\partial \varepsilon}{\partial y} = \frac{\partial \varepsilon}{\partial z} = 0. \tag{4.51}$$

d) Wall boundary conditions:

$$\Psi = 0 \tag{4.52}$$

$$\Psi_p = \omega_n + \frac{(z_p - z_n)}{(z_n - z_m)} (\omega_n - \omega_m), \tag{4.53}$$

where p is the node at the wall, n is the node at the first string adjacaent to the wall and m is the node twice removed from the wall in the direction normal to the wall i.e. z-direction.

Further,

$$\bar{U}_n = u^*\left[A \ln \left(\frac{\rho u^* |Z_m - Z_p|}{\mu}\right) + B\right] \tag{4.54}$$

$$k_n = u^{*2}/C_\mu^{1/2}, \tag{4.55}$$

$$\varepsilon_n = u^{*3}/\kappa \cdot z, \tag{4.56}$$

where,

$$u^* = \{C\mu^{1/4} k_m^{1/2} \bar{U}_m / [A \ln \left(\frac{\rho C\mu^{1/4} k_m^{1/2} |Z_m - Z_p|}{\mu}\right) + B]\}^{1/2}. \tag{4.57}$$

4.5 Various Constants of the Models

A summary of models constants has been presented in Table 1. The values of the constants employed in present work have been compared with those adopted by other workers in Table 2.

5.0 THE NUMERICAL PROCEDURE

5.1 Introduction

Equations 4.29 to 4.34 can be generalized by one standard elliptic partial differential equation as follows:

$$a_\phi \left[\frac{\partial}{\partial y}\left(\phi \frac{\partial \Psi}{\partial z}\right) - \frac{\partial}{\partial z}\left(\phi \frac{\partial \Psi}{\partial y}\right)\right] - \left[\frac{\partial}{\partial y}\left(b_{\phi,y} \frac{\partial \phi}{\partial y}\right) + \frac{\partial}{\partial z}\left(b_{\phi,z} \frac{\partial \phi}{\partial z}\right)\right] + S_\phi = 0. \quad (5.1)$$

The representative new symbols in this equation are identified for each equation from(4.29) to (4.34) in Table 3. The finite-difference technique was employed in solving these equations numerically. There are two possible ways to approximate differential equations by finite difference equations. One is by Taylor-series expansions whereas the other is by integration over finite areas in the primary flow cell along with appropriate assumptions about the distributions of the variables between the nodes of the grid. For all three models, an upwind finite difference technique of Gosman et al [4] together with Gauss-Seidel iteration was employed with a Cartesian grid over the primary flow cell. The grid is presented in Fig. 2.

5.2 The Finite Difference Equations

A part of the finite difference grid has been

displayed in Fig. 3, which shows a typical node P with four other surrounding nodes viz., E, W, N and S.

The integration of the differential equations is performed over the hatched area (Fig. 3). The sides of this small square/rectangular area (depending upon the square/rectangular grid) lie midway between the neighbouring grid lines.

The double integration over the domain shown in Fig. 3 yields:

$$a_\phi \int_{z,s}^{n} \int_{y,w}^{e} \left[\frac{\partial}{\partial y}\left(\phi \frac{\partial \Psi}{\partial z}\right) - \frac{\partial}{\partial z}\left(\phi \frac{\partial \Psi}{\partial y}\right)\right] dy\, dz$$

Convection terms = I_c

$$- \int_{z,s}^{n} \int_{y,w}^{e} \left[\frac{\partial}{\partial y}\left(b_{\phi,y} \frac{\partial \phi}{\partial y}\right) + \frac{\partial}{\partial z}\left(b_{\phi,z} \frac{\partial \phi}{\partial z}\right)\right] dy\, dz$$

Diffusion terms = I_d

$$= - \int_{z,s}^{n} \int_{y,w}^{e} S_\phi \, dy\, dz. \quad (5.2)$$

Source term = I_s

Equation (5.2) can also be written in symbolic form as:

$$I_c - I_d + I_s = 0. \quad (5.3)$$

The integrals for each term appearing in equation (5.2) are evaluated individually in the following subsections.

5.2.1 Convection Terms

The following assumptions were made before integrating the convection terms:

a) The function ϕ is uniform within each square/rectangle and has the value of node P.

b) The value of the stream function at a particular corner of the square/rectangle is equal to the average of the values on the four neighbouring nodes.

c) The average value of the function ϕ takes the value possessed by the fluid upstream of the specific face under consideration, i.e. the so-called "upwind technique".

The integration of the convection terms of equation (5.2) yields:

$$I_c = a_\phi \{ \int_{z,s}^{n} [\phi_e \, (\frac{\partial \Psi}{\partial z})_e - \phi_w \, (\frac{\partial \Psi}{\partial z})_w] \, dz - \int_{y,w}^{e} [\phi_n \, (\frac{\partial \Psi}{\partial y})_n - \phi_s \, (\frac{\partial \Psi}{\partial y})_s] \, dy \}, \quad (5.4)$$

which can be further expressed as:

$$I_c = I_{c1} + I_{c2} + I_{c3} + I_{c4}, \quad (5.5)$$

where,

$$I_{c1} = a_\phi \int_{z,s}^{n} \phi_e \, (\frac{\partial \Psi}{\partial z})_e \, dz, \quad (5.6)$$

and so on.

If ϕ and Ψ are assumed to be well-behaved

function, then there exists an average value of ϕ_e which is $\bar{\phi}_e$ such that:

$$\bar{\phi}_e = \frac{\int_{z,s}^{n} \phi_e \left(\frac{\partial \Psi}{\partial z}\right)_e dz}{\int_{z,s}^{n} \left(\frac{\partial \Psi}{\partial z}\right)_e dz} \quad \frac{I_{c1}}{a_\phi \, (\Psi_{ne} - \Psi_{se})}, \quad (5.7),$$

where the subscripts express the values of variables at the corresponding corners of the integration domain shown in Fig. 3. Therefore, I_{c1} can be given as:

$$I_{c1} = a_\phi \, \bar{\phi}_e \, (\Psi_{ne} - \Psi_{se}). \quad (5.8)$$

Applying upwind difference techinque [4], I_{c1} can be rewritten as:

$$I_{c1} = a_\phi \{\phi_P \left[\frac{(\Psi_{ne} - \Psi_{se}) - |\Psi_{ne} - \Psi_{se}|}{2}\right] +$$

$$\phi_E \left[\frac{(\Psi_{ne} - \Psi_{se}) - |\Psi_{ne} - \Psi_{se}|}{2}\right] \}, \quad (5.9)$$

whereas assumption b) can be mathematically expressed as:

$$\Psi_{ne} = \tfrac{1}{4} \, [\Psi_{NE} + \Psi_N + \Psi_P + \Psi_E], \quad (5.10)$$

and,

$$\Psi_{se} = \tfrac{1}{4} \, [\Psi_{SE} + \Psi_E + \Psi_P + \Psi_S]. \quad (5.11)$$

The other terms of equation (5.5), i.e. I_{c2}, I_{c3} and I_{c4} can be obtained by a similar treatment for each of them. Assembling and rearrangment of various terms produces the following expression:

$$I_c = A_E (\phi_P - \phi_E) + A_W (\phi_P - \phi_W) + A_N (\phi_P - \phi_N) + A_S (\phi_P - \phi_S), \quad (5.12)$$

where the coefficients A are:

$$A_E = \frac{a\phi}{8} \{[\Psi_{SE} + \Psi_S - \Psi_{NE} - \Psi_N] + |\Psi_{SE} + \Psi_S - \Psi_{NE} - \Psi_N|\} ,$$

$$A_W = \frac{a\phi}{8} \{[\Psi_{NW} + \Psi_N - \Psi_{SW} - \Psi_S] + |\Psi_{NW} + \Psi_N - \Psi_{SW} - \Psi_S|\} ,$$

$$A_N = \frac{a\phi}{8} \{[\Psi_{NE} + \Psi_E - \Psi_{NW} - \Psi_W] + |\Psi_{NE} + \Psi_E - \Psi_{NW} - \Psi_W|\} ,$$

and,

$$A_S = \frac{a\phi}{8} \{[\Psi_{SW} + \Psi_W - \Psi_{SE} - \Psi_E] + |\Psi_{SW} + \Psi_W - \Psi_{SE} - \Psi_E|\} . \quad (5.13)$$

It is obvious that coefficients A's can never become negative, however, they may assume a value of zero. This is one of the features which enables a stable solution procedure. The above equations (5.13) are not suitable for nodes near the corner bisector and special provision is made in the computer program to deal with them.

5.2.2 Diffusion Terms

The integration of diffusion terms of equation

(5.2) yields:

$$I_d = \int_{z,s}^{e} [(b_{\phi,y})_e \left(\frac{\partial \phi}{\partial y}\right)_e - (b_{\phi,y})_w \left(\frac{\partial \phi}{\partial y}\right)_w] \, dz$$

$$+ \int_{y,w}^{e} [(b_{\phi,z})_n - \left(\frac{\partial \phi}{\partial z}\right)_n - (b_{\phi,z})_s \left(\frac{\partial \phi}{\partial z}\right)_s] \, dy, \quad (5.14)$$

which can be symbolically represented as:

$$I_d = I_{d1} + I_{d2} + I_{d3} + I_{d4}, \quad (5.15)$$

where,

$$I_{d1} = \int_{z,s}^{n} [(b_{\phi,y})_e \left(\frac{\partial \phi}{\partial y}\right)_e] \, dz, \quad (5.16)$$

and so on.

If the quantities $b_{\phi,y}$ and ϕ vary linearly then following assumptions can be made in the domain under consideration;

$$(b_{\phi,y})_e \cong \tfrac{1}{2} [(b_{\phi,y})_E + (b_{\phi,y})_P] \ ,$$

$$\left(\frac{\partial \phi}{\partial y}\right)_e \cong (\phi_E - \phi_P)/(y_E - y_P) \ ,$$

and,

$$z_n - z_s = \tfrac{1}{2} (z_N - z_S). \quad (5.17)$$

With these assumptions, equation (5.16) can be integrated to give:

$$I_{d1} = \tfrac{1}{2} [(b_{\phi,y})_E + (b_{\phi,y})_P] \frac{1}{y_E - y_P} (\phi_E - \phi_P)$$

$$(z_n - z_s). \quad (5.18)$$

The integration of other terms of equation (5.15)

can be evaluated in a similar way. Assembling and rearranging gives:

$$I_d = B_E\,(\phi_E - \phi_P) + B_W\,(\phi_W - \phi_P) + B_N\,(\phi_N - \phi_P) + B_S\,(\phi_S - \phi_P), \quad (5.19)$$

where,

$$B_E = \tfrac{1}{4}\,[(b_{\phi,y})_E + (b_{\phi,y})_P] \cdot \frac{1}{y_E - y_P} \cdot (z_n - z_s),$$

$$B_W = \tfrac{1}{4}\,[(b_{\phi,y})_W + (b_{\phi,y})_P] \cdot \frac{1}{y_P - y_W} \cdot (z_n - z_s),$$

$$B_N = \tfrac{1}{4}\,[(b_{\phi,z})_N + (b_{\phi,z})_P] \cdot \frac{1}{z_N - z_P} \cdot (y_E - y_W),$$

and,

$$B_s = \tfrac{1}{4}\,[(b_{\phi,z})_S + (b_{\phi,z})_P] \cdot \frac{1}{z_P - z_S} \cdot (y_E - y_W). \quad (5.20)$$

It is noticeable that like A's, B's will never be negative, thus endowing a stable solution procedure.

5.2.3 Source Term

The source term of equation (5.2) can be integrated to give:

$$I_s = \int_{z,s}^{n} \int_{y,w}^{e} S_\phi \, dy \, dz \quad (5.21)$$

To evaluate source terms for the different transport equations, S_ϕ is considered to be constant within the domain of integration and assumed to have the value at the particular node under consideration i.e. P. The validity of this assumption depends mainly on grid

size, the finer the better.

Therefore, the integration of equation (5.21) finally yields:

$$I_s = S_{\phi,P} (y_e - y_w) (z_n - z_s) . \quad (5.22)$$

Since y and z are the space-average value as given in assumption [equation (5.17)], equation (5.22) takes the form:

$$I_s = S_{\phi,P} \cdot V_P , \quad (5.23)$$

where,

$$V_P = \tfrac{1}{4} (y_E - y_W) \cdot (z_N - z_S) . \quad (5.24)$$

The values of the functions $b_{\phi,y}$, $b_{\phi,z}$, and $S_{\phi P}$ are presented in Table 3.

5.2.4 The Complete Finite-Difference Equation

Assembling and rearranging convection, diffusion and source terms gives:

$$A_E (\phi_P - \phi_E) + AW (\phi_P - \phi_W) + A_N (\phi_P - \phi_N) + AS$$

$$(\phi_P - \phi_S) - [B_E (\phi_E - \phi_P) + B_W (\phi_W - \phi P) + B_N$$

$$(\phi_N - \phi_P) + B_S (\phi_S - \phi_P)] + S_{\phi,P} \cdot V_P = 0, \quad (5.25)$$

which ultimately yields successive-substitution formula which may be written in the form:

$$\phi_P = C_E \phi_E + C_W \phi_W + C_N \phi_N + C_S \phi_S + Q, \quad (5.26)$$

where,

$$C_E = (A_E + B_E)/\Sigma AB,$$

$$C_W = (A_W + B_W)/\Sigma AB,$$

$$C_N = (A_N + B_N)/\Sigma AB,$$

$$C_S = (A_S + B_S)/\Sigma AB,$$

$$Q = - S_{\phi,p}\ V_p/\Sigma AB,$$

and,

$$\Sigma AB = A_E + A_W + A_N + A_S + B_E + B_W + B_N + B_S. \quad (5.27)$$

The A's and B's are identified by equations (5.13) and (5.20).

5.2.5 Boundary Conditions

a) Solid Wall

The various conditions were presented in section 4.2.(iii)(d).

b) Midwall Bisector

The conditions for this boundary are given in section 4.2.(iii)(a). For $\bar{U}$, k and ε, gradients along the normal-to-the midwall bisector were set to zero. This was achieved by expanding the parameters in Taylor series as illustrated in the above section. If the mesh is 'really fine' this condition can be met by simply assigning the values at nodes on the midwall bisector to take the values of adjacent nodes on the

normal-to-the boundary direction.

c) Corner Bisector

The conditions for this boundary are given in section 4.2.(iii)(b). $\bar{U}$, k and ε gradients along the normal to the corner bisector were set to zero. The following figure illustrates the procedure employed:

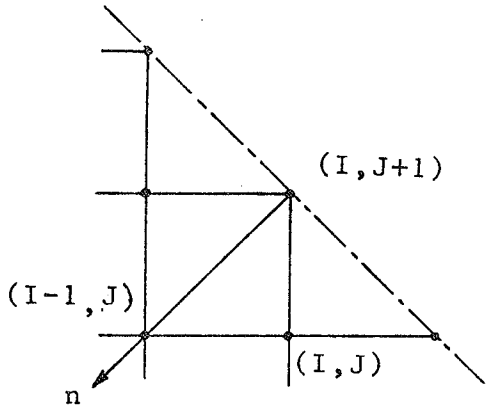

To have a zero gradient in the n-direction, the following condition was applied:

$$U_{i,j+1} = U_{i-1,j}. \qquad (5.27)$$

The same treatment was applied for both k and .

However, it should be noted that interpolation is necessary in the case when the grid is not square (rather rectangular) which does not permit the existence of nodes on the direction normal to the corner bisector. A procedure to handle such a situation has been described in the work of Aly [64].

5.3 Stability Analysis of the Successive Substitution Formula

In order to ensure the convergence of an iterative solution to equations of the form (5.26), certain stability conditions must be satisfied. These conditions have been stipulated in Said's [49] work (Section 6.3, pp. 69-72) and is referred to interested readers. For the sake of completeness, however, the modified k and ε source term for stability is given respectively as follows:

$$k_P = \frac{C_E k_E + C_W k_W + C_N k_N + C_S k_S + \mu_{t,P} \frac{V_P}{\Sigma AB} \left[\left(\frac{\partial \bar{U}}{\partial y}\right)^2 \right. \cdots}{\frac{1}{\Sigma AB} \left[\Sigma AB + \frac{\rho \varepsilon_P V_P}{k_P}\right]}$$

$$\cdots \frac{\left. + \left(\frac{\partial \bar{U}}{\partial z}\right)^2 \right]}{\frac{1}{\Sigma AB} \left[\Sigma AB + \frac{\rho \varepsilon_P V_P}{k_P}\right]} \quad , \quad (5.28)$$

and,

$$\varepsilon_P = \frac{C_E \varepsilon_E + C_W \varepsilon_W + C_N \varepsilon_N + C_S \varepsilon_S + C_1 \mu_{t,P} \left[\left(\frac{\partial \bar{U}}{\partial y}\right)^2 \right. \cdots}{\frac{1}{\Sigma AB} \left[\Sigma AB + C_2 \rho \left(\frac{\varepsilon_P}{k_P}\right) V_P\right]}$$

$$\cdots \frac{\left. + \left(\frac{\partial \bar{U}}{\partial z}\right)^2 \right] \left[\frac{V_P}{\Sigma AB} \frac{\varepsilon_P}{k_P}\right]}{\frac{1}{\Sigma AB} \left[\Sigma AB + C_2 \rho \left(\frac{\varepsilon_P}{k_P}\right) V_P\right]} \quad . \quad (5.29)$$

Equation (5.28) was obtained using Table 3 with equation (5.26), after rearrangement. A similar approach

was used for equation (5.29) as well.

5.4 Iterative Technique

The 'Gauss-Seidel' iterative technique was employed in the solution procedure. A provision for under-relaxation was included in the computer program for ω, k and ε, in the following form:

$$\phi_{i,j}^{T} = \phi_{i,j}^{T-1} + \alpha_R \, (\phi_{i,j}^{T} - \phi_{i,j}^{T-1}), \quad (5.30)$$

where ϕ stands for ω, k and ε; $\phi_{i,j}^{T}$ is the value at iteration number T; $\phi_{i,j}^{T-1}$ is the value at the same node in the previous iteration (T-1) and α_R is the under-relaxation factor. Despite the provision, none of the variables needed under-relaxation for a converged solution in all three models.

5.5 Convergence Criterion

The computation time is proportional to the number of iterations which must be executed before the change effected by an iteration cycle is acceptably small. What is acceptable is, of course, tied up with the question of the accuracy desired. However, over stringent demands may result in excessive computing times, with little gain in accuracy.

The criterion employed in this work, dictates that the maximum fractional change of ϕ in the field from one cycle of iteration to the next must not exceed a

prescribed value, i.e.:

$$\left| \frac{(\phi_{i,j}^{T} - \phi_{i,j}^{T-1})}{\phi_{i,j}^{T}} \right|_{max} \leq \xi, \quad (5.31)$$

where ξ was taken as 0.001 for all the parameters i.e. ω, Ψ, k, ε and $\bar{U}$. In general, the mean axial velocity field undergoes most rapid convergence whereas ω controlled the complete convergence and hence the actual exit criteria for Ψ, k, ε and $\bar{U}$ were beyond the specified value of 0.001.

5.6 Initial Conditions

The ω and Ψ were initially assumed to be zero everywhere. At the first string of nodes adjacent to the wall, the initial values for $\bar{U}$, k and ε were determined by using wall functions [equations (4.54) to (4.56)] with an initial arbitrary value given to u*. For the rest of the field, $\bar{U}$ was given the value U_b, k was given the value at the boundary while ε was given half of the boundary value. Even with these unrealistic initial conditions, the fields converged well.

5.7 The Employed Grid Spacing

A grid constituting of regular 21 x 21 mesh (Fig. 2), for a quadrant of the square duct, was used in the analysis for all three models. This mesh was purposely held fixed for all three models in order to facilitate

the comparative study of their respective performances. Regarding mesh size, much coarser grids have been satisfactorily employed by others; e.g., 11 x 11 by Launder and Ying [2] and 15 x 15 by Gerard [65]. At any rate, for turbulent flows, any inadequacy in grid size can, to some extent, be compensated for by adjusting vorticity source model constants (mostly C', C", and C"'). Furthermore, it is generally considered (see e.g., [66]) that even with a coarse grid (which is all one can afford in most practical problems), the upwind-difference scheme (as employed in this work) usually gives reasonable results.

In view of these considerations, the 21 x 21 grid in the present work, for a quadrant of the square duct, is considered adequate in regard to accuracy of the numerical solution.

6.0 NUMERICAL RESULTS AND DISCUSSIONS

6.1 General

As mentioned earlier, three computation schemes pertaining to three different vorticity source term models were used to obtain converged solutions. Model I used both normal and shear stresses, whereas Model II and Model III used only normal stresses in the calculations. Since the contribution to vorticity source by shear stress is considered negligible as compared to the normal stresses, the predicted results of Model I can be compared with those of Model II and Model III without significant bias. Finally, the results of all three models are compared to the available experimental data to evaluate their performance. For this purpose, the experimental results of Hoagland [9], Leutheusser [10], Brundrett and Baines [11], Gessner and Jones [13], Launder and Ying [14] and Kokorev et al [15] were used. The Reynolds number range was confined to the practical range of 60,000 to 300,000 and converged solutions were obtained for all three models without under-relaxing any variable. A few results are also presented without secondary flow and are compared with the results with secondary flow in order to illustrate the effects of the secondary flow.

A flow-chart and a complete listing of the

employed computer program for numerical predictions, have been presented in Appendix E. All calculations were performed on the AMDAHL 470/V7 computer whereas plots were taken with a Hewlett-Packard computer-plotter (HP 7220C) which was connected to the AMDAHL. Most of the computer-plots have been presented as produced on the plotter, however, in some cases, the curves were smoothed in certain places to improve continuity. The plots of experimental results were overlaid on computer-plots manually except for a few instances, where sufficient experimental data were available to plot them using the HP-plotter.

The predicted results are presented and discussed in the following subsections.

6.2 Secondary Velocity Profiles

Figures 4 and 5 compare the predicted contour plots of normalized secondary velocity components i.e. $\bar{V}$ and $\bar{W}$ respectively for all three models at Re = 75,000. Models I, II and III are very close to each other. This similarity was also found at other Reynolds numbers. Accordingly, Model II was arbitrarily chosen to represent the predicted resultant secondary velocity and these results are compared to the available experimental data in Figs. 6 to 8 inclusive.

Hoagland [9] has reported resultant secondary

velocity contours at Re = 75,000, in the plane of the channel, which can be compared in Fig. 6 to the predictions of Model II. The present results are in reasonable agreement with the experimental data except for the position close to the wall. In addition, the V_{sec} predictions appear somewhat overestimated in the core region and underestimated close to the wall. Hoagland [9] admitted that the probe interference might have impaired the accuracy of the experimental data near the wall. Also, the continuity relation requires that the flow rate towards the wall should equal that away from it. The predicted profiles do, of course, obey this continuity constraint and hence are supposed to be more correct.

Figure 7 illustrates the secondary velocity profiles at Re = 215,000 for Model II, at different lateral cross-sectional planes. The predicted results agree reasonably with the measurements of Launder and Ying [14] considering the difficulties of secondary flow measurements. It is noted, for example, that whereas the predicted results for y/L = 0.5 are symmetrical about z/L = 0.5 (as should be the case), the data of [14] exhibits considerable asymmetry.

In Fig. 8, the secondary velocity profile of Kokorev et al [15], who measured secondary velocity at Re

= 100,000 by using inclined taps, has been compared with the predictions of Model II at a section y/L = 0.4. As can be seen, the predictions agree fairly well.

For all three models, secondary velocities normalized with either the average bulk velocities or duct centre line velocities, were found to decrease with increase in Reynolds number in the range considered (over 60,000). Launder and Ying [14] found that the secondary velocity in a fully developed flow through a square-sectioned duct is sensibly independent of Reynolds number whether the duct is rough or smooth, provided that the velocity is normalized with the average friction velocity. In Figs. 9 to 12, the secondary velocity profiles for Reynolds number 215,000 and 83,000 have been presented for Model I and III respectively. The main purpose behind the presentations of secondary velocity profiles for Re = 83,000 (ref. Figs. 10 and 12) was to compare the profiles with the ones predicted at Re = 215,000. They are almost identical as expected since the secondary velocity ($\bar{V}$) has been normalized with average friction velocity ($\bar{u}^*$) and thus is independent of Reynolds number. This observation is in accordance, therefore, with Launder and Ying [14].

Finally, in Fig. 13, the predictions of Models I, II and II at y/L = 0.5 and 0.8, have been combined to

illustrate that the three models give very close predictions. It can also be observed that the predictions of Model II are generally closest to the experimental measurements.

On the basis of Figs. 6-13, it is concluded that the predicted secondary velocities are in reasonable agreement with the available experimental data.

6.3 Mean Axial Velocity Distributions

Contour plots of mean axial velocity are presented in Fig. 14 for all three models at Re = 83,000. The predicted results are very similar and can be compared with Leutheusser's [10] experimental data which is included in Fig. 14. As can be seen, the predictions are in fair agreement with the measurements near the wall, displaying faithfully the distortion of the contours towards the corner as a result of movement of high momentum fluid from near the center outwards along the corner bisector. Near the corner, distortions in the predicted contours are somewhat over-estimated, hence velocities are under-estimated. On the other hand, velocities are over-estimated near the center of the duct. These discrepancies indicate the under-estimation of the secondary flow magnitude along the diagonal of the square (directed toward the corner) and also its over-estimation along the wall bisector (directed toward

the core).

In Figs. 15 to 17, the variations of axial velocity along several fixed vertical sections in the flow have been presented and are seen to be in reasonable agreement with the measurements of Launder and Ying [14]. These figures illustrate the accustomed bulges in axial velocity caused by the secondary motions. Due to these bulges, in Figs. 15 to 17, the magnitude of axial velocity is lower for the $y/L = 0.0$ section than for the $y/L = 0.4$ section for distances for z/L approximately less than 0.5.

Figure 18 illustrates the effect of Reynolds number on isovels. For the larger Reynolds number, the axial velocity is at a lower level near the core region and at a higher level near the wall region. It is obvious that axial velocity scaled by bulk velocity (or, for that matter, centre line velocity) is not completely independent of Reynolds number. A large difference between two employed Reynolds number is chosen to demonstrate the effect prominently.

Isovels are shown also in Fig. 19 for computed results without secondary flow, for Re = 83,000. For zero secondary flow, Ψ and ω were simply set to zero and only the equations for axial velocity, turbulent kinetic energy and its dissipation rate were solved. For this

case, as expected, the bulges in the contours are absent. For the sake of comparison, the predicted contour plots of Model II and experimental measurements (with secondary flow) have been included in the same figure. It is noticeable that if secondary flow is neglected, the predictions fall into serious discrepancy, generally under-estimating the velocity along the corner bisector (especially near the corner) and significantly over-estimating along the midwall bisector.

6.4 Vorticity and Stream Function Distributions

The stream function contours for Models I, II and III, for Re = 70,000, are shown in Fig. 20. The predicted results are very close to each other and are compared with Hoagland's [9] measurements. The contours of all three models are qualitatively similar to those obtained experimentally but they are high in levels near the centre and less penetrating near the corner. This is due to the reasons already described in section 6.3 regarding discrepancies in the isovels patterns. As far as the stream function distribution is concerned, Model II is close to the experimental data [9] than the other two models whereas Model I and Model III are very close (see Fig. 20) to each other.

One conflicting observation exists. Model I includes shear stress in its source term and, this

(supposedly) has some direct effect on secondary flow magnitudes in the corner region. In fact, of the three models, Model I is supposed to be the most penetrating in the corner region. However, this is not the case. Brundrett and Baines' [11] measurements strongly suggested that in the case of square ducts, the normal stress term predominates over the shear stress term throughout the cross-section. Not only for square, but the validity of their suggestion was claimed for all ducts having parallel sides. Under this supportive argument, the above discrepancy can be understood.

Fig. 21 illustrates the normalized vorticity distribution for Model II at Re = 60,000. The predictions for all three models, in general, are qualitatively similar to each other and also to those derived experimentally by Brundrett and Baines [11] with higher magnitudes in the corner region and close to the solid wall. However, the predictions with Model III was considerably low in levels.

6.5 Mean Turbulent Kinetic Energy Distributions

Contours of turbulent kinetic energy for all three models, normalized by the square of the average friction velocity, are shown in Fig. 22 at Re = 83,000. The predicted results are quite close to each other and can be compared with the experimental data of Brundrett and

Baines [11]. The predicted results confirm Brundrett and Baines' overall conclusion that the energy contours are much more distorted by the secondary flow than those of axial velocity. The detailed agreement between experiment and calculation, however, is not particularly good, the measured energy levels being appreciably higher than the predicted. The contrast between the prediction and the experiment is especially evident near the corner. This is consistent with the under-prediction of the secondary flow velocity near the corner region (as discussed in section 6.2), since the dilution process near the corner due to the secondary flow current which carries the fluid of low kinetic energy at the core toward the corner, becomes less efficient for a lower secondary flow velocity.

The turbulent kinetic energy profiles along the mid-wall bisector are presented in Fig. 23 for Models I to III respectively. As discussed earlier, they were found at a lower level than the experimental measurements [11].

In a bid to improve the turbulent kinetic energy contours, the model constant (C') of Model I was increased from 0.0035 to 0.006, thus improving the kinetic energy contours (ref. Figs. 24 and 25) as expected, since the magnitude of secondary velocities

went up (from 1.5% to 2.0%) causing more bulges. the isovels also improved slightly (Fig. 26), i.e. closer to the experimental data, but the wall shear stress distribution (Fig. 27) was adversely affected and obviously secondary velocities distribution were also seriously disturbed. As can be seen from Fig. 24-27, the increased C' does not improve the secondary flow absolutely and hence this attempt was abandoned and C' was restored to the original value of 0.0035.

Concerning scaling, the contours of turbulent kinetic energy (k), normalized with the square of the average friction velocity, are shown for Re = 75,000 and 215,000 in Fig. 28. It is observed that kinetic energy normalized by $\bar{u}^*$ is essentially independent of Reynolds number.

6.6 Local Wall Shear Stress Distribution

The predicted shear stress distributions, for all three models, have been normalized by average and center-point shear stress and have been presented in Figs. 29 and 30 respectively. The predictions are quite similar and in fair agreement with experimental data.

The tendency of the secondary velocity to smooth out variations in wall shear stress around the perimeter of the duct is well brought out in these figures. The predicted results of Models I, II and III, display

substantially the same variation as Leuthuesser's [10] measurements with the peak shear stress actually occurring about midway between the corner and the mid-point of the sides. This behavior is in marked contrast with the numerical solution obtained with secondary velocities suppressed (Fig. 29).

In Fig. 30, the shear stress was normalized by centre line shear stress in order to facilitate direct comparison with Hoagland's [9] experimental points. As can be seen, predictions of Model II are closer to Hoagland's [9] data as compared to Model I and Model III.

6.7 Effect of Reynolds Number

The friction factor dependence on Reynolds number was investigated by conducting a series of computations (for various Reynolds numbers) with Model III. The predicted results are compared to the experimental data of Leutheusser [10], for smooth square duct, in Fig. 31. On the same figure, comparison with the prediction obtained by the Blasius correlation for friction factors in smooth circular tubes is shown. The predicted friction factors are in good agreement with the experimental measurements.

The distributions of predicted local wall shear stress (for Model II) for three different Reynolds number is compared in Fig. 32. The effect of Reynolds number on

τ/τ_w is not significant and it can be concluded that normalized wall shear stress scales fairly well with Reynolds number and, therefore, can be compared with experimental data of Leutheusser [10] taken at a different Reynolds number. It is, however, noticeable that with increased Reynolds number a slightly smoother (less bulged) shear stress distribution is obtained, which is expected. Higher Reynolds number causes higher secondary flow, which in turn, evens out the shear stress along the wall more effectively and hence a slightly flatter curve results. This trend remains unaffected whether the local shear stress is normalized by τ_w or $\tau_{c/p}$.

6.8 Comparison of Three Models

The following criteria were chosen as a basis for the comparison of three models, viz., 1) accuracy, 2) speed of convergence, 3) vorticity source comparison and 4) potential for multi-cell geometries.

1) Accuracy:

All three models performed reasonably well in predicting the fully developed turbulent flow in a square duct. The predictions of all three models were close except for vorticity source predictions (as discussed later). As compared to experimental data, Model II was slightly more accurate than Model I and Model III in

predicting vorticity, stream function, secondary velocities fields and wall shear stress distribution. The predictions of vorticity source by Model II was also more accurate than the other two models. For Model II, the turbulent kinetic energy predictions were slightly better near the corner region whereas they were slightly poorer near the center region, as compared to other two models. Overall, Model II is slightly more accurate as compared to Model I and Model III.

2) Speed of Convergence:

For each model, a number of computer programs were run using different size of ducts and different Reynolds number. However, it was not possible to pin-point a single factor or constant affecting the speed of convergence significantly and consistently. This is expected due to the complex coupling of a number of integro-differential equations involved in the solutions procedure.

Typically, at a Reynolds number of 75,000, Model I, II and III required approximately 320, 360 and 240 iterations respectively, for the converged solutions. Similarly, at a Reynolds number of 107,000, about 340, 280 and 260 iterations were needed to obtain converged solutions for Model I, II and III respectively. Overall, Model III converged faster than Model I and II, under

exactly similar circumstances.

3) Vorticity Source Comparison:

Figure 33 to 35, show the predictions of vorticity production for Model I, II and III respectively. The predicted vorticity production contours, for all three models, are qualitatively similar to those given by Brundrett and Baines [11]. Quantitatively, Model I and Model II generally have the same levels as [11], whereas Model III levels are comparatively low. In fact, the predictions of Model III are one order of magnitude lower than the experimental data [11]. This discrepancy seems to be due to an inherent characteristics of this synthetic model.

4) Potential for Multi-cell Geometries:

In the past, Model I has been successfully employed for various types of flow geometries. The inventors of this model, i.e. Launder and Ying [2], claimed it to give reasonably good predictions in ducts of more complicated cross-section, such as commonly arise in nuclear fuel rod bundles and certain other heat-exchanger types. Aly, Trupp and Gerrard [30], and Gosman and Rapley [52] used this model for an equilateral triangular duct and Carajilescov and Todreas [32] used it for triangular rod bundles. It was also successfully employed by Said [49] for internally finned tubes. In

many ways, this model has shown promise in tackling complicated geometries involving multi-cells.

Less can be said about Model II. Not much historical background is available except that Seale [3] can be given the credit of initiating the idea. Alshamani's [5] [47] turbulent properties correlations, paved a way towards the development of this model. However, this model seems very promising and is shown here to be very successful in predicting turbulent flow characteristics (being the best out of the three models tested) in a square duct.

The algebraic expression of Model III, which allows the source of axial vorticity to be calculated directly and without iteration, successfully reproduced secondary velocities in square and triangular ducts and in a duct consisting of two inter-connected subchannels (simulated rod bundle, SRB) due to Seale [3]. Thus it can be stated that Model III is as promising as Model I and may be exploited for use for complicated geometrics of other types.

7.0 CONCLUSIONS AND RECOMMENDATIONS FOR FUTURE WORK

The two equation ($k-\varepsilon$) turbulence model developed in the present work, performed quite well in conjunction with three different types of vorticity source term models, in predicting the fully developed turbulent flow characteristics for square ducts. The predicted results appear logical qualitatively and quantitatively. The overall level of agreement between predicted and experimental data is considered satisfactory (except for vorticity source predictions).

The following observations and conclusions are drawn from the study of comparative performance of Models I, II and III with respect to each other and (in turn) the published experimental data:

(i) The most impressive finding is the close similarity in the predictions of all three models, despite the different models of vorticity source term. Overall, the predicted results of all the three models are quite close to each other and no significant differences were noticed. The predictions of Model I and Model III (except for vorticity source production predictions) were extremely close, despite the fact that Model I takes into account both Reynolds normal and shear stresses whereas Model III only includes normal stresses. It truly supports the common belief that

Reynolds shear stress contribution is negligible as compared to normal stress (as discussed in section 4.3) and satisfactory predictions can be obtained without its inclusion (in order to save computer time) in the numerical analysis.

(ii) Even though the mean-velocity field is predicted adequately by all three models, the models fail to give satisfactory agreement between prediction and experimental data [11] of vorticity source production. The vorticity production contours of Models I, II and II are qualitatively similar to those of Brundrett and Baines [11]. Quantitatively, the predicted magnitudes of Model I and Model II are of the same order as that of experiment [11] whereas the predictions of Model III are one order lower in magnitude than the experimental results [11]. This phenomena appears to be inherent to in Model III.

(iii) The turbulent kinetic energy assumes relatively higher values near the wall, which is due to the usual high turbulence production zone very near the wall. It decreases leaving the wall to reach a minimum value at the duct centreline.

The turbulence fields are clearly influenced by the presence of secondary flows. The present study confirms previous observations (eg. [11]) that the effect

on the turbulent kinetic energy field is more pronounced than on the axial velocity field.

(iv) Reportedly, the secondary velocities, normalized with either the average mean velocity or centre-line axial velocity, are found to decrease with increasing Reynolds number. This confirms the findings of Gessner and Jones [13].

(v) The mean axial velocity when normalized by bulk velocity or centre-line axial velocity, does not scale well with Reynolds number. However, the secondary velocities and turbulent kinetic energy when normalized by average friction velocity, and the wall shear stress normalized by average wall shear stress (or centre-point stress), all scale well with Reynolds number.

(vi) Due to momentum transport by secondary flows, the predicted wall shear stress of all three models, over the central half of each wall is constant to within a few percent. The effect of Reynolds number on the normalized wall shear stress distribution for Model II was studied and found not very significant in the range 60,000 to 300,000 (Figs. 29 and 30). However, increasing Reynolds number slightly flattens the shear stress distribution curve.

(vii) The friction factor dependence on Reynolds number is investigated for Model III and found

to agree with the measurements of Leutheusser [10] for smooth square ducts.

As per previous discussions and observations, it is considered that Model II is slightly more accurate overall, as compared to the other two models. Hence, the exploitation of Model II for different geometries (both simple and complicated e.g., isosceles triangular duct, trapezoidal duct, eccentric annuli, etc.) may be highly rewarding. On the other hand, in the light of closeness of predictions of Model II with Models I and III and chiefly the speed of convergence of Model III, it appears that Model III has several attractive features. Furthermore, Model III has already been employed for a complicated geometry (Simulated Rod Bundle) by Seale [3], and presumably has many promises in reserve for a variety of complicated geometries. It is therefore recommended that the use of both Models II and III to complicated geometries be explored in future studies.

8.0 REFERENCES

1. Kacker, S. C., "Some Aspects of Fully Developed Turbulent Flow in Non-circular Ducts", J. Fluid Mech., Vol. 57, Part 3, pp. 583-602, 1973.

2. Launder, B. E. and Ying, W. M., "Prediction of Flow and Heat Transfer in Ducts of Square Cross-section", Proc. Instn. Mech. Engrs., Vol. 187, pp. 455-61, 1973.

3. Seale, W. J., "Turbulence Generated Secondary Flows in Ducts of Non-circular Cross-section", Journal Mechanical Engineering Science, Vol. 24 No. 3, pp. 119-27, 1982.

4. Gosman, A. D., Pun, W. M., Runchal, A. K., Spalding, D. B. and Wolfshtein, M., "Heat and Mass Transfer in Recirculating Flows", Academic Press, 1969.

5. Alshamani, K. M. M., "Relationships between Turbulent Intensities in Turbulent Pipe and Channel Flows" Journal of Royal Aeronautical Society, London, Vol. 83, pp. 159-61, 1979.

6. Launder, B. E. and Singham, J. R., "The Prediction of Fully-developed Flow in Non-circular Ducts," Symp. Internal Flow, Paper 12 (University of Salford), 1971.

7. Prandtl, L., "Proc. Second Int. Congr. of Applied Mech., 1926, p. 71 et seq Zurich, 1927 (Also translated as NACA TM-435).

8. Nikuradse, J., "Untersuchungen uber die Geschwindikeitsverteitung in Turbulenten Stromungen", Ph. D. Thesis Gottingen, 1926. Also VDI Forschungsheft 281, Berlin, 1926.

9. Hoagland, L. C., "Fully Developed Turbulent Flow in Straight Rectangular Ducts-Secondary Flow, its Causes and Effect on the Primary Flow", Ph.D. Thesis, Massachussets Institute of Technology, 1960.

10. Leutheusser, H. J., "Turbulent Flow in Rectangular Ducts", American Society of Civil Engineers, Journal of the Hydraulics Division, Vol. 89, No. HY3. pp. 1-19, May, 1963.

11. Brundrett, E. and Baines, W. D., "The Production and

Diffusion of Vorticity in Duct Flow", J. Fluid Mech., Vol. 19, pp. 375-94, 1964.

12. Gessner, F. B., "The Origin of Secondary Flow in Turbulent Flow along a Corner", J. Fluid Mech., Vol. 58, Pt. 1, pp. 1-25, 1973.

13. Gessner, F. B. and Jones, J. B., "On Some Aspects of Fully Developed Turbulent Flow in Rectangular Channels", J. Fluid Mech., Vol. 23, Pt. 4, pp. 689-713, 1965.

14. Launder, B. E. and Ying, W. M., "Secondary Flows in Ducts of Square Cross-section", J. Fluid Mech., Vol. 54, pp. 289-95, 1972.

15. Kokorev, L. S. Korsun, A. S., Kostyunin, B. N., Petrovichev, V. I. and Struenze, R. L., "Effect of Secondary Flows on the Velocity Distribution and Hydraulic Drag in Turbulent Liquid Flows in Noncircular Channels", Heat Trans. - Soviet Res. Vol. 3, No. 1, p. 78, 1971.

16. Ahmed, S. and Brundrett, E., "Turbulent Flow in Non-circular Ducts. Part 1", Int. J. Heat Mass Transfer, Vol. 14, pp. 365-75, 1971.

17. Melling, A. and Whitelaw, J. H., "Turbulent Flow in a Rectangular Duct", J. Fluid Mech., Vol. 78, part 2, pp.289-315, 1976.

18. Gessner, F. B., Po, J. K. and Emery, A. F., "Measurements of Developing Turbulent Flow in a Square Duct", Symp. on Turbulent Shear Flows, Univ. Park, Pennsylvania, Vol. 1, p. 9.7, April, 1977.

19. Comte-Bellot, G., Strohl, A. and Alcaraz, E., "On Aerodynamic Disturbances Caused by Single Hot-wire Probes", Journal of Applied Mechanics, Trans. ASME, Series E, Vol. 38, pp. 767-74, 1971.

20. Reynolds, W. C., "Computation of Turbulent Flows-State-of-The-Art," Report MD-27, Thermo-sciences Division, Department of Mechanical Engineering, Stanford University, 1970.

21. Reynolds, W. C., "Recent Advances in the Computation of Turbulent Flows", Advances in Chemical Engineering, Vol. 9, pp. 193-246, 1974.

22. Wolfshtein, M., Naot, D. and Lin, A., "Models of

Turbulence", Topics in Transport Phenomenon, Editor: Gutfinger, C., John Wiley & Sons, pp. 3-45, 1975.

23. Launder, B. E. and Spalding, D. B., "Mathematical Models of Turbulence", Academic Press, London, 1972.

24. Bradshaw, P., "The Understanding and Prediction of Turbulent Flow", Aeronautidcal Journal, pp. 403-18, 1972.

25. Bradshaw, P., "Turbulence Research - Progress and Problems", Proceedings of the 1976 Heat Transfer and Fluid Mechanics Institute, Held at the University of California, Davis, California, June 21-23, pp. 128-39, 1976.

26. Spalding, D. B., "Turbulence Models for Heat Transfer", Proc. of the Sixth International Heat Transfer Conference, Toronto, Canada, Vol. 6, pp. 33-43, 1978.

27. Buleev, N.I., "Theoretical Model for Turbulent Transfer in Three Dimensional Fluid Flow", Paper presented at the Third United Nations Conference on the Peaceful Uses of Atomic Energy, Paper A/CONF. 28/P/329, May, 1964.

28. Hanjalic, K. and Launder, B. E., "A Reynolds Stress Model of Turbulence and Its Application to Thin Shear Flows", J. Fluid Mechanics, Vol. 52, pp. 609-38, 1972.

29. Launder, B. E., Reece, G. J. and Rodi, W., "Progress in the Development of a Reynolds Stress Turbulence Closure", J. Fluid Mech., Vol. 68, Part 3, pp. 537-66, 1975.

30. Aly, A. M. M., Trupp, A. C. and Gerrard, A. D., "Measurements and Predictions of Fully Developed Turbulent Flow in an Equilateral Trangular Duct", J. Fluid Mech., Vol. 85, Part 1, pp. 57-83, 1978.

31. Trupp, A. C. and Aly, A. M. M., "Predicted Secondary Flows in Triangular Array Rod Bundles", ASME Journal of Fluids Engineering, Vol. 101, pp. 354-63, 1979.

32. Carajilescov, P. and Todreas, N. E., "Experimental and Analytical Study of Axial Turbulent Flows in an Interior Sub-channel of a Bare Rod Bundle" Transactions of the ASME, J. of Heat Transfer, Vol. 98, pp. 262-8, 1976.

33. Tennankore, K. N. and Steward, F. R., "Comparison of Several Turbulence Models for Predicting Flow Patterns with Confined Jets", Symposium on Turbulent Shear Flows, University Park, Pennsylvania, Vol. 1, pp. 10.9-10.16, 1977.

34. Launder, B. E. and Spalding, D. B., "The Numerical Computation of Turbulent Flows", Computer Methods in Applied Mechanics and Engineering, Vol. 3, pp. 269-89, 1974.

35. Jones, W. P. and Launder, B. E., "The Prediction of Laminarization with a Two-Equation Model of Turbulence", Int. J. Heat Mass Transfer, Vol. 15, pp. 301-14, 1972.

36. Jones, W. P. and Launder, B. E., "The Calculation of Low-Reynolds-Number Phenomena with a Two-Equation Model of Turbulence", Int. J. Heat Mass Transfer, Vol. 16, pp. 1119-30, 1973.

37. Deissler, R. G. and Taylor, M. F., "Analyses of Turbulent Flow and Heat Transfer in Non-circular Passages", NASA Tech. Rep. R-31, 1959.

38. Krajewski, B., "Determination of Turbulent Velocity Field in A Rectilinear Duct with Non-circular Cross-section", Int. J. Heat Mass Transfer, Vol. 13, pp. 1819-24, 1970.

39. Buleev, N. I., "Theoretical Model of the Mechanism of Turbulent Exchange in Fluid Flow", AERE Translation 957, 1963.

40. Ibragimov, M. H., Petrishchev, V. S. and Sabelev, G. I., "Calculation of Heat Transfer in Turbulent Flow with Allowance for Secondary Flow", Int. J. Heat Mass Transfer, Vol. 14, pp. 1033-8, 1971.

41. Ibragimov, M. H., Petrischev, V. S. and Sabelev, G. I., "Calculation of a Secondary Flow in Turbulent Fluid Flow", Izv. Akad. Nauk. Mekhanica Zuid. Gaza, No. 4, 1969.

42. Wilson, N. W., Azad, R. S. and Trupp, A. C., "An Analysis of the Effect of Secondary Flows on the Longitudinal Velocity Distribution in Square Ducts", Symp. Internal Flows, Univ. of Salford, Paper 11, April 1971.

43. Ying, W. M., "Fully-developed Flow with Swirl in Non-circular Ducts, Ph.D. Thesis, University of London, 1971.

44. Tatchell, D. G., "Convection Processes in Confined, Three Dimensional Boundary Layers", Ph.D. Thesis, University of London, 1975.

45. Wolfshtein, M., Naot, D. and Shavit, A., "Numerical Calculation of Reynolds Stresses in a Square Duct with Secondary Flow", Warme-und Stoffubertragung, Vol. 7, pp. 151-61, 1974.

46. Hornby, R. P., Mistry, J. and Barrow, H., "A Mixing Length Model for Turbulent Flow in Constant Cross-section Ducts", Warme-und Stoffubertragung, Vol. 10, pp. 125-29, 1977.

47. Alshamani, K. M. M., "Correlations Among Turbulent Shear Stress, Turbulent Kinetic Energy and Axial Turbulence Intensity", AIAA Journal, Vol. 16, No. 8, 1978.

48. Nakayama, A., Chow, W. L. and Sharma, D., "Calculation of Fully Developed Turbulent Flows in Ducts of Arbitrary Cross-section", Journal of Fluid Mechanics, Vol. 128, pp. 199-217, 1983.

49. Said, M. N. A. A., "Predictions and Measurements of Fully Developed Turbulent Flow in Longitudinal Internally Finned Tubes", Ph. D. Thesis, University of Manitoba, Manitoba, Canada, 1981.

50. Gosman, A. D., Neilsen, P. V., Restivo, A. and Whitelaw, J. H., "The Flow Properties of Rooms With Small Ventilation Openings", Transactions of the ASME, Journal of Fluids Engineering, Vol. 102, pp. 316-32, 1980.

51. Hinze, J. O., "Turbulence", 2nd Edition, McGraw Hill, 1975.

52. Gosman, A. D. and Rapley, C. W., "A Prediction Method for Fully Developed Flow Through Non-circular Passages", Int. Proc. I Intl. Conf. on Num. Methods in Laminar and Turbulent Flow, University College, Swansea, pp. 271-85, 1978.

53. Date, A. W., "Prediction of Fully Developed Flow in a Tube Containing a Twisted Tape", Int. J. Heat Mass Transfer, Vol. 17, pp. 845-59, 1974.

54. Harsha, P. T. and Lee, S. C., "Correlation between Turbulent Shear Stress and Turbulent Kinetic Energy", AIAA Journal, Vol. 8, pp. 1508-10, 1970.

55. Sandborn, V. A., "Experimental Evaluation of Momentum Terms in Turbulent Pipe Flow", NACA TN 3266, 1954.

56. Laufer, J., "The Structure of Turbulence in Fully Developed Pipe Flow", NACA TN 2934, 1953.

57. Laufer, J., "Investigation of Turbulent Flow in a Two Dimensional Channel", NACA Tn 2123, 1950.

58. Lawn, C. J., "Application of the Turbulent Energy Equation to Fully Developed Flow in Simple Ducts", Central Electricity Generating Board, RD/B/R/1575, A, B, C, 1970.

59. Lawn, C. J., "The Determination of the Rate of Dissipation in Turbulent Pipe Flow", Journal of Fluid Mechanics, Vol. 48, Pt. 3, pp. 477-505, 1971.

60. Clark, J. A., "Study of Incompressible Turbulent Boundary Layers in a Two Dimensional Wind Tunnel", Ph. d. Thesis, Queen's Univ. of Belfast, 1966.

61. Clark, J. A., "A Study of Incompressible Turbulent Boundary Layers in Channel Flows", Journal of Basic Engineering, No. 90, pp. 455-68, 1968.

62. Comte-Bellot, G., "Turbulent Flow between Two Parallel Walls", Ph. D. Thesis, Univ. of Grenoble, 1963 (transl. into English by P. Bradshaw in Aeronautical Research Council ARC 31 609, F.M. 4102, 1969).

63. Laufer, J., "The Structure of Turbulence in Fully Developed Pipe Flows", NACA Report TN1174, 1954.

64. Aly, A. M. M., "Turbulent Flows in Equilateral Triangular Ducts and Rod Bundle Sub-channels", Ph. D. Thesis, Univ. of Manitoba, 1977.

65. Gerard, R., "Finite Element Solution for Flow in Non-circular Conduits", J. of the Hydraulics Division, ASCE, Vol. 100,1 No. HY3, pp. 425-41, 1974.

66. Patankar, S. V., "Numerical Heat Transfer and Fluid

Flow", McGraw-Hill, 1980.

67. Gerrard, A. D., "Turbulent Flow in an Equilateral Triangular Duct", M. Sc. Thesis, U. of Manitoba, Canada, February 1976.

APPENDIX A

DERIVATION OF TURBULENT KINETIC ENERGY EQUATION

It is worth recalling that the turbulent flow, in question, is assumed to be fully developed, steady, incompressible with constant property fluid and negligible body forces.

The turbulent kinetic energy is derived (in Cartesian coordinate) from the Navier-Stokes equation by multiplying the momentum equation for the fluctuating flow for each direction by the corresponding fluctuating velocity component, averaging in time and then adding the three equations.

The continuity equation may be written as:

$$\frac{\partial \bar{V}}{\partial y} + \frac{\partial \bar{W}}{\partial z} = 0, \quad (A.1)$$

and,

$$\frac{\partial u}{\partial x} + \frac{\partial v}{\partial y} + \frac{\partial w}{\partial z} = 0. \quad (A.2)$$

The instantaneous value of a turbulent quantity is supposed to be composed of a mean value alongwith a fluctuating component, such that

$$\tilde{U} = \bar{U} + u, \qquad \tilde{V} = \bar{V} + v,$$
$$\tilde{W} = \bar{W} + w, \quad \text{and} \quad \tilde{P} = \bar{P} + p, \quad (A.3)$$

where tilde ($\sim$) indicates the instaneous value.

1. Axial Direction (x-Direction)

The axial momentum equation may be written in the following form:

$$\frac{\partial \tilde{U}}{\partial t} + \tilde{U}\frac{\partial \tilde{U}}{\partial x} + \tilde{V}\frac{\partial \tilde{U}}{\partial y} + \tilde{W}\frac{\partial \tilde{U}}{\partial z} = -\frac{1}{\rho}\frac{\partial \tilde{P}}{\partial x} + \nu \nabla^2 \tilde{U} ,$$

where,

$$\nabla^2 = \frac{\partial^2}{\partial x^2} + \frac{\partial^2}{\partial y^2} + \frac{\partial}{\partial z^2} . \quad (A.4)$$

Substitution of equations (A.3) into equation (A.4) and taking time average gives:

$$\frac{\partial \bar{U}}{\partial t} + \bar{U}\frac{\partial \bar{U}}{\partial x} + \bar{V}\frac{\partial \bar{U}}{\partial y} + \bar{W}\frac{\partial \bar{U}}{\partial z} + \frac{\partial}{\partial x}\overline{u^2} + \frac{\partial}{\partial y}\overline{uv} + \frac{\partial}{\partial z}\overline{uw}$$

$$= -\frac{1}{\rho}\frac{\partial P}{\partial x} + \nu \nabla^2 \bar{U} . \quad (A.5)$$

Equation (A.5) is the axial mean flow or Reynold's equation which, when subtracted from equation (A.4), gives the following equation for the fluctuating flow in the axial direction:

$$\frac{\partial u}{\partial t} + \bar{U}\frac{\partial u}{\partial x} + u\frac{\partial \bar{U}}{\partial x} + u\frac{\partial u}{\partial x} + \bar{V}\frac{\partial u}{\partial y} + v\frac{\partial \bar{U}}{\partial y} + v\frac{\partial u}{\partial y}$$

$$+ \bar{W}\frac{\partial u}{\partial z} + w\frac{\partial \bar{U}}{\partial z} + w\frac{\partial u}{\partial z} = -\frac{1}{\rho}\frac{\partial p}{\partial x} + \nu \nabla^2 u . \quad (A.6)$$

Multiplying equation (A.6) by u and taking time average yields:

$$\overline{u\frac{\partial u}{\partial t}} + \bar{U}\,\overline{u\frac{\partial u}{\partial x}} + \bar{u}^2\frac{\partial \bar{U}}{\partial x} + \overline{u^2\frac{\partial u}{\partial x}} + \bar{V}\,\overline{u\frac{\partial u}{\partial y}} + \overline{uv} \quad \ldots$$

$$\ldots \quad \frac{\partial \bar{U}}{\partial y} + \overline{uv \frac{\partial u}{\partial y}} + \bar{W} \overline{u \frac{\partial u}{\partial z}} + \overline{wu} \frac{\partial \bar{U}}{\partial z} + \overline{uw \frac{\partial u}{\partial z}} =$$

$$- \frac{1}{\rho} \overline{u \frac{\partial p}{\partial x}} + \nu \overline{u \nabla^2 u} . \quad (A.7)$$

2. Lateral Horizontal Direction (y-Direction)

The momentum equation in y-direction may be similarly written as:

$$\frac{\partial \tilde{V}}{\partial t} + \tilde{U} \frac{\partial \tilde{V}}{\partial x} + \tilde{V} \frac{\partial \tilde{V}}{\partial y} + \tilde{W} \frac{\partial \tilde{V}}{\partial z} = - \frac{1}{\rho} \frac{\partial \tilde{P}}{\partial y} + \nu \nabla^2 \tilde{V} . \quad (A.8)$$

Substitutions of equations (A.3) into equation (A.8) and taking time average yields:

$$\frac{\partial \bar{V}}{\partial t} + \bar{U} \frac{\partial \bar{V}}{\partial x} + \bar{V} \frac{\partial \bar{V}}{\partial y} + \bar{W} \frac{\partial \bar{V}}{\partial z} + \frac{\partial}{\partial x} \overline{uv} + \frac{\partial}{\partial y} \overline{v^2} + \frac{\partial}{\partial z} \overline{vw}$$

$$= - \frac{1}{\rho} \frac{\partial P}{\partial y} + \nu \nabla^2 \bar{V} . \quad (A.9)$$

Equation (A.9) is the mean flow (Reynolds) equation in y-direction which, when subtracted from equation (A.8), yields the following equation for the fluctuating flow in the y-direction.

$$\frac{\partial v}{\partial t} + \bar{U} \frac{\partial v}{\partial x} + u \frac{\partial \bar{V}}{\partial x} + u \frac{\partial v}{\partial x} + \bar{V} \frac{\partial v}{\partial y} + v \frac{\partial \bar{V}}{\partial y} + v \frac{\partial v}{\partial y} +$$

$$\bar{W} \frac{\partial v}{\partial z} + w \frac{\partial \bar{V}}{\partial z} + w \frac{\partial v}{\partial z} = - \frac{1}{\rho} \frac{\partial p}{\partial y} + \nu \nabla^2 v . \quad (A.10)$$

Multiplying equation (A.10) by v and taking time average yields:

$$\overline{v \frac{\partial v}{\partial t}} + \bar{U} \overline{v \frac{\partial v}{\partial x}} + \overline{uv} \frac{\partial \bar{V}}{\partial x} + \overline{uv \frac{\partial v}{\partial x}} + \bar{V} \overline{v \frac{\partial v}{\partial y}} + \bar{v}^2 \frac{\partial \bar{V}}{\partial y} +$$

$$\overline{v^2 \frac{\partial v}{\partial y}} + \bar{W} \overline{v \frac{\partial v}{\partial z}} + \overline{vw} \frac{\partial \bar{V}}{\partial z} + \overline{vw \frac{\partial v}{\partial z}} = - \frac{1}{\rho} \overline{v \frac{\partial p}{\partial y}} +$$

$$\nu \overline{v \nabla^2 v} . \quad (A.11)$$

3. Lateral-Vertical Direction (z-Direction)

The momentum equation in z-direction is given as:

$$\frac{\partial \tilde{W}}{\partial t} + \tilde{U} \frac{\partial \tilde{W}}{\partial x} + \tilde{V} \frac{\partial \tilde{W}}{\partial y} + \tilde{W} \frac{\partial \tilde{W}}{\partial z} = - \frac{1}{\rho} \frac{\partial \tilde{P}}{\partial z} + \nu \nabla^2 \tilde{V} . \quad (A.12)$$

Applying equation (A.3) into equation (A.12) and averaging in time yields:

$$\frac{\partial \bar{W}}{\partial t} + \bar{U} \frac{\partial \bar{W}}{\partial x} + \bar{V} \frac{\partial \bar{W}}{\partial y} + \bar{W} \frac{\partial \bar{W}}{\partial z} + \frac{\partial}{\partial x} \overline{wu} + \frac{\partial}{\partial y} \overline{vw} + \frac{\partial}{\partial z} \bar{w}^2 =$$

$$- \frac{1}{\rho} \frac{\partial P}{\partial z} + \nu \nabla^2 \bar{W} . \quad (A.13)$$

Equation (A.13) is the mean flow (Reynolds) equation in z-direction which, when subtracted from equation (A.8), gives the following equation for the fluctuating flow in the z-direction:

$$\frac{\partial w}{\partial t} + \bar{U} \frac{\partial w}{\partial x} + u \frac{\partial \bar{W}}{\partial x} + u \frac{\partial w}{\partial x} + \bar{V} \frac{\partial w}{\partial y} + v \frac{\partial \bar{W}}{\partial y} + v \frac{\partial w}{\partial y} + \bar{W} \frac{\partial w}{\partial z}$$

$$+ w \frac{\partial \bar{W}}{\partial z} + w \frac{\partial w}{\partial z} = - \frac{1}{\rho} \frac{\partial p}{\partial z} + \nu \nabla^2 w . \quad (A.14)$$

Multiplying equation (A.14) by w and taking time average yields:

$$\overline{w \frac{\partial w}{\partial t}} + \bar{U} \overline{w \frac{\partial w}{\partial x}} + \overline{uw} \frac{\partial \bar{W}}{\partial x} + \overline{uw \frac{\partial w}{\partial x}} + \bar{V} \overline{w \frac{\partial w}{\partial y}} + \overline{vw} \frac{\partial \bar{W}}{\partial y} +$$

$$\overline{vw \frac{\partial w}{\partial y}} + \bar{W} \overline{w \frac{\partial w}{\partial z}} + \bar{w}^2 \frac{\partial \bar{W}}{\partial z} + \overline{w^2 \frac{\partial w}{\partial z}} = - \frac{1}{\rho} \overline{w \frac{\partial p}{\partial z}} +$$

$$\nu \overline{w \nabla^2 w} . \quad (A.15)$$

Adding equations (A.7), (A.11) and (A.15) and making use of the continuity equations (A.1) and (A.2) gives:

$$[\frac{\partial k}{\partial t} + \bar{V} \frac{\partial k}{\partial y} + \bar{W} \frac{\partial k}{\partial z} + \bar{U} \frac{\partial k}{\partial x}] + [\frac{\partial}{\partial x} \overline{uk'} + \frac{\partial}{\partial y} \overline{vk'} +$$

$$\frac{\partial}{\partial z} \overline{wk'}] = \nu [\nabla^2 k] + S_1 + S_2 + S_3 , \quad (A.16)$$

where,

$$S_1 = - \frac{1}{\rho} (\overline{u \frac{\partial p}{\partial x}} + \overline{v \frac{\partial p}{\partial y}} + \overline{w \frac{\partial p}{\partial z}}),$$

$$S_2 = -\nu [\overline{(\frac{\partial u}{\partial x})^2} + \overline{(\frac{\partial v}{\partial x})^2} + \overline{(\frac{\partial w}{\partial x})^2} + \overline{(\frac{\partial u}{\partial y})^2} + \overline{(\frac{\partial v}{\partial y})^2} +$$

$$\overline{(\frac{\partial w}{\partial y})^2} + \overline{(\frac{\partial u}{\partial z})^2} + \overline{(\frac{\partial v}{\partial z})^2} + \overline{(\frac{\partial w}{\partial z})^2}], \text{ and}$$

$$S_3 = - \{[\bar{u}^2 \frac{\partial \bar{U}}{\partial x} + \overline{uv} \frac{\partial \bar{V}}{\partial x} + \overline{uw} \frac{\partial \bar{W}}{\partial x}] + [\bar{v}^2 \frac{\partial \bar{V}}{\partial y} + \overline{vw} \frac{\partial \bar{W}}{\partial y} +$$

$$\overline{uv} \frac{\partial \bar{U}}{\partial y}] + [\bar{w}^2 \frac{\partial \bar{W}}{\partial z} + \overline{wu} \frac{\partial \bar{U}}{\partial z} + \overline{vw} \frac{\partial \bar{V}}{\partial z}]\}.$$

In the above equations, the mean turbulent kinetic energy (time-averaged) i.e. k is defined as:

$$k = \tfrac{1}{2} (\bar{u}^2 + \bar{v}^2 + \bar{w}^2),$$

whereas the fluctuating component of k is given by:

$$k' = \tfrac{1}{2} (u^2 + v^2 + w^2).$$

Equation (A.16) is the exact transport equation for k. The following assumptions were made to obtain the approximate transport equation:

a) The terms S_1 in equation (A.16) representing diffusion of k by fluctuating pressure effects is assumed to be negligible.

b) The terms S_2 and S_4 represent the rate of dissipation of k by molecular visiosity and their sum is given as:

$$S_2 + S_4 \cong - \varepsilon.$$

c) The term S_3 represents the rate of energy transferred from the main flow to the turbulent eddies. This transfer is, however, controlled by the gradients of the main velocity. If we neglect the gradients of secondary velocities, S_3 can be expressed as:

$$S_3 \cong - [\bar{u}^2 \frac{\partial \bar{U}}{\partial x} + \overline{uv} \frac{\partial \bar{U}}{\partial y} + \overline{uw} \frac{\partial \bar{U}}{\partial z}].$$

Under the above assumptions and fully developed turbulent flow conditions (i.e. $\frac{\partial}{\partial t} = o = \frac{\partial}{\partial x}$), the approximate transport equation for k may be written as:

$$[\bar{V}\frac{\partial k}{\partial y} + \bar{W}\frac{\partial k}{\partial z}] = [\frac{\partial}{\partial y}(\nu\frac{\partial k}{\partial y} - \overline{vk'}) + \frac{\partial}{\partial z}(\nu\frac{\partial k}{\partial z} - \overline{wk'})] -$$

$$[\overline{uv}\frac{\partial \bar{U}}{\partial y} + \overline{uw}\frac{\partial \bar{U}}{\partial z}] - \varepsilon. \quad (A.17)$$

Applying equations (3.7), (3.8), (4.1), (4.2) and (4.3), to equation (A.17) yields:

$$[\frac{1}{\rho}\frac{\partial \Psi}{\partial z}\cdot\frac{\partial k}{\partial y} - \frac{1}{\rho}\frac{\partial \Psi}{\partial y}\cdot\frac{\partial k}{\partial z}] = [\frac{\partial}{\partial y}(\nu\frac{\partial k}{\partial y} + \frac{1}{\rho}\frac{\mu_t}{k}\frac{\partial k}{\partial y}) +$$

$$\frac{\partial}{\partial z}(\nu\frac{\partial k}{\partial z} + \frac{1}{\rho}\frac{\mu_t}{\sigma_k}\frac{\partial k}{\partial z})] + [\frac{1}{\rho}\mu_t(\frac{\partial \bar{U}}{\partial y})^2 + \frac{1}{\rho}\mu_t(\frac{\partial \bar{U}}{\partial z})^2] - \varepsilon,$$

which when rearranged, gives:

$$[\frac{\partial}{\partial y}(k\frac{\partial \Psi}{\partial z}) - \frac{\partial}{\partial z}(k\frac{\partial \Psi}{\partial y})] - \frac{\partial}{\partial y}[(\mu + \frac{\mu_t}{\sigma_k})\frac{\partial k}{\partial y}] - \frac{\partial}{\partial z}$$

$$[(\mu + \frac{\mu_t}{\sigma_k})\frac{\partial k}{\partial z}] - \mu_t[(\frac{\partial \bar{U}}{\partial y})^2 + (\frac{\partial \bar{U}}{\partial z})^2] + \rho\varepsilon = 0,$$

which is same as equation (4.33).

APPENDIX B

DERIVATION OF TURBULENCE ENERGY DISSIPATION RATE EQUATION

The equations of motion for the fluctuating flow i.e. equations (A.6), (A.10) and (A.14) may be expressed in Cartesian tensor form as:

$$\frac{\partial v_e}{\partial t} + \bar{V}_f \frac{\partial v_e}{\partial x_f} + v_f \frac{\partial \bar{V}_e}{\partial x_f} + v_f \frac{\partial v_e}{\partial x_f} = - \frac{1}{\rho} \frac{\partial P}{\partial x_e} + \frac{\partial}{\partial x_f}$$

$$(\nu \frac{\partial v_e}{\partial x_f} + \overline{v_e v_f}). \quad (B.1)$$

Differentiating equation (B.1) with respect to x_g yields:

$$\frac{\partial}{\partial t} (\frac{\partial v_e}{\partial x_g}) + [\bar{V}_f \frac{\partial}{\partial x_f} (\frac{\partial v_e}{\partial x_g}) + \frac{\partial \bar{V}_f}{\partial x_g} \frac{\partial v_e}{\partial x_f}] + [v_f \frac{\partial^2 \bar{V}_e}{\partial x_f \partial x_g} +$$

$$\frac{\partial v_f}{\partial x_g} \frac{\partial \bar{V}_e}{\partial x_f}] + [v_f \frac{\partial}{\partial x_f} (\frac{\partial v_e}{\partial x_g}) + \frac{\partial v_f}{\partial x_g} \frac{\partial v_e}{\partial x_f}] = - \frac{1}{\rho} \frac{\partial^2 P}{\partial x_e \partial x_g} +$$

$$\frac{\partial^2}{\partial x_f \partial x_g} [\nu \frac{\partial v_e}{\partial x_f} + \overline{v_e v_f}]. \quad (B.2)$$

Multiplying equation (B.2) by $2 \nu \frac{\partial v_e}{\partial x_g}$ throughout, taking time average and making use of the definition of the turbulent energy dissipation rate i.e.,

$$\epsilon = \nu \overline{(\frac{\partial v_e}{\partial x_g})^2} \text{ and } \epsilon' = \nu (\frac{\partial v_e}{\partial x_g})^2$$

and continuity equation, we get the following expression

after rearrangement:

$$\frac{\partial \varepsilon}{\partial t} + \bar{V}_f \frac{\partial \varepsilon}{\partial x_f} = \nu \frac{\partial^2 \varepsilon}{\partial x_f^2} - \frac{\partial \overline{(v_f \varepsilon')}}{\partial x_f} - 2\nu \frac{\partial \bar{V}_e}{\partial x_f} \overline{\frac{\partial v_e}{\partial x_g} \frac{\partial v_f}{\partial x_g}}$$

$$- 2\nu \frac{\partial \bar{V}_f}{\partial x_g} \overline{\frac{\partial v_e}{\partial x_f} \frac{\partial v_e}{\partial x_g}} - 2\nu \overline{\frac{\partial v_e}{\partial x_f} \frac{\partial v_e}{\partial x_g} \frac{\partial v_f}{\partial x_f}} - 2$$

$$\overline{[\nu \frac{\partial}{\partial x_f} (\frac{\partial v_e}{\partial x_g})]^2} - 2 \frac{\nu}{\rho} \frac{\partial}{\partial x_e} \overline{(\frac{\partial v_e}{\partial x_g} \frac{\partial p}{\partial x_g})} - \nu \frac{\partial \overline{v_e v_f v_f}}{\partial x_g}$$

$$\frac{\partial^2 \bar{V}_e}{\partial x_f \partial x_g} . \quad (B.3)$$

After changing the indices of fourth term on right hand side of equation (B.3), it can be written as:

$$\frac{\partial \varepsilon}{\partial t} + \bar{V}_f \frac{\partial \varepsilon}{\partial x_f} = \nu \frac{\partial^2 \varepsilon}{\partial x_f^2} - \frac{\partial \overline{(v_f \varepsilon')}}{\partial x_f} - S_5 - S_6 - S_7,$$

(B.4)

where,

$$S_5 = 2\nu \frac{\partial \bar{V}_e}{\partial x_f} [\overline{\frac{\partial v_e}{\partial x_g} \frac{\partial v_f}{\partial x_g}} + \overline{\frac{\partial v_g}{\partial x_e} \frac{\partial v_g}{\partial x_f}}],$$

$$S_6 = 2 \{\nu \overline{\frac{\partial v_e}{\partial x_f} \frac{\partial v_e}{\partial x_g} \frac{\partial v_f}{\partial x_g}} + \overline{[\nu \frac{\partial}{\partial x_f} (\frac{\partial v_e}{\partial x_g})]^2} ,$$

and,

$$S_7 = \nu [\frac{2}{\rho} \frac{\partial}{\partial x_e} \overline{(\frac{\partial v_e}{\partial x_g} \frac{\partial p}{\partial x_g})} + \overline{\frac{\partial v_e v_f v_f}{\partial x_g}} \frac{\partial^2 \bar{V}_j}{\partial x_f \partial x_g}].$$

This is the exact transport equation for the turbulence energy dissipation rate. However, the following approximation is employed in closing the ε equation:

$$S_5 \cong C_1 \frac{\varepsilon}{k} \overline{v_e v_f} \frac{\partial \bar{V}_e}{\partial x_f} \text{ , (Generation term)}$$

$$S_6 \cong C_2 \frac{\varepsilon^2}{k} \text{ , (Decay term)}$$

where C_1 and C_2 are constants. The term S_7 represents diffusion of ε by fluctuating pressure and fluctuating flow effects and is assumed to be negligible.

Thus equation (B.4) is reduced to the following approximate equation:

$$\frac{\partial \varepsilon}{\partial t} + \bar{V}_f \frac{\partial \varepsilon}{\partial x_f} = \nu \frac{\partial^2 \varepsilon}{\partial x_f{}^2} - \frac{\partial}{\partial x_f} \overline{(v_f \varepsilon')} - C_1 \frac{\varepsilon}{k} \overline{v_e v_f}$$

$$\frac{\partial \bar{V}_e}{\partial x_f} - C_2 \frac{\varepsilon^2}{k} . \quad \text{(B.5)}$$

Invoking fully developed turbulent flow conditions i.e. $\frac{\partial}{\partial t} = o = \frac{\partial}{\partial x}$, the transport equation for the turbulence energy dissipation rate (ε) takes the following form due to equation (B.5):

$$[\bar{V} \frac{\partial \varepsilon}{\partial y} + \bar{W} \frac{\partial \varepsilon}{\partial z}] = [\frac{\partial}{\partial y} (\nu \frac{\partial \varepsilon}{\partial y} - \overline{v\varepsilon'}) + \frac{\partial}{\partial z} (\nu \frac{\partial \varepsilon}{\partial w} - w\varepsilon')]$$

$$- C_1 \frac{\varepsilon}{k} [\overline{uv} \frac{\partial \bar{U}}{\partial y} + \overline{wu} \frac{\partial \bar{U}}{\partial z}] - C_2 \frac{\varepsilon^2}{k} . \quad \text{(B.6)}$$

In reaching equation (B.6), the secondary velocity

gradients in the generation term ($C_1 \frac{\varepsilon}{k} \overline{v_e v_f} \frac{\partial \bar{V}_e}{\partial x_f}$) were neglected on the basis that gradients of the main flow dominate on this term.

Applying equations (3.7), (3.8), (4.1), (4.2) and (4.4) to equation (B.6) yields:

$$[\frac{1}{\rho} \frac{\partial \Psi}{\partial z} \cdot \frac{\partial \varepsilon}{\partial y} - \frac{1}{\rho} \frac{\partial \Psi}{\partial y} \cdot \frac{\partial \varepsilon}{\partial z}] = [\frac{\partial}{\partial y} (\nu \frac{\partial \varepsilon}{\partial y} + \frac{1}{\rho} \frac{\mu_t}{\sigma_\varepsilon} \frac{\partial \varepsilon}{\partial y}) + \frac{\partial}{\partial z} (\nu \frac{\partial \varepsilon}{\partial w} + \frac{1}{\rho} \frac{\mu_t}{\sigma_\varepsilon} \frac{\partial \varepsilon}{\partial z})] + C_1 \frac{\varepsilon}{k} [\frac{1}{\rho} \mu_t (\frac{\partial \bar{U}}{\partial y})^2 + \frac{1}{\rho} \mu_t (\frac{\partial \bar{U}}{\partial z})^2] - C_2 \frac{\varepsilon^2}{k},$$

which when rearranged, gives:

$$[\frac{\partial}{\partial y} (\varepsilon \frac{\partial \Psi}{\partial z}) - \frac{\partial}{\partial z} (\varepsilon \frac{\partial \Psi}{\partial y})] - \frac{\partial}{\partial y} [(\mu + \frac{\mu_t}{\sigma_\varepsilon}) \frac{\partial \varepsilon}{\partial y}] - \frac{\partial}{\partial z} [(\mu + \frac{\mu_t}{\sigma_\varepsilon}) \frac{\partial \varepsilon}{\partial z}] - C_1 \frac{\mu_t \varepsilon}{k} [(\frac{\partial \bar{U}}{\partial y})^2 + (\frac{\partial \bar{U}}{\partial z})^2 + C_2 \rho \frac{\varepsilon^2}{k},$$

which is same as equation (4.34).

APPENDIX C

DERIVATION OF EQUATION FOR SOURCE OF VORTICITY FOR MODEL II

The relationships between $\tilde{u}^+$ and $\tilde{v}^+$ as well as $\tilde{u}^+$ and $\tilde{w}^+$ for fully developed flow in square duct were studied [47], for a wide range of Reynolds number. The published experimental data were used to carry out the investigation. It was found that $\tilde{u}^+$ and $\tilde{v}^+$ as well as $\tilde{u}^+$ and $\tilde{w}^+$ are related very nearly by the following linear form (for square duct):

$$\bar{v}^+ = 0.213\ \bar{u}^+ + 0.767, \quad (C.1)$$

and,

$$\bar{w}^+ = 0.487\ \bar{u}^+ + 0.443. \quad (C.2)$$

Furthermore, the non-dimensional turbulent kinetic energy is given as:

$$k^+ = \tfrac{1}{2}\ (\overline{u^{+2}} + \overline{v^{+2}} + \overline{w^{+2}}). \quad (C.3)$$

Substituting equations (C.1) and (C.2) into equation (C.3) for $\tilde{v}^+$ and $\tilde{w}^+$ respectively, we obtain:

$$k^+ = \alpha\ \bar{u}^{+2} + \bar{u}^{+2} + \nu, \quad (C.4)$$

where,

$$\alpha = \tfrac{1}{2}\{1 + (.213)^2 + (.487)^2\} = 0.64127,$$

$$= 0.213 \times 0.767 + 0.487 \times 0.443 = 0.379112,$$

and,

$$\nu = \tfrac{1}{2}\{(0.767)^2 + (0.443)^2\} = 0.39227.$$

Therefore,

$$k^+ = 0.64127\ \bar{u}^{+2} + 0.379112\ \bar{u}^{+2} + 0.39227. \quad (C.5)$$

The above equation was plotted for k^+ versus $\bar{u}^+$ (Fig. 36). Almost linear relationship between them (for approximately $\bar{u}^+ > 0.8$) was found to exist, as follows:

$$k^+ = 2.59\ \bar{u}^+ - 1.47. \quad (C.6)$$

Now, $\bar{v}^+$ and $\bar{w}^+$ can be expressed in terms of $\bar{u}^+$ through equations (C.1) and (C.2), therefore $(\bar{v}^{+2} - \bar{w}^{+2})$ can also be represented in terms of $\bar{u}^+$. Furthermore, $\bar{u}^+$ can be represented in terms of k^+ via equation (C.6) and hence $(\bar{v}^{+2} - \bar{w}^{+2})$ can be expressed in terms of k^+ as well. After substitutions and rearrangement, the following expression for $(\bar{v}^{+2} - \bar{w}^{+2})$ was obtained in terms of k^+:

$$(\bar{v}^{+2} - \bar{w}^{+2}) = (0.2708 - 0.1245\ k^+ - 0.0286\ k^{+2}), \quad (C.7)$$

or,

$$(\overline{v}^2 - \overline{w}^2) = u^{*2} \ (0.2708 - 0.1245\ k^+ - 0.0286\ k^{+2}), \quad (C.8)$$

which is same as equation (4.22).

Differentiating equation (C.8) with respect to z yields :

$$\frac{\partial}{\partial z} (\overline{v}^2 - \overline{w}^2) = u^{*2} \ (-0.1245 \frac{\partial k^+}{\partial z} - 0.0572\ k^+ \frac{\partial k}{\partial z}). \quad (C.9)$$

Again differentiating equation (C.9) with respect to y yields:

$$\frac{\partial^2}{\partial y \partial z} (\overline{v}^2 - \overline{w}^2) = u^{*2} \ [- 0.0572 \frac{\partial k^+}{\partial y} - (0.1245 + 0.0572\ k^+) \frac{\partial^2 k^+}{\partial y \partial z}],$$

or,

$$\frac{\partial^2}{\partial y \partial z} (\overline{v}^2 - \overline{w}^2) = \rho u^{*2} \ [- 0.0572 \frac{\partial k^+}{\partial y} \frac{\partial k^+}{\partial z} - (0.1245 + 0.0572\ k^+) \frac{\partial^2 k^+}{\partial y \partial z}] = S_w,$$

which is the source term for Model II for axial vorticity equation (4.31) and has been used in computer program in the present form.

APPENDIX D

DERIVATION OF EQUATION FOR SOURCE OF VORTICITY FOR MODEL III

The equation (4.26) for the source of axial vorticity can be rewritten in terms of the normalized variables defined in the nomenclature (and noting that Y_P is a function of the coordinate z) as follows:

$$S\omega = C''' \frac{\rho\, u^{*2}}{\hat{y}^2_{max}} \frac{\partial \hat{y}}{\partial z} \frac{\partial^2}{\partial Y_L \partial Y_P} (k^{+2} + 4.0\, k^+). \quad (D.1)$$

Now,

$$\frac{\partial^2}{\partial Y_L Y_P} (k^{+2} + 4.0\, k^+) = \frac{\partial}{\partial Y_P} [2\, k^+ \frac{\partial k^+}{\partial Y_L} + 4.0 \frac{\partial k^+}{\partial Y_L}]$$

$$= 2 \cdot \frac{\partial}{\partial Y_P} [(k^+ + 2) \frac{\partial k^+}{\partial Y_L}]$$

$$= 2 [\frac{\partial k^+}{\partial Y_P} \cdot \frac{\partial k^+}{\partial Y_L} + (k^+ + 2) \frac{\partial}{\partial Y_P} (\frac{\partial k^+}{\partial Y_L})], \quad (D.2)$$

and,

$$k^+ = k_{i,+} + (k_{w,+} - k_{i,+}) (1 - \hat{y}/y_{max})^2. \quad (4.27)$$

By making use of the definitions of nondimensional distances Y_L, Y_M and Y_P, equation (4.27) can be rewritten as:

$$k^+ = \{1 - m\, Y_P^2\} + \{k_{w,+} - 1 + m\, Y_P^2\}\, Y_L^2$$

$$= Y_M + (k_{w,+} - Y_M)\, Y_L^2, \quad (D.3)$$

therefore,

$$\frac{\partial k^+}{\partial Y_L} = 2\, Y_L\, (k_{w,+} - Y_M)\ , \quad (D.4)$$

$$\frac{\partial}{\partial Y_P}\left(\frac{\partial k^+}{\partial Y_L}\right) = \frac{\partial}{\partial Y_P}\{2\, k_{w,+}\, Y_L - 2\, Y_M\, Y_L\}$$

$$= -\,2\, Y_L\, \frac{\partial Y_M}{\partial Y_P}$$

$$= -\,2\, Y_L\, \frac{\partial}{\partial Y_P}\,(1 - m\, Y_P^2)\, k_{c,+}$$

$$= -\,2\, Y_L\, k_{c,+}\, (-\, m \cdot 2\, Y_P)$$

$$= 4\, k_{c,+}\, Y_L\, Y_P\, m. \quad (D.5)$$

Also,

$$\frac{\partial k^+}{\partial Y_P} = \frac{\partial}{\partial Y_P}\,[Y_M + (k_{w,+} - Y_M)\, Y_L^2\,],$$

where Y_P is a function of z.

Therefore,

$$\frac{\partial k}{\partial Y_P} = \frac{\partial}{\partial Y_P}\,[k_{c,+}\,(1 - m\, Y_P^2) + k_{w,+}\, Y_L^2 - k_{c,+}$$

$$(1 - m\, Y_P^2)\, Y_L^2\,]$$

$$= -\,2\, m\, k_{c,+}\, Y_P + 2\, m\, k_{c,+}\, Y_P\, Y_L^2$$

$$= -\,2\, k_{c,+}\, m\, Y_P\, (1 - Y_L^2)\ . \quad (D.6)$$

Therefore,

$$(k^+ + 2)\, \frac{\partial}{\partial Y_P}\left(\frac{\partial k^+}{\partial Y_L}\right) = (k^+ + 2)\, 4\, m\, k_{c,+}\, Y_L\, Y_P$$

$$= 4\, k_{c,+}\, m\, Y_L\, Y_P\, \{2 + Y_M + (k_{w,+} - Y_M)\, Y_L^2\,\}. \quad (D.7)$$

Similarly,

$$\frac{\partial k^+}{\partial Y_L} \cdot \frac{\partial k^+}{\partial Y_P} = 2\ (k_{w,+} - Y_M)\ Y_L \cdot (-\ 2\ k_{c,+})\ m\ Y_P$$

$$(1 - Y_L{}^2),$$

$$= -\ 4\ k_{c,+}\ m\ Y_L\ Y_P\ (1 - Y_L^2\ )\ (k_{w,+} - Y_M). \quad (D.8)$$

Now, substituting equations (D.7) and (D.8) into equation (D.2) and finally substituting equation (D.2) into equation (D.1) yields:

$$Sw = 8\ C'''\ \frac{\rho u^{*2}}{\hat{y}^2_{max}}\ k_{c,+}\ m\ Y_L\ Y_P \{2 + Y_M + (k_{w,+} - Y_M)$$

$$Y_L^2\ \} - \{(1 - Y_L^2\ )\ (k_{w,+} - Y_M)\}]\ \frac{\partial \hat{y}}{\partial z}\ , \quad (D.9)$$

which is the source term for model III for axial vorticity equation (4.31) and has been used in computer program in the present form.

APPENDIX E

"COMPUTER PROGRAM"

A computer program was developed to facilitate predictions of flow characteristics of fully developed turbulent flow in a square duct. The main program has been presented in Appendix E-1 with calculation procedure for vorticity source term for Model I. However, the calculation procedure for vorticity source term for Model II and Model III has been presented separately in Appendices E-2 and E-3 respectively. The statements from number 259 to 429 of the main program must be replaced by the statements given in Appendix E-2, before starting computation for Model II. Similarly, they should be replaced by the procedure given in Appendix E-3 for Model III. A flow-chart for the computer program has been presented in figure (D.1). The following is a representation of the input constant values:

Fortran Symbol	Representation
M	Numerical grid parameter (M x M)
SIDE	Size of the square duct, meter
RE	Reynolds number
ROW	Density of fluid, kg/m^3
CMU	C_μ

CE1	C_1
CE2	C_2
SIGMK	σ_k
CAPA	κ
CPRIME	C'
CPRPR	C''
CA	C'''
CM	m
CK	$k_{c,+}$
CW	$k_{w,+}$
A	Law of the wall constants
SIGMU	σ_μ
ALFAW	Under-relaxation factor for ω
ALPAEP	Under-relaxation factor for Ψ
ALFAK	Under-relaxation factor for k
ALFAE	Under-relaxation factor for ε
ALFAU	Under-relaxation factor for $\bar{U}$
IVORT	Control numbers for vorticity source term calculation
INORML	IVORT=1, secondary flows suppressed
	IVORT=1, secondary flows included
	INORML=1, normal stress suppressed exclusively
ISHEAR	ISHEAR=1, shear stress suppressed exclusively
	[Note: IVORT=1 ignores INORML and/or ISHEAR]

IMAX	Maximum number of iterations
IPRINT	Number of iterations between print-out of data
IRPRNT	Number of iterations between print-out of residuals.
ALMD	Convergence criterion for $\bar{U}$, Ψ, k and ε
ALMDW	Convergence criterion for ω
AMU	Dynamic visiosity of fluid, (kg/m.s)

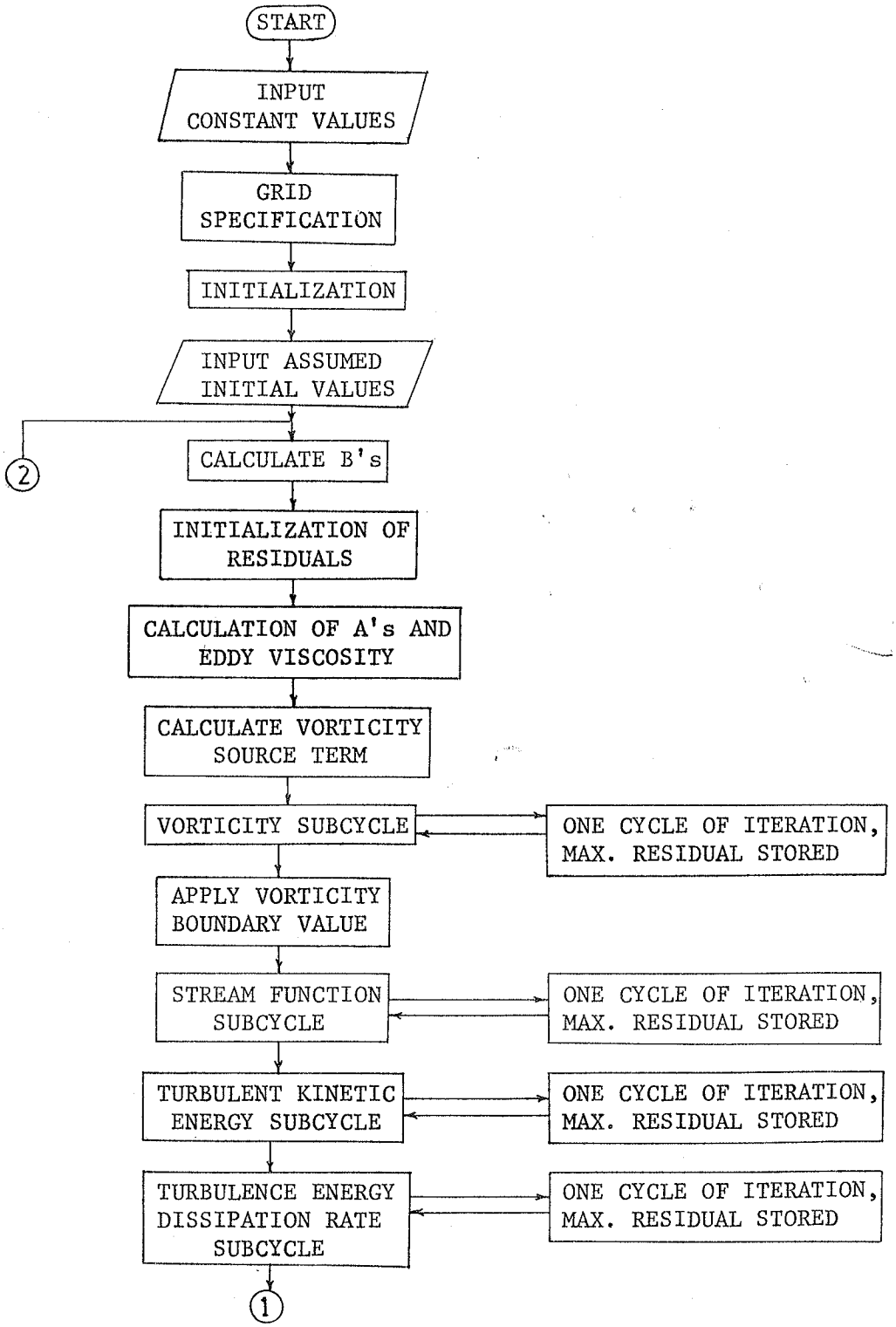

Fig. (D.1). Flow-chart of the Computer Program.

Fig. (D.1) contd...

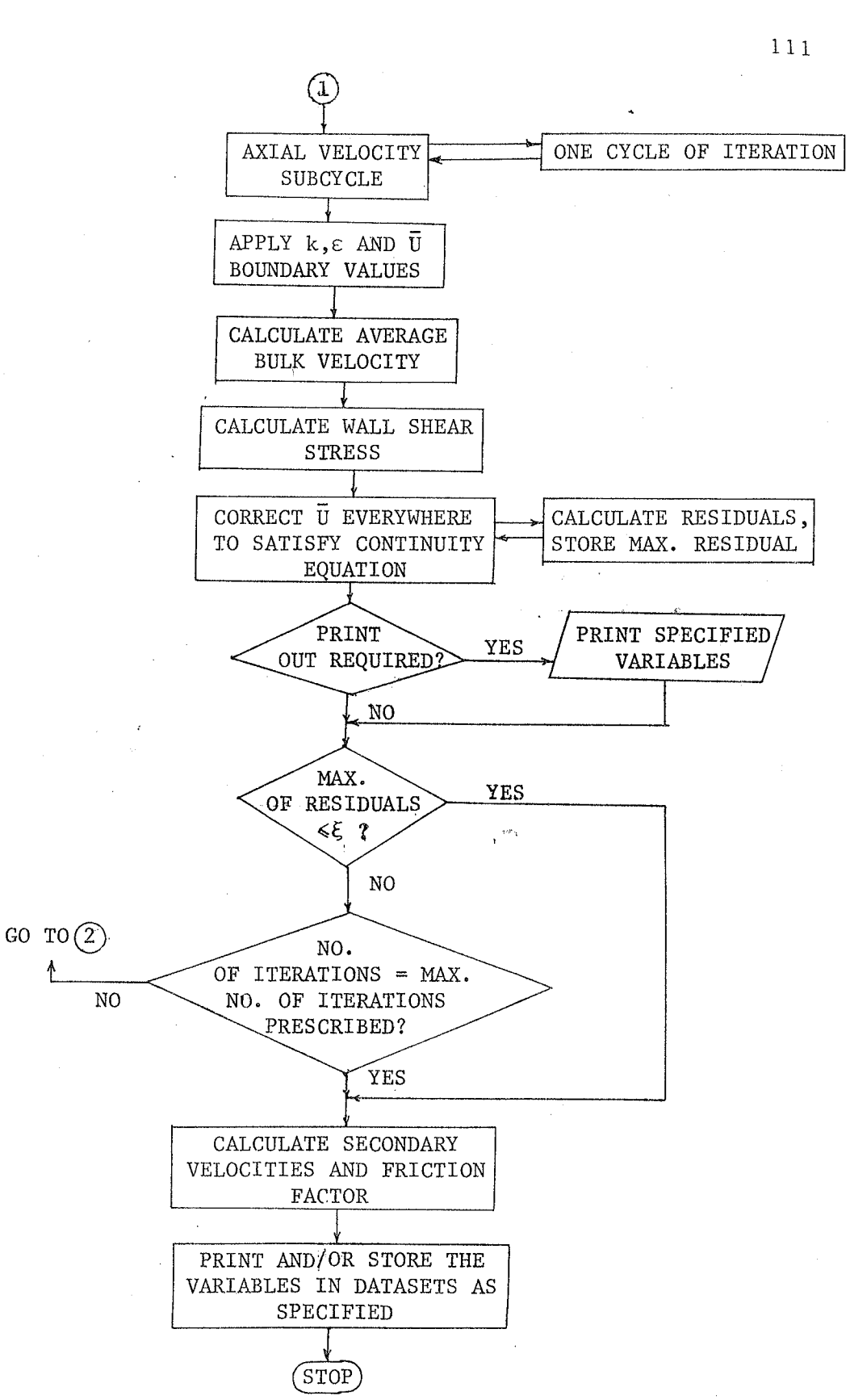

Fig. (D.1). Flow-chart of the Computer Program.

```
C
C       **** SANKATMOCHAN TERA SAHARA ****
C
        DIMENSION OMEG(31,31),EPS(31,31),TKE(31,31),TED(31,31),U(31,31),
       *V(31,31),W(31,31),AMUT(31,31),AE(31,31),AW(31,31),AN(31,31),AS
       *(31,31),BEF(31,31),BWF(31,31),BNF(31,31),BSF(31,31),VP(31,31)
        DIMENSION DUY(31,31),DUZ(31,31),F1(31,31),F2(31,31),F3(31,31),
       *F4(31,31),Y(31),Z(31),UPIUSW(31),TOWW(31),UFW(31),RSWF(31,31),RSE
       *PF(31,31),RSUF(31,31),DA(31,31),DAT(31,31),YSTR(31),YRAT(31,31)
       *,ZRAT(31,31),VORSOR(31,31),UP(31),TKEP(31),TEDP(31),ZPLUSP(31)
       *,UOLD(31,31),VSEC(31,31),VSBCI(31,31),TOWWCL(31),UBCI(31,31)
        DIMENSION VSBUFW(31,31),UBUBAV(31,31),SISNML(31,31),DUZS(31,31)
       *,CHCK(31,31)
C
        DATA M,SIDE/21,.1270/,RE,ROW/75000.0,1.2047/,CMU,CE1,
       *CE2,SIGMK,CAPA,CPRIME/0.09,1.44,1.92,1.0,.41,.0035/,A,E/2.44,5.0/
        DATA SIGMU,ALFAW,ALFAEP,ALFAK,ALFAE,ALFAU/1.0,1.0,1.0,1.0,1.0,
       *1.0/,IVORT,INORML,ISHEAR/2,2,2/,IMAX,IPRINT,IRPRNT,ALMD,ALMDW
       */1000,200,20,0.001,0.001/
C
        AMU = 0.00001817
C
        M1 = M - 1
        M2 = M - 2
        M3 = M - 3
        SIGME = CAPA * CAPA / ((CE2 - CE1) * SQRT(CMU))
        AREA = SIDE * SIDE
        CLAREA = SIDE * SIDE / 8.0
        CLWIPR = SIDE / 2.0
        GRSPG = CLWIPR / M1
        DEQ = 4.0 * CLAREA / CLWIPR
        UBAV = RE * AMU / (ROW * DEQ)
        AMASS = ROW * UBAV * CLAREA
        ANU = AMU / ROW
C
        PRINT 400, M,SIDE,DEQ,RE,UBAV,ROW,AMU,GRSPG
        PRINT 401, CMU,CE1,CE2,SIGMK,SIGME,CAPA,CPRIME
        PRINT 485, A,E
        PRINT 439, SIGMU
        PRINT 402, ALFAW,ALFAEP,ALFAK,ALFAE,ALFAU,ALMD,ALMDW
        PRINT 455, AREA,CLAREA
C
C     **** GRID SPECIFICATIONS ****
C
        Y(1) = 0.0
        Z(1) = 0.0
        DO 10 I=2,M
        Y(I) = Y(I-1) + GRSPG
   10 CONTINUE
C
        DO 79 J=2,M
        Z(J) = Z(J-1) + GRSPG
   79 CONTINUE
        YFLAG = (Y(M) - CLWIPR) / CLWIPR
        ZFLAG = (Z(M) - CLWIPR) / CLWIPR
        IF((ABS(YFLAG) .GT. 0.001) .OR. (ABS(ZFLAG) .GT. 0.001)) GO
       *TO 9999
C
        PRINT 305
        PRINT 432
        WRITE(6,433) (Y(I),I=1,M)
        PRINT 306
        PRINT 434
        WRITE(6,433) (Z(J),J=1,M)
```

```
C
C     **** INITIALIZATION BY ZERO ****
C
      DO 4 I=1,M
      DO 4 J=1,M
      OMEG(I,J) = 0.0
      EPS(I,J) = 0.0
      TKE(I,J) = 0.0
      TED(I,J) = 0.0
      U(I,J) = 0.0
      V(I,J) = 0.0
      W(I,J) = 0.0
      AMUT(I,J) = 0.0
      VP(I,J) = 0.0
      VORSOR(I,J) = 0.0
      AE(I,J) = 0.0
      AW(I,J) = 0.0
      AN(I,J) = 0.0
      AS(I,J) = 0.0
    4 CONTINUE
C
C     **** ASSUMED INITIAL VALUES ****
C
      UFAVW = 0.150
      TOWAVW = ROW * UFAVW * UFAVW
      DPDX = 4.0 * TOWAVW / DEQ
      TKEI = UFAVW * UFAVW / SQRT(CMU)
      TEDI = UFAVW**3 / (CAPA * Z(2))
      ZPLUS = ROW * UFAVW * Z(2) / AMU
      UIN = UFAVW * (A * ALOG(ZPLUS) + B)
      DO 902 I=1,M1
      UFW(I) = UFAVW
      UP(I) = UIN
      TKEP(I) = TKEI
      TEDP(I) = TEDI
  902 CONTINUE
C
      DO 8 J=2,M
      K = M-(J-1)
      DO 8 I=1,K
      U(I,J) = UBAV
      TKE(I,J) = TKEI
      TED(I,J) = 0.5 * TEDI
    8 CONTINUE
C
      PRINT 484
      WRITE(6,*) ZPLUS
      PRINT 418
      WRITE(6,*) (TED(I,2),I=1,M2)
      PRINT 407, UFAVW,TOWAVW,DPDX,TKEI,TEDI
C
C     **** COEFFICIENT CALCULATIONS FOR VORTICITY AND STREAM FUNCTION
C     EQUATIONS ****
C
      DO 58 J=2,M2
      K = M-J
      DO 58 I=2,K
      BEP(I,J) = 0.25 * (Z(J+1)-Z(J-1)) / (Y(I+1)-Y(I))
      BWP(I,J) = 0.25 * (Z(J+1)-Z(J-1)) / (Y(I)-Y(I-1))
      BNP(I,J) = 0.25 * (Y(I+1)-Y(I-1)) / (Z(J+1) - Z(J))
      BSP(I,J) = 0.25 * (Y(I+1)-Y(I-1)) / (Z(J) - Z(J-1))
      VP(I,J) = 0.25 * (Y(I+1)-Y(I-1)) * (Z(J+1)-Z(J-1))
   58 CONTINUE
C
```

```
      SUMDA = 0.0
      DO 96 J=2,M1
      K = M-(J-1)
      DO 96 I=2,K
      DA(I,J) = (Y(I)-Y(I-1)) * (Z(J)-Z(J-1))
      SUMDA = SUMDA + DA(I,J)
   96 CONTINUE
      DO 99 J=2,M
      K = M-(J-1)
      I = K
      DAT(I,J) = (Y(I+1) - Y(I)) * (Z(J) - Z(J-1)) / 2.0
      SUMDA = SUMDA + DAT(I,J)
   99 CONTINUE
      PRINT 425, SUMDA
C
      ROWCMU = ROW * CMU**0.25
      DO 136 I=1,M
      YSTR(I) = Y(I) / CLWTPR
  136 CONTINUE
C
C     **** MAIN LOOP OF ITERATIONS ****
C
      ICOUNT = 0
  900 ICOUNT = ICOUNT + 1
C
C     **** INITIALIZATION OF RESIDUALS ****
C
      RSWM = 0.0
      RSEPM = 0.0
      RSKM = 0.0
      RSEM = 0.0
      RSUM = 0.0
C
      DO 180 I=1,M
      DO 180 J=1,M
      F1(I,J) = 0.0
      F2(I,J) = 0.0
      F3(I,J) = 0.0
      F4(I,J) = 0.0
      DUY(I,J) = 0.0
      DUZ(I,J) = 0.0
      STSNML(I,J) = 0.0
      DUZS(I,J) = 0.0
      CHCK(I,J) = 0.0
  180 CONTINUE
C
      IF(IVORT .EQ. 1) GO TO 703
C
C     **** A'S CALCULATIONS ****
C
C
      DO 31 J=2,M2
      K = M-J
      DO 31 I=2,K
      AEP = EPS(I+1,J-1) + EPS(I,J-1) - EPS(I+1,J+1) - EPS(I,J+1)
      AE(I,J) = (AEP + ABS(AEP)) / 8.0
      AWP = EPS(I-1,J+1) + EPS(I,J+1) - EPS(I-1,J-1) - EPS(I,J-1)
      AW(I,J) = (AWP + ABS(AWP)) / 8.0
      ANP = EPS(I+1,J+1) + EPS(I+1,J) - EPS(I-1,J+1) - EPS(I-1,J)
      AN(I,J) = (ANP + ABS(ANP)) / 8.0
      ASP = EPS(I-1,J-1) + EPS(I-1,J) - EPS(I+1,J-1) - EPS(I+1,J)
      AS(I,J) = (ASP + ABS(ASP)) / 8.0
   31 CONTINUE
C
```

```
  703 CONTINUE
C
C     **** EDDY VISCOSITY ( MUT ) ****
C
      DO 42 J=2,M
      K = M-(J-1)
      DO 42 I=1,K
      IF(TED(I,J) .EQ. 0.0) GO TO 43
      AMUT(I,J) = CMU * ROW * (TKE(I,J)**2) / TED(I,J)
      GO TO 42
   43 AMUT(I,J) = 0.0
   42 CONTINUE
C
C     **** COEFFICIENT FOR THE VORTICITY SOURCE TERM ****
C     **** DUY AND DUZ ARE TRANSIENT LOCATIONS ****
C
      DO 555 J=1,M2
      K = M-J
      DO 555 I=2,K
      YRAT(I,J) = (Y(I) - Y(I-1)) / (Y(I+1) - Y(I))
  555 CONTINUE
C
      DO 666 J=2,M2
      K = M-J
      DO 666 I=1,K
      ZRAT(I,J) = (Z(J) - Z(J-1)) / (Z(J+1) - Z(J))
  666 CONTINUE
C
      DO 34 J=2,M2
      K = M-J
      DO 34 I=1,K
      DUZ(I,J) = ((U(I,J+1) - U(I,J)) * ZRAT(I,J) + (U(I,J) - U(I,
     *J-1)) / ZRAT(I,J)) / (Z(J+1) - Z(J-1))
   34 CONTINUE
C
      DO 65 J=2,M2
      K = M-J
      DO 65 I=2,K
      DUY(I,J) = ((U(I+1,J) - U(I,J)) * YRAT(I,J) + (U(I,J) - U(I-1,
     *J)) / YRAT(I,J)) / (Y(I+1) - Y(I-1))
   65 CONTINUE
C
C     **** DV/DY AND DW/DZ BOUNDARY VALUES ****
C     **** AT THE WALL ( NOTE: DUY = 0 ) ****
C
C
      DO 14 I=1,M1
      DUZ(I,1) = U(I,2) / (Z(2) - Z(1))
   14 CONTINUE
      DUZ(1,M1) = (U(1,M1) - U(1,M2)) / (Z(M1) - Z(M2))
      DO 111 J=2,M1
      K = M-(J-1)
      I = K
      DUZ(I,J) = (U(I,J) - U(I,J-1)) / (Z(J) - Z(J-1))
  111 CONTINUE
C
      DO 554 I=1,M
      DUY(I,1) = 0.0
  554 CONTINUE
C
      DO 206 J=2,M1
      K = M-(J-1)
      I = K
      DUY(I,J) = (U(I,J) - U(I-1,J)) / (Y(I) - Y(I-1))
```

```
  206 CONTINUE
      DUZ(M,1) = 0.0
C
C     **** LAUNDER AND YING APPROXIMATION ****
C     **** FOR VORTICITY SOURCE TERM CALCULATIONS ****
C
C     **** F1: THE NORMAL STRESSES ****
C     **** F2: COEFFICIENT FOR K & E SOURCE TERM ****
C     **** F4: THE SHEAR STRESSES ****
C
      DO 173 J=1,M
      K = M-(J-1)
      DO 173 I=1,K
      DUYSQ = DUY(I,J)**2
      DUZSQ = DUZ(I,J)**2
      F2(I,J) = (DUYSQ + DUZSQ) / SIGMU
      IF(IVORT .EQ. 1) GO TO 173
      IF(TED(I,J) .EQ. 0.0) GO TO 178
      FACTOR = CPRIME * AMUT(I,J) * TKE(I,J) / TED(I,J)
      GO TO 179
  178 FACTOR = 0.0
  179 CONTINUE
      IF(INORML .EQ. 1) GO TO 716
      F1(I,J) = FACTOR * (DUZSQ - DUYSQ)
  716 CONTINUE
      IF(ISHEAR .EQ. 1) GO TO 173
      F4(I,J) = FACTOR * DUY(I,J) * DUZ(I,J)
  173 CONTINUE
C
      IF(IVORT .EQ. 1) GO TO 704
      IF(INORML .EQ. 1) GO TO 717
C
C     **** CLEAR LOCATIONS DUY AND DUZ ****
C
      DO 126 I=1,M
      DO 126 J=1,M
      DUY(I,J) = 0.0
      DUZ(I,J) = 0.0
  126 CONTINUE
C
C     **** NOTE: F3 IS A TRANSIENT LOCATION ****
C
      DO 49 J=2,M2
      K = M-J
      DO 49 I=1,K
      F3(I,J) = ((F1(I,J+1) - F1(I,J)) * ZRAT(I,J) + (F1(I,J) - F1
     *(I,J-1)) / ZRAT(I,J)) / (Z(J+1) - Z(J-1))
   49 CONTINUE
C
C     **** BOUNDARY VALUES ****
C
      DO 68 J=2,M1
      K = M-(J-1)
      I = K
      F3(I,J) = (F1(I,J) - F1(I,J-1)) / (Z(J) - Z(J-1))
   68 CONTINUE
      DO 903 I=1,M1
      F3(I,1) = (F1(I,2) - F1(I,1)) / (Z(2) - Z(1))
  903 CONTINUE
C
      DO 48 J=2,M2
      K = M-J
      DO 48 I=2,K
      DUY(I,J) = ((F3(I+1,J) - F3(I,J)) * YRAT(I,J) + (F3(I,J) - F3
```

```
321.       *(I-1,J)) / YRAT(I,J)) / (Y(I+1) - Y(I-1))
322.     48 CONTINUE
323.  C
324.  C      **** CLEAR LOCATION F1 ****
325.  C
326.        DO 137 I=1,M
327.        DO 137 J=1,M
328.        F1(I,J) = 0.0
329.    137 CONTINUE
330.  C
331.  C      **** VORT. SOURCE TERM - NORMAL STRESSES - STORED IN F1 LOCN. ****
332.  C
333.        DO 40 J=2,M2
334.        K = M-J
335.        DO 40 I=2,K
336.        F1(I,J) = DUY(I,J)
337.        STSNML(I,J) = (F1(I,J) * CLWTPR * CLWTPR) /(ROW * UFN(I) * UFN(I))
338.     40 CONTINUE
339.  C
340.  C
341.    717 CONTINUE
342.  C
343.  C      **** CLEAR LOCATIONS DUY ****
344.  C
345.        DO 171 I=1,M
346.        DO 171 J=1,M
347.        DUY(I,J) = 0.0
348.  C     DUZ(I,J) = 0.0
349.        IF(INORML .EQ. 1) F1(I,J) = 0.0
350.    171 CONTINUE
351.  C
352.        IF(ISHEAR .EQ. 1) GO TO 718
353.  C
354.  C
355.  C      **** VORTICITY SOURCE TERM - SHEAR STRESS CALCULATIONS ****
356.  C
357.        DO 51 J=2,M2
358.        K = M-J
359.        DO 51 I=1,K
360.        DUZ(I,J) = ((F4(I,J+1) - F4(I,J)) * ZRAT(I,J) + (F4(I,J) - F4
361.       *(I,J-1)) / ZRAT(I,J)) / (Z(J+1) - Z(J-1))
362.     51 CONTINUE
363.  C
364.  C      **** BOUNDARY VALUES ****
365.  C
366.        DO 24 J=2,M1
367.        K = M-(J-1)
368.        I = K
369.        DUZ(I,J) = (F4(I,J) - F4(I,J-1)) / (Z(J) - Z(J-1))
370.     24 CONTINUE
371.  C
372.        DO 17 I=1,M1
373.        DUZ(I,1) = F4(I,2) / (Z(2) - Z(1))
374.     17 CONTINUE
375.  C
376.        DO 15 J=2,M2
377.        K = M-J
378.        DO 15 I=2,K
379.        DUY(I,J) = ((F4(I+1,J) - F4(I,J)) * YRAT(I,J) + (F4(I,J) - F4
380.       *(I-1,J)) / YRAT(I,J)) / (Y(I+1) - Y(I-1))
381.     15 CONTINUE
382.  C
383.  C      **** BOUNDARY VALUES ****
384.  C
```

```
      DO 138 J=2,M1
      K = M-(J-1)
      I = K
      DUY(I,J) = (F4(I,J) - F4(I-1,J)) / (Y(I) - Y(I-1))
  138 CONTINUE
C
C     **** CLEAR LOCATIONS F3 AND F4 ****
C
      DO 172 I=1,M
      DO 172 J=1,M
      F3(I,J) = 0.0
      F4(I,J) = 0.0
  172 CONTINUE
C
      DO 53 J=2,M2
      K = M-J
      DO 53 I=2,K
      F4(I,J) = ((DUZ(I,J+1) - DUZ(I,J)) * ZRAT(I,J) + (DUZ(I,J) -
     *DUZ(I,J-1)) / ZRAT(I,J)) / (Z(J+1) - Z(J-1))
      F3(I,J) = ((DUY(I+1,J) - DUY(I,J)) * YRAT(I,J) + (DUY(I,J) -
     *DUY(I-1,J)) / YRAT(I,J)) / (Y(I+1) - Y(I-1))
   53 CONTINUE
C
  718 CONTINUE
C
C     **** CLEAR LOCATION DUDZ ****
C
      DO 175 I=1,M
      DO 175 J=1,M
      DUZ(I,J) = 0.0
  175 CONTINUE
C
C     **** VORTICITY SOURCE TERM : NORMAL + SHEAR STRESSES ****
C     **** VORTICITY SOURCE TERM - SHEAR STRESS - STORED IN LOCN DUZ ***
C
      DO 55 J=2,M2
      K = M-J
      DO 55 I=2,K
      IF(ISHEAR .EQ. 1) GO TO 54
C
      DUZ(I,J) = F3(I,J) - F4(I,J)
      DUZS(I,J) = DUZ(I,J)
   54 VORSOR(I,J) = + (F1(I,J) + DUZ(I,J))
      CHCK(I,J) = (VORSOR(I,J) * CLWTPR*CLWTPR)/(ROW* UPW(I) * UPW(I))
   55 CONTINUE
C
C     **** VORTICITY SUBCYCLE ****
C
      DO 56 J=2,M2
      K = M-J
      DO 56 I=2,K
      CE = AE(I,J) + 2.0 * AMU * BEP(I,J)
      CW = AW(I,J) + 2.0 * AMU * BWP(I,J)
      CN = AN(I,J) + 2.0 * AMU * BNP(I,J)
      CS = AS(I,J) + 2.0 * AMU * BSP(I,J)
      SGMAB = CE + CW + CN + CS
      SOURCE = VP(I,J) * VORSOR(I,J)
      OMEGA = (CE * OMEG(I+1,J) + CW * OMEG(I-1,J) + CN * OMEG(I,J+1)
     *+ CS * OMEG(I,J-1) + SOURCE) / SGMAB
C
C     **** CALCULATE RESIDUALS ****
C
      IF(OMEGA .EQ. 0.0) GO TO 182
      RSW = (OMEGA - OMEG(I,J)) / OMEGA
```

```
449.          RSWF(I,J) = RSW
450.          IF(ABS(RSW) .GT. ABS(RSWM)) RSWM=RSW
451.      182 OMEG(I,J) = ALFAW * OMEGA + (1.0 - ALFAW) * OMEG(I,J)
452.       56 CONTINUE
453.  C
454.  C       **** THE VORTICITY BOUNDARY VALUE ( AT THE WALL ) ****
455.  C       **** OMEGA IS ZERO AT CORNER & MIDWALL BISECTORS ****
456.  C
457.          SLOPW = Z(2) / (Z(3) - Z(2))
458.          DO 26 I=2,M3
459.          OMEG(I,1) = OMEG(I,2) + SLOPW * (OMEG(I,2) - OMEG(I,3))
460.       26 CONTINUE
461.          OMEG(M2,1) = OMEG(M3,1) * (Y(M) - Y(M2)) / (Y(M) - Y(M3))
462.          OMEG(M1,1) = OMEG(M2,1) * (Y(M) - Y(M1)) / (Y(M) - Y(M2))
463.  C
464.  C       **** STREAM FUNCTION SUBCYCLE ****
465.  C
466.          DO 62 J=2,M2
467.          K = M-J
468.          DO 62 I=2,K
469.          SGMB = 2.0 * (BEF(I,J) + BWF(I,J) + BNF(I,J) + BSF(I,J))
470.          SOURCE = OMEG(I,J) * VP(I,J) * ROW
471.  C
472.  C       **** HERE C'S = B'S AS A'S ARE ZERO ****
473.  C
474.          EPSI = (2.0 * (BEF(I,J) * EPS(I+1,J) + BWF(I,J) * EPS(I-1,J) +
475.         *BNF(I,J) * EPS(I,J+1) + BSF(I,J) * EPS(I,J-1)) + SOURCE) / SGMB
476.  C
477.  C       **** CALCULATE RESIDUALS ****
478.  C
479.          IF(EPSI .EQ. 0.0) GO TO 183
480.          RSEP = (EPSI - EPS(I,J)) / EPSI
481.          RSEPF(I,J) = RSEP
482.          IF(ABS(RSEP) .GT. ABS(RSEPM)) RSEPM=RSEP
483.      183 EPS(I,J) = ALFAEP * EPSI + (1.0 - ALFAEP) * EPS(I,J)
484.       62 CONTINUE
485.  C
486.      704 CONTINUE
487.  C
488.  C       **** CLEAR LOCATIONS F3 AND F4 ****
489.  C
490.          DO 69 I=1,M
491.          DO 69 J=1,M
492.          F3(I,J) = 0.0
493.          F4(I,J) = 0.0
494.       69 CONTINUE
495.  C
496.  C       **** COEFFICIENT FOR K EQUATION ****
497.  C
498.          DO 146 J=2,M2
499.          K = M-J
500.          DO 146 I=2,K
501.          IF(TKE(I,J) .EQ. 0.0) GO TO 146
502.          F4(I,J) = ROW * VP(I,J) * TED(I,J) / TKE(I,J)
503.      146 CONTINUE
504.  C
505.  C       **** K SUBCYCLE ****
506.  C
507.          DO 67 J=3,M2
508.          K = M-J
509.          DO 67 I=2,K
510.          CE = AE(I,J) + BEF(I,J) * (2.0 * AMU + (AMUT(I,J) + AMUT(I+1,J))
511.         */ SIGMK)
512.          CW = AW(I,J) + BWF(I,J) * (2.0 * AMU + (AMUT(I,J) + AMUT(I-1,J))
```

```
513.       */ SIGMK)
514.        CN = AN(I,J) + BNF(I,J) * (2.0 * AMU + (AMUT(I,J) + AMUT(I,J+1))
515.       */ SIGMK)
516.        CS = AS(I,J) + BSF(I,J) * (2.0 * AMU + (AMUT(I,J) + AMUT(I,J-1))
517.       */ SIGMK)
518.        SGMABK = CE + CW + CN + CS
519.        TKEY = (CE * TKE(I+1,J) + CW * TKE(I-1,J) + CN * TKE(I,J+1) + CS
520.       **TKE(I,J-1) + AMUT(I,J) * F2(I,J) * VP(I,J)) / (SGMABK + F4(I,J))
521. C
522. C      **** CALCULATE RESIDUALS ****
523. C
524.        IF(TKEY .EQ. 0.0) GO TO 184
525.        RSK = (TKEY - TKE(I,J)) / TKEY
526.        IF(ABS(RSK) .GT. ABS(RSKM)) RSKM=RSK
527.    184 TKE(I,J) = ALFAK * TKEY + (1.0 - ALFAK) * TKE(I,J)
528.     67 CONTINUE
529. C
530. C      **** DISSIPATION SOURCE TERM STORED IN LOCATION F3 ****
531. C
532.        DO 71 J=2,M2
533.        K = M-J
534.        DO 71 I=2,K
535.        F3(I,J) = CE1 * CMU * TKE(I,J) * F2(I,J) * VP(I,J) * RCW
536.     71 CONTINUE
537. C
538. C      **** DISSIPATION SUBCYCLE ****
539. C
540.        DO 73 J=3,M2
541.        K = M-J
542.        DO 73 I=2,K
543.        CE = AE(I,J) + BEF(I,J) * (2.0 * AMU + (AMUT(I,J) + AMUT(I+1,J))
544.       */ SIGME)
545.        CW = AW(I,J) + BWF(I,J) * (2.0 * AMU + (AMUT(I,J) + AMUT(I-1,J))
546.       */ SIGME)
547.        CN = AN(I,J) + BNF(I,J) * (2.0 * AMU + (AMUT(I,J) + AMUT(I,J+1))
548.       */ SIGME)
549.        CS = AS(I,J) + BSF(I,J) * (2.0 * AMU + (AMUT(I,J) + AMUT(I,J-1))
550.       */ SIGME)
551.        SGMABE = CE + CW + CN + CS
552.        TEDN = (CE * TED(I+1,J) + CW * TED(I-1,J) + CN * TED(I,J+1) + CS
553.       ** TED(I,J-1) + F3(I,J)) / (SGMABE + CE2 * F4(I,J))
554. C
555.        IF(TEDN .LT. 0.0) WRITE(6,*) ICOUNT,I,J,CE,CW,CN,CS
556.        IF(TEDN .LT. 0.0) CALL PRNPUN(F3,M,1,2)
557.        IF(TEDN .LT. 0.0) CALL PRNPUN(F4,M,1,2)
558.        IF(TEDN .LT. 0.0) GO TO 101
559. C
560. C      **** CALCULATE RESIDUALS ****
561. C
562.        IF(TEDN .EQ. 0.0) GO TO 185
563.        RSE = (TEDN - TED(I,J)) / TEDN
564.        IF(ABS(RSE) .GT. ABS(RSEM)) RSEM=RSE
565.    185 TED(I,J) = ALFAE * TEDN + (1.0 - ALFAE) * TED(I,J)
566.     73 CONTINUE
567. C
568. C      **** AXIAL VELOCITY (U) SUBCYCLE ****
569. C
570.        DO 74 J=3,M2
571.        K = M-J
572.        DO 74 I=2,K
573.        CE = AE(I,J) + BEP(I,J) * (2.0 * AMU + (AMUT(I,J) + AMUT(I+1,J))
574.       */ SIGMU)
575.        CW = AW(I,J) + BWF(I,J) * (2.0 * AMU + (AMUT(I,J) + AMUT(I-1,J))
576.       */ SIGMU)
```

```
      CN = AN(I,J) + BNF(I,J) * (2.0 * AMU + (AMUT(I,J) + AMUT(I,J+1))
     */ SIGMU)
      CS = AS(I,J) + BSF(I,J) * (2.0 * AMU + (AMUT(I,J) + AMUT(I,J-1))
     */ SIGMU)
      SGMABU = CE + CW + CN + CS
      U(I,J) = (CE * U(I+1,J) + CW * U(I-1,J) + CN * U(I,J+1) + CS *
     *U(I,J-1) + DPDX * VF(I,J)) / SGMABU
   74 CONTINUE
C
C     **** U, K AND E BOUNDARY CONDITIONS ****
C
C     **** NEAR THE WALL ****
C
C
      DO 155 I=1,M1
      U(I,2) = UP(I)
      TKE(I,2) = TKEP(I)
      TED(I,2) = TEDP(I)
  155 CONTINUE
C
C
C     **** AT THE MIDWALL BISECTOR ****
C
      YRA = ((Y(2) - Y(1))**2 - (Y(3) - Y(1))**2)
      YRB = ((Y(2) - Y(1))**2) / YRA
      YRC = ((Y(3) - Y(1))**2) / YRA
      DO 77 J=2,M2
      TKE(1,J) = YRB * TKE(3,J) - YRC * TKE(2,J)
      TED(1,J) = YRB * TED(3,J) - YRC * TED(2,J)
      U(1,J) = YRB * U(3,J) - YRC * U(2,J)
      IF(TKE(1,J) .LT. 0.0) TKE(1,J)=0.0
      IF(TED(1,J) .LT. 0.0) TED(1,J)=0.0
      IF(U(1,J) .LT. 0.0) U(1,J)=0.0
   77 CONTINUE
C
C     **** AT CORNER BISECTOR ****
C
      DO 76 J=3,M2
      K = M-(J-1)
      I = K
      U(I,J) = U(I-1,J-1)
      TKE(I,J) = TKE(I-1,J-1)
      TED(I,J) = TED(I-1,J-1)
      IF(TKE(I,J) .LT. 0.0) TKE(I,J)=0.0
      IF(TED(I,J+1) .LT. 0.0) TED(I,J+1)=0.0
      IF(U(I,J) .LT. 0.0) U(I,J)=0.0
   76 CONTINUE
C
C     **** NODES NEAR DUCT CENTER ****
C
      YRD = (0.25 * (Z(M) - Z(M1))) / (Z(M) - Z(M2))
      TKE(1,M1) = (TKE(1,M2) * (Z(M1) - Z(M3)) - TKE(1,M3) * (Z(M1)-
     *Z(M2))) / (Z(M2) - Z(M3))
      TED(1,M1) = (TED(1,M2) * (Z(M1) - Z(M3)) - TED(1,M3) * (Z(M1) -
     *Z(M2))) / (Z(M2) - Z(M3))
      U(1,M1) = U(1,M3) + (U(1,M2) - U(1,M3)) * (Z(M1) - Z(M3)) /
     *(Z(M2) - Z(M3))
      U(1,M) = U(1,M1) + YRD * (U(1,M1) - U(1,M2))
      TKE(1,M) = TKE(1,M1) + YRD * (TKE(1,M1) - TKE(1,M2))
      TED(1,M) = TED(1,M1) + YRD * (TED(1,M1) - TED(1,M2))
      U(2,M1) = 0.5 * (U(1,M) + U(3,M2))
      TKE(2,M1) = 0.5 * (TKE(1,M) + TKE(3,M2))
      TED(2,M1) = 0.5 * (TED(1,M) + TED(3,M2))
      L = M
```

```
      DO 545 I=1,2
      IF(I .EQ. 2) L=M1
      DO 545 J=M1,L
      IF(TKE(I,J) .LT. 0.0) TKE(I,J)=0.0
      IF(TED(I,J) .LT. 0.0) TED(I,J)=0.0
      IF(U(I,J) .LT. 0.0) U(I,J)=0.0
  545 CONTINUE
C
C     **** AVERAGE BULK VELOCITY CALCULATION ****
C
      SUM = 0.0
      DO 83 J=2,M1
      K = M-(J-1)
      DO 83 I=2,K
      UAV = (U(I,J) + U(I-1,J) + U(I-1,J-1) + U(I,J-1)) / 4.0
      DV = UAV * DA(I,J)
      SUM = SUM + DV
   83 CONTINUE
C
C     **** TRIANGLES ALONG CORNER BISECTOR ****
C
      DO 82 J=2,M
      K= M-(J-1)
      I = K
      UL = (U(I,J) + U(I,J-1)) / 2.0
      UAV = (2.0 / 3.0) * UL + (1.0 / 3.0) * U(I+1,J-1)
      DV = UAV * DAT(I,J)
      SUM = SUM + DV
   82 CONTINUE
C
      UB = SUM / CLAREA
C
      DO 27 I=1,M2
      RWMUK = ROWCMU * SQRT(TKE(I,3))
      ZDPLS = RWMUK * Z(3) / AMU
      IF(ZDPLS .EQ. 0.0) ZDPLS=ZPLUS
      UPLS4 = A * ALOG(ZDPLS) + E
      TOWW(I) = RWMUK * U(I,3) / UPLS4
   27 CONTINUE
      TOWW(M) = 0.0
      TOWW(M1) = TOWW(M2) * ((Y(M) - Y(M1)) / (Y(M) - Y(M2)))
C
C     **** CALCULATE AVERAGE WALL SHEAR STRESSES ****
C
      SUMW = 0.0
      DO 28 I=2,M
      TOWM = (TOWW(I) + TOWW(I-1)) / 2.0
      SUMW = SUMW + TOWM * (Y(I) - Y(I-1))
   28 CONTINUE
      TOWAVW = SUMW / CLWTPR
      UFAVW = SQRT(TOWAVW / ROW)
      DPDX = 4.0 * TOWAVW / DEQ
C
      DO 29 I=1,M1
      UFW(I) = SQRT(TOWW(I) / ROW)
      TKEP(I) = UFW(I) * UFW(I) / SQRT(CMU)
      TEDP(I) = UFW(I) * UFW(I) * UFW(I) / (CAPA * Z(2))
      ZPLUSP(I) = UFW(I) * Z(2) / ANU
      UP(I) = UFW(I) * (A * ALOG(ZPLUSP(I)) + E)
      TKE(I,2) = TKEP(I)
      TED(I,2) = TEDP(I)
      U(I,2) = UP(I)
   29 CONTINUE
      UFW(M) = 0.0
```

```
705.  C
706.  C     **** CORRCTN OF U EVERYWEERE IN ORDER TO SATISFY CONT EQ ****
707.  C
708.        DO 84 J=2,M
709.        K = M-(J-1)
710.        DO 84 I=1,K
711.        U(I,J) = U(I,J) * UBAV / UB
712.     84 CONTINUE
713.        DO 500 J=2,M
714.        K = M-(J-1)
715.        DO 500 I=1,K
716.        IF(ICOUNT .EQ. 1) GO TO 300
717.        IF(U(I,J) .EQ. 0.0) GO TO 186
718.        RSU = (U(I,J) - UOLD(I,J)) / U(I,J)
719.        IF(ABS(RSU) .GT. ABS(RSUM)) RSUM=RSU
720.    186 U(I,J) = ALFAU * U(I,J) + (1.0 - ALFAU) * UOLD(I,J)
721.    300 UOLD(I,J) = U(I,J)
722.    500 CONTINUE
723.  C
724.        UPLUSW(M) = 0.0
725.        DO 92 I=1,M1
726.        IF(UFW(I) .EQ. 0.0) GO TO 92
727.        UPLUSW(I) = U(I,2) / UFW(I)
729.     92 CONTINUE
729.        IFREQ = ICOUNT / IRPRNT
730.        IFREQ = IFREQ * IRPRNT
731.        IF(ICOUNT .NE. IFREQ) GO TO 91
732.        PRINT 421, ICOUNT
733.        PRINT 422, RSWM,RSEPM,RSKM,RSEM,RSUM
734.  C
735.     91 IF(ABS(RSWM) .LE. ALEDW .AND. ABS(RSEPM) .LE. ALMD .AND. ABS(RSK
736.       *M) .LE. ALMD .AND. ABS(RSEM) .LE. ALMD .AND. ABS(RSUM) .LE. ALMD)
737.       *GO TO 101
738.  C
739.        IFREQ = ICOUNT / IPRINT
740.        IFREQ = IFREQ * IPRINT
741.        IF(ICOUNT .NE. IFREQ) GO TO 100
742.  C
743.        CALL PRINTC(ICOUNT,RSWM,RSEPM,RSKM,RSEM,RSUM,UB,DPDX,UFW,TOWW,
744.       *TOWAVW,UFAVW,ZPLUS,UPLUSW,M1,M)
745.  C
746.        IF(IVORT .EQ. 1) GO TO 708
747.  C
748.        CALL PRVORT(F1,DUZ,VORSOR,INORML,ISHEAR,M)
749.  C
750.    708 CONTINUE
751.  C
752.        CALL PRFILD(OMEG,EPS,TKE,TED,U,AMUT,IVORT,M,2)
753.  C
754.        IF(IVORT .EQ. 1) GO TO 714
755.  C
756.        PRINT 456
757.        CALL PRNPUN(RSWF,M,1)
758.        PRINT 457
759.        CALL PRNPUN(RSEPF,M,1)
760.  C
761.    714 CONTINUE
762.  C
763.    100 IF(ICOUNT .LT. IMAX) GO TO 900
764.  C
765.    101 CONTINUE
766.  C
767.        IF(IVORT .EQ. 1) GO TO 705
768.  C
```

```
C      **** SECONDARY VELOCITIES ****
C
C      **** CLEAR LOCATION DUY AND DUZ ****
C
       DO 208 I=1,M
C      K = M- (J-1)
       DO 208 J=1,M
       DUY(I,J) = 0.0
       DUZ(I,J) = 0.0
  208 CONTINUE
C
       DO 177 J=2,M2
       K = M-J
       DO 177 I=2,K
       DUY(I,J) = ((EPS(I+1,J) - EPS(I,J)) * YRAT(I,J) + (EPS(I,J) -
      *EPS(I-1,J)) / YRAT(I,J)) / (Y(I+1) - Y(I-1))
  177 CONTINUE
C
       DO 278 J=2,M2
       K = M-J
       DO 278 I=1,K
       DUZ(I,J) = ((EPS(I,J+1) - EPS(I,J)) * ZRAT(I,J) + (EPS(I,J) -
      *EPS(I,J-1)) / ZRAT(I,J)) / (Z(J+1) - Z(J-1))
  278 CONTINUE
C
C      **** BOUNDARY VALUES ****
C      **** AT THE WALL ****
C
       DO 88 I=2,M1
       DUZ(I,1) = EPS(I,2) / (Z(2) - Z(1))
   88 CONTINUE
       DUZ(M,1) = 0.0
       DUZ(1,1) = 0.0
C      **** AT THE CORNER BISECTOR ****
       DO 86 J=2,M1
       K = M- (J-1)
       I = K
       DUZ(I,J) = (EPS(I,J) - EPS(I,J-1)) / (Z(J) - Z(J-1))
   86 CONTINUE
       DUZ(1,M1) = (EPS(1,M1) - EPS(1,M2)) / (Z(M1) - Z(M2))
       DO 1111 I=1,M
       DUY(I,1) = 0.0
 1111 CONTINUE
       DO 2222 J=2,M1
       DUY(1,J) = (EPS(2,J) - EPS(1,J)) / (Y(2) - Y(1))
 2222 CONTINUE
C      **** AT THE CORNER BISECTOR ****
       DO 3333 J=2,M1
       K = M- (J-1)
       I = K
       DUY(I,J) = (EPS(I,J) - EPS(I-1,J)) / (Y(I) - Y(I-1))
 3333 CONTINUE
C
       DO 4444 J=1,M
       K = M- (J-1)
       DO 4444 I=1,K
       V(I,J) = (1.0 / ROW) * DUZ(I,J)
       W(I,J) = -(1.0 / ROW) * DUY(I,J)
 4444 CONTINUE
C
  705 CONTINUE
C
C      **** FRICTION FACTOR CALCULATION ****
C
```

```
      FF = 8.0 * TOWAVW / (ROW * UBAV**2)
C
      PRINT 428, FF
      PRINT 498, AMASS
C
      DO 90 I=1,M
      TOWWCL(I) = TOWW(I) / TOWW(1)
   90 CONTINUE
      DO 89 I=1,M
      TOWW(I) = TOWW(I) / TOWAVW
      UFW(I) = UFW(I) / UFAVW
   89 CONTINUE
      PRINT 423
      WRITE(6,*) (UFW(I),I=1,M)
      PRINT 424
      WRITE(6,*) (TOWW(I),I=1,M)
      PRINT 426
      WRITE(6,*) (TOWWCL(I),I=1,M)
C
      WRITE(9,*) (TOWW(I),I=1,M)
      WRITE(19,*) (TOWWCL(I),I=1,M)
C
      PRINT 453
      WRITE(6,*) (YSTR(I),I=1,M)
C
      IF(IVORT .EQ. 1) GO TO 709
C
      CALL PRVORT(F1,DUZS,VORSCR,INCRML,ISHEAR,M)
  709 CONTINUE
C
      CALL PRFILD(OMEG,EPS,TKE,TED,U,AMUT,2,M,2)
C
      IF(IVORT .EQ. 1) GO TO 711
C
      PRINT 415
      CALL PRNPUN (V,M,1)
      PRINT 416
      CALL PRNPUN (W,M,1)
  711 CONTINUE
C
      DO 94 J=1,M
      K = M-(J-1)
      DO 94 I=1,K
      IF(F3(I,J) .NE. 0.0) F3(I,J)=0.0
      F3(I,J) = TKE(I,J) / UFAVW**2
      TKE(I,J) = TKE(I,J) * 100.0 / (UBAV * UBAV)
      EPS(I,J) = EPS(I,J) * 1000.0
      UBCL(I,J) = U(I,J) / U(1,M)
      UBUBAV(I,J) = U(I,J) / UBAV
      OMEG(I,J) = OMEG(I,J) * CLWIPR / U(1,M)
C
C
   94 CONTINUE
C
      DO 307 J=2,M
      K = M-(J-2)
      DO 307 I=K,M
      UBUBAV(I,J) = UBUBAV(M-J+1,M-I+1)
      UBCL(I,J) = UBCL(M-J+1,M-I+1)
      OMEG(I,J) = OMEG(M-J+1,M-I+1)
      TKE(I,J) = TKE(M-J+1,M-I+1)
      F3(I,J) = F3(M-J+1,M-I+1)
C
      IF(IVORT.EQ.1) GO TO 307
```

```
C
      V(I,J) = -W(M-J+1,M-I+1)
      W(I,J) = -V(M-J+1,M-I+1)
  307 CONTINUE
C
      IF(IVORT .EQ. 1) GO TO 324
C
      VMAX = 0.0
      WMAX = 0.0
      SECMAX = 0.0
      DO 323 J=1,M
      DO 323 I=1,M
      VSEC(I,J) = SQRT(V(I,J) * V(I,J) + W(I,J) * W(I,J))
      V(I,J) = V(I,J) / UEAV * 100.0
      W(I,J) = W(I,J) / UEAV * 100.0
      VSBCL(I,J) = VSEC(I,J) / U(1,M) * 100.0
      VSBUFW(I,J) = VSEC(I,J) / UFAVW
      IF(ABS(W(I,J)) .GT. ABS(WMAX)) WMAX=W(I,J)
      IF(ABS(V(I,J)) .GT. ABS(VMAX)) VMAX=V(I,J)
      IF(VSBCL(I,J) .GT. SECMAX) SECMAX=VSBCL(I,J)
  323 CONTINUE
C
  324 CONTINUE
      WRITE(8,*) ((UBCL(I,J),I=1,M),J=1,M)
      WRITE(11,*) ((EPS(I,J),I=1,M),J=1,M)
      WRITE(12,*) ((UBUBAV(I,J),I=1,M),J=1,M)
      WRITE(20,*) ((OMEG(I,J),I=1,M),J=1,M)
      WRITE(13,*) ((TKE(I,J),I=1,M),J=1,M)
      WRITE(21,*) ((F3(I,J),I=1,M),J=1,M)
      IF(IVORT .EQ. 1) GO TO 322
      WRITE(14,*) ((SISNMI(I,J),I=1,M),J=1,M)
      WRITE(15,*) ((VSEC(I,J),I=1,M),J=1,M)
      WRITE(22,*) ((CHCK(I,J),I=1,M),J=1,M)
      WRITE(16,*) ((VSBCL(I,J),I=1,M),J=1,M)
      WRITE(10,*) ((VSBUFW(I,J),I=1,M),J=1,M)
      WRITE(17,*) ((V(I,J),I=1,M),J=1,M)
      WRITE(18,*) ((W(I,J),I=1,M),J=1,M)
  322 CONTINUE
C
C
      PRINT 499
      CALL PRNPUN(F3,M,2)
      PRINT 448
      CALL PRNPUN(TKE,M,2)
      PRINT 449
      CALL PRNPUN(UBUBAV,M,2)
      PRINT 454
      CALL PRNPUN(UBCL,M,2)
C
      IF(IVORT .EQ. 1) GO TO 713
C
      PRINT 450
      CALL PRNPUN(V,M,2)
      PRINT 451
      CALL PRNPUN(W,M,2)
      PRINT 437,VMAX,WMAX,SECMAX
      PRINT 452
      CALL PRNPUN(VSEC,M,2)
      PRINT 454
      CALL PRNPUN(VSBCL,M,2)
      PRINT 458
      CALL PRNPUN(VSBUFW,M,2)
C
  713 CONTINUE
```

```
      C
            IF(IVORT .EQ. 1) GO TO 715
      C
            PRINT 456
            CALL PRNPUN(RSWF,M,1)
            PRINT 457
            CALL PRNPUN(RSEPF,M,1)
            CALL PRNPUN(STSNML,M,1)
      C
        715 CONTINUE
      C
      C
        305 FORMAT(//4X,'THE NODAL DISTANCE IN THE Y - DIRN. (METER) :'/)
        306 FORMAT(//4X,'THE NODAL DISTANCE IN THE Z - DIRN. (METER) :'/)
        400 FORMAT('1',40X,'**** INPUT VALUES ****'///4X,'M  =',I4/4X,'SIZE =
           *',F9.6,2X,'(METER)'/4X,'DEQ  =',F9.6,2X,'(METER)'/4X,'RE  =',F10.2
           */4X,'UBAV  =',E12.5,2X,'(M/SEC)'/4X,'ROW  =',F8.5,2X,'(KG/CU. M)'/
           *4X,'AMU  =',E12.5,2X,'(KG/M SEC)'/4X,'GRSPG  =',F9.6,2X,'(METER)')
        401 FORMAT(//4X,'CONSTANT VALUES :'/4X,'CMU  =',F7.3/4X,'CE1  =',
           *F7.3/4X,'CE2  =',F7.3/4X,'SIGMK  =',F7.3/4X,'SIGME  =',F7.3/4X,
           *'CAPA  =',F8.4/4X,'CPRIME  =',F7.4/)
        399 FORMAT(///10X,'?? FIAG : WRONG SIDE, GRSPG ?? XXX'///)
        402 FORMAT( 4X,'UNDER RELAXATION FACTORS :'/4X,'ALFAW  =',F7.4/4X,
           *'ALFAEP  =',F7.4/4X,'ALFAK  =',F7.4/4X,'ALFAE  =',F7.4/4X,'
           *ALFAU  =',F7.4//4X,'CONVERGENCE VALUES :'/4X,'ALMD  =',F8.5,
           */4X,'ALMDW  =',F8.5/)
        407 FORMAT(//4X,'ASSUMED INITIAL AND BOUNDARY VALUES ARE :'/4X,
           *'UFAVW =',E12.5/4X,'TOWAVW =',E12.5/4X,'DPDX  =',
           *E12.5/4X,'TKEI  =',E12.5/4X,'TEDI  =',E12.5/)
        415 FORMAT( /10X,'THE VELOCITY DISTRIBUTION IN Y - DIRN. (M/SEC) :'/)
        416 FORMAT( /10X,'THE VELOCITY DISTRIBUTION IN Z - DIRN. (M/SEC) :'/)
        418 FORMAT(//4X,'ASSUMED DISSIPTN. I.V. (TED(I,2)) :'/)
        421 FORMAT(///51X,'ICOUNT  =',2X,I5//)
        422 FORMAT(  4X,'RSWM=',E13.6,9X,'RSEPM=',E13.6,9X,'RSKM=',
           *E13.6,9X,'RSEM=',E13.6,9X,'RSOM=',E13.6)
        423 FORMAT(/10X,'FRICTN. VEL. DISTBN. ALONG THE DUCT SURFACE :'/25
           *X,'NORMALIZED BY UFAVW' /)
        424 FORMAT(/10X,'WALL SHEAR STRESS DISTBN. ALONG THE DUCT SURFACE :'
           *,20X,'NORMALIZED BY TOWAVW'/)
        425 FORMAT(/4X,'SUM. DA :',E14.6,2X,'(SQ. M.)')
        426 FORMAT(/10X,'WALL SHEAR STRESS DISTBN. ALONG THE DUCT SURFACE :'
           *,20X,'NORMALIZED BY TOWWCI'/)
        428 FORMAT( /4X,'E.F.  =',E14.6)
        432 FORMAT( 1X,'     I=',3X,'1',10X,'2',10X,'3',10X,'4',10X,'5',10X,'
           *6',10X,'7',10X,'8',10X,'9',10X,'10',10X,'11'/)
        433 FORMAT(5X,11E11.4/5X,10E11.4)
        434 FORMAT( 1X,'     J=',3X,'1',10X,'2',10X,'3',10X,'4',10X,'5',10X,'
           *6',10X,'7',10X,'8',10X,'9',10X,'10',10X,'11'/)
        437 FORMAT(/4X,'VMAX =',E12.5,2X,'(% UB)',20X,'WMAX =',E12.5,2X,
           *'(% UB)',20X,'SECMAX =',E12.5,2X,'(% UB)'/)
        439 FORMAT(/4X,'SIGMU  =',F7.3//)
        448 FORMAT(/10X,'THE T.K.E. DISTBN. NORMALIZED BY (UBAV SQ) :'/)
        449 FORMAT(/10X,'THE AXIAL VEL. DISTBN. NRMALIZED BY UBAV :'/)
        450 FORMAT(/10X,'THE VEL. DISTBN. IN Y - DIRN. %AGE OF UBAV :'/)
        451 FORMAT(/10X,'THE VEL. DISTBN. IN Z - DIRN. %AGE OF UBAV :'/)
        452 FORMAT(/10X,'THE SECONDARY VELOCITY - %AGE OF UBAV :'/)
        453 FORMAT  (/4X,'DISTANCE FROM MIDWALL BISECTOR NORMALIZED BY DUCT
           * LENGTH UNDER CONSIDERATION (Y*)'/)
        454 FORMAT(/10X,'THE SECY. VEL.DISTBN. NORMALIZED BY UCI :'/)
        455 FORMAT(/4X,'DUCT CROSS SECTN. AREA :',E14.6,2X,'(SQ. M)',/4X,
           *'CELL CROSS SECTN. AREA :',E14.6,2X,'(SQ. M)')
        456 FORMAT(//10X,'THE VORTICITY RESIDUALS :'/)
        457 FORMAT(//10X,'THE STREAM FUNCTION RESIDUALS :'/)
        458 FORMAT(/10X,'THE SECY. VEL. DISTIBN. NORMALIZED BY UFAVW :'/)
```

```
1025.    484 FORMAT(//4X,'THE DIMNSNLESS NORMAL DISTANCE FROM THE WALL :',5X,
1026.       *E12.5//)
1027.    485 FORMAT(/4X,'LAW OF THE WALL CONSTANTS :'/4X,'A  =',E10.4/4X,
1028.       *'E  =',F10.4/)
1029.    498 FORMAT(/4X,'MASS RATE OF FLOW (KG/SEC) :',E12.4/)
1030.    499 FORMAT(/4X,'       K / UF**2 :'/)
1031.        GO TO 1112
1032.   9999 CONTINUE
1033.        WRITE(6,399)
1034.   1112 STOP
1035.        END
1036.  C
1037.  C
1038.        SUBROUTINE PRNPUN(PHI,M,N)
1039.  C
1040.        REAL PHI(31,31)
1041.  C
1042.        IF(N .EQ. 2) GO TO 509
1043.        PRINT 432
1044.        DO 507 J=1,M
1045.        K = M-(J-1)
1046.        PRINT 433,J,(PHI(I,J),I=1,K)
1047.    507 CONTINUE
1048.    509 CONTINUE
1049.        IF(N .EQ. 1) GO TO 510
1050.        DO 508 J=1,M
1051.        PRINT 433,J,(PHI(I,J),I=1,M)
1052.    508 CONTINUE
1053.    510 CONTINUE
1054.  C
1055.    432 FORMAT( 1X,'(J)  I=',3X,'1',10X,'2',10X,'3',10X,'4',10X,'5',10X,'
1056.       *6',10X,'7',10X,'8',10X,'9',10X,'10',10X,'11'//)
1057.    433 FORMAT(1X,I2,2X,11E11.4/5X,10E11.4)
1058.        RETURN
1059.        END
1060.  C
1061.  C
1062.        SUBROUTINE PRINTC(ICOUNT,RSWM,RSEPM,RSKM,RSEM,RSUM,UB,DPDX,UFW,
1063.       *TOWW,TOWAVW,UFAVW,ZPLUS,UPLUSW,M1,M)
1064.        REAL TOWW(31),UFW(31),UPLUSW(31)
1065.        PRINT 421,ICOUNT
1066.        PRINT 422,RSWM,RSEPM,RSKM,RSEM,RSUM
1067.        PRINT 485
1068.        WRITE(6,*) UB
1069.        PRINT 423,UFAVW,TOWAVW,DPDX
1070.        PRINT 481
1071.        WRITE(6,*) (UFW(I),I=1,M)
1072.        PRINT 480
1073.        WRITE(6,*) (TOWW(I),I=1,M)
1074.        PRINT 483
1075.        WRITE(6,*) (UPLUSW(I),I=1,M)
1076.        PRINT 484
1077.        WRITE(6,*) ZPLUS
1078.    421 FORMAT(///51X,'ICOUNT=',2X,I5//)
1079.    422 FORMAT( 4X,'RSWM=',E13.6,9X,'RSEPM=',E13.6,9X,'RSKM=',E13.6,9X,'
1080.       *RSEM=',E13.6,9X,'RSUM=',E13.6//)
1081.    423 FORMAT(/4X,'UFAVW=',E12.5,2X,'(M/SEC)'//4X,'TOWAVW=',E12.5,2X,
1082.       *'(N/SQ M)'//4X,'DPDX=',E12.5,2X,'(PA/M)'/)
1083.    480 FORMAT(/10X,'THE WALL SHEAR STRESS DISTBN. ALONG THE DUCT SURFACE
1084.       * : (N/SQ.M)'/)
1085.    481 FORMAT(/10X,'THE FRICTION VELOCITY DISTRIBUTION ALONG THE DUCT SU
1086.       *FACE : (M/SEC)'/)
1087.    483 FORMAT(/10X,'THE LOG-LAW VEL. DISTBN. ALONG THE WALL :'/)
1088.    484 FORMAT(/10X,'THE DIMNSNLESS NORMAL DISTANCE FROM THE WALL (ZPLUS)
```

```
1089.       *=',E12.5//)
1090.    485 FORMAT(4X,'UB = ',5X,E12.5,2X,'(M/SEC)'/)
1091.       RETURN
1092.       END
1093. C
1094. C
1095.       SUBROUTINE PRVORT(F1,DUZ,VORSOR,INORML,ISHEAR,M)
1096. C
1097.       REAL F1(31,31),DUZ(31,31),VORSOR(31,31)
1098. C
1099.       IF(INORML .EQ. 1) GO TO 719
1100. C
1101.       PRINT 418
1102.       PRINT 432
1103.       DO 112 J=1,M
1104.       K = M-(J-1)
1105.       PRINT 433,J,(F1(I,J),I=1,K)
1106.   112 CONTINUE
1107. C
1108.   719 CONTINUE
1109. C
1110.       IF(ISHEAR .EQ. 1) GO TO 720
1111. C
1112.       PRINT 444
1113.       PRINT 432
1114.       DO 212 J=1,M
1115.       K = M-(J-1)
1116.       PRINT 433,J,(DUZ(I,J),I=1,K)
1117.   212 CONTINUE
1118. C
1119.   720 CONTINUE
1120. C
1121.       PRINT 419
1122.       PRINT 432
1123.       DO 114 J=1,M
1124.       K = M-(J-1)
1125.       PRINT 433,J,(VORSOR(I,J),I=1,K)
1126.   114 CONTINUE
1127. C
1128. C
1129.   418 FORMAT(//10X,'THE VORTICITY SOURCE TERM (NORMAL STRESSES) DISTBN.
1130.      * :'/)
1131.   419 FORMAT(//10X,'THE VORT. SOURCE TERM (NORMAL & SHEAR STRESSES) :'/)
1132.   432 FORMAT( 1X,'(J)  I=',3X,'1',10X,'2',10X,'3',10X,'4',10X,'5',10X,'
1133.      *6',10X,'7',10X,'8',10X,'9',10X,'10',10X,'11'//)
1134.   444 FORMAT(//10X,'VORTICITY SOURCE TERM - SHEAR STRESSES DISTBN. :'/)
1135.   433 FORMAT(1X,I2,2X,11E11.4/5X,10E11.4)
1136.       RETURN
1137.       END
1138. C
1139. C
1140.       SUBROUTINE PRFILD(OMEG,EPS,TKE,TED,U,AMUT,IVORT,M,NPOINT)
1141.       REAL OMEG(31,31),EPS(31,31),TKE(31,31),TED(31,31),U(31,31),AMUT
1142.      *(31,31)
1143. C
1144.       IF(IVORT .EQ. 1) GO TO 708
1145. C
1146.       PRINT 410
1147.       PRINT 432
1148.       DO 92 J=1,M
1149.       K = M-(J-1)
1150.       PRINT 433,J,(OMEG(I,J),I=1,K)
1151.    92 CONTINUE
1152.       PRINT 411
```

```
1153.          PRINT 432
1154.          DO 93 J=1,M
1155.          K = M-(J-1)
1156.          PRINT 433,J,(EPS(I,J),I=1,K)
1157.       93 CONTINUE
1158.  C
1159.      708 CONTINUE
1160.  C
1161.          PRINT 412
1162.          PRINT 432
1163.          DO 94 J=1,M
1164.          K = M-(J-1)
1165.          PRINT 433,J,(TKE(I,J),I=1,K)
1166.       94 CONTINUE
1167.          PRINT 413
1168.          PRINT 432
1169.          DO 95 J=1,M
1170.          K = M-(J-1)
1171.          PRINT 433,J,(TED(I,J),I=1,K)
1172.       95 CONTINUE
1173.          PRINT 414
1174.          PRINT 432
1175.          DO 96 J=1,M
1176.          K = M-(J-1)
1177.          PRINT 433,J,(U(I,J),I=1,K)
1178.       96 CONTINUE
1179.          IF(NPRNT .EQ. 1) GO TO 100
1180.          PRINT 417
1181.          PRINT 432
1182.          DO 99 J=1,M
1183.          K = M-(J-1)
1184.          PRINT 433,J,(AMUT(I,J),I=1,K)
1185.       99 CONTINUE
1186.  C
1187.      100 CONTINUE
1188.      410 FORMAT( //10X,'THE VORTICITY DISTRIBUTION (1/SEC) :'/)
1189.      411 FORMAT( //10X,'THE STREAM FUNCTION DISTRIBUTION (KG/M SEC) :'/)
1190.      412 FORMAT( //10X,'THE TURBULENT K.E. DISTRIBUTION (SQ M/SQ SEC) :'/)
1191.      413 FORMAT( //10X,'THE TURBULENT ENERGY DISSPTN. DISTRIBUTION (SQ M/
1192.         *CU SEC):'/)
1193.      414 FORMAT( //10X,'THE AXIAL VELOCITY DISTRIBUTION (M/SEC) :'/)
1194.      417 FORMAT( //10X,'THE EDDY VISCOSITY DISTRIBUTION (KG/M SEC) :'/)
1195.      432 FORMAT( 1X,'(J)  I=',3X,'1',10X,'2',10X,'3',10X,'4',10X,'5',10X,'
1196.         *6',10X,'7',10X,'8',10X,'9',10X,'10',10X,'11'//)
1197.      433 FORMAT(1X,I2,2X,11E11.4/5X,10E11.4)
1198.          RETURN
1199.          END
1200.  $ENTRY
1201.  /*
```

```
C
C     **** SEALE'S SOURCE TERM FOR VORTICITY EQUATION ****
C
      DO 173 J=1,M
      K = M- (J- 1)
      DO 173 I=1,K
      DUYSQ = DUY(I,J)**2
      DUZSQ = DUZ(I,J)**2
      F2(I,J) = (DUYSQ + DUZSQ) / SIGMU
  173 CONTINUE
      IF(IVORT .EQ. 1) GO TO 704
C
C     **** CLEAR LOCATIONS DUY AND DUZ ****
C
      DO 126 I=1,M
      DO 126 J=1,M
      DUY(I,J) = 0.0
      DUZ(I,J) = 0.0
  126 CONTINUE
      DO 49 I=1,M
      DUMMY(I) = Z(M- (I-1))
   49 CONTINUE
C
      DO 68 J=1,M
      K = M- (J- 1)
      DO 68 I=1,K
      ZTOP(I,J) = DUMMY(I)
   68 CONTINUE
C
      DO 48 J=2,M2
      K = M-J
      DO 48 I=2,K
      DTDY(I,J) = ((ZTOP(I+1,J) - ZTOP(I,J)) * YRAT(I,J) + (ZTOP(I,J)
     *- ZTOP(I-1,J)) / YRAT(I,J)) / (Y(I+1) - Y(I-1))
   48 CONTINUE
C
      ZMAX = CLWTPR
C
      CA = 0.0110
      CM = 2.4
      CK = 1.0
      CW = 4.0
C
      DO 40 J=1,M
      K = M- (J- 1)
      DO 40 I=1,K
      ZP(I,J) = (1.0 - (ZTOP(I,J) / ZMAX))
      ZL(I,J) = (1.0 - (Z(J) / ZMAX))
      ZM(I,J) = CK * (1.0 - CM * ZP(I,J) * ZP(I,J))
      ZN(I,J) = (2.0 + ZM(I,J) + ((CW - ZM(I,J)) * ZL(I,J) * ZL(I,J)))
     *- ((1.0 - ZL(I,J) * ZL(I,J)) * (CW - ZM(I,J)))
   40 CONTINUE
C
      FACTOR = 8.0 * CA * CM * BOW * UFAVW * UFAVW *
     *(CK / (CLWTPR * CLWTPR))
C
      DO 51 J=2,M2
      K = M-J
      DO 51 I=2,K
      VORSOR(I,J) = FACTOR * ZP(I,J) * ZL(I,J) * ZN(I,J) * DTDY(I,J)
      STSNML(I,J) = VORSOR(I,J) / BOW * CLWTPR * CLWTPR
   51 CONTINUE
C
C
```

```
C
C     **** ALSHAMANI'S SOURCE TERM FOR VORTICITY EQUATION ****
C
      CPRPR = 0.210
      DO 173 J=1,M
      K = M-(J-1)
      DO 173 I=1,K
      DUYSQ = DUY(I,J)**2
      DUZSQ = DUZ(I,J)**2
      F2(I,J) = (DUYSQ + DUZSQ) / SIGMU
  173 CONTINUE
      IF(IVORT .EQ. 1) GO TO 704
C
C     **** CLEAR LOCATIONS DUY AND DUZ ****
C
      DO 126 I=1,M
      DO 126 J=1,M
      DUY(I,J) = 0.0
      DUZ(I,J) = 0.0
  126 CONTINUE
C
      DO 49 J=1,M
      K = M-(J-1)
      DO 49 I=1,K
      IF(UFW(I) .EQ. 0.0) GO TO 49
      F1(I,J) = TKE(I,J) / (UFW(I) * UFW(I))
   49 CONTINUE
C
      DO 68 J=2,M2
      K = M-J
      DO 68 I=2,K
      DUY(I,J) = ((F1(I+1,J) - F1(I,J)) * YRAT(I,J) +
     *(F1(I,J) - F1(I-1,J)) / YRAT(I,J)) / (Y(I+1) - Y(I-1))
   68 CONTINUE
C     **** BOUNDARY VALUE ****
      DO 48 J=2,M1
      K = M-(J-1)
      I = K
      DUY(I,J) = (F1(I,J) - F1(I-1,J)) / (Y(I) - Y(I-1))
   48 CONTINUE
C
      DO 40 J=2,M2
      K = M-J
      DO 40 I=1,K
      DUZ(I,J) = ((F1(I,J+1) - F1(I,J)) * ZRAT(I,J) + (F1(I,J) -
     *F1(I,J-1)) / ZRAT(I,J)) / (Z(J+1) - Z(J-1))
   40 CONTINUE
C     **** BOUNDARY VALUES ****
      DO 51 J=2,M1
      K = M-(J-1)
      I = K
      DUZ(I,J) = (F1(I,J) - F1(I,J-1)) / (Z(J) - Z(J-1))
   51 CONTINUE
C     DO 52 I=2,M1
C     DUZ(I,1) = (F1(I,2) - F1(I,1)) / (Z(2) - Z(1))
C  52 CONTINUE
C
      DO 24 J=2,M2
      K = M-J
      DO 24 I=2,K
      F4(I,J) = ((DUZ(I+1,J) - DUZ(I,J)) * YRAT(I,J) + (DUZ(1,J) -
     *DUZ(I-1,J)) / YRAT(I,J)) / (Y(I+1) - Y(I-1))
   24 CONTINUE
C
```

```
65.         DO 55 J=2,M2
66.         K = M-J
67.         DO 55 I=2,K
68.         FACTOR = ROW *(UFW(I) * UFW(I)) *  CPRPR
69.         VORSOR(I,J) = FACTOR * ( -.0572 * DUY(I,J) * DUZ(I,J) -
70.        *(( .1245 + .0572 * F1(I,J)) * F4(I,J)))
71.         STSNML(I,J) = VORSOR(I,J) / FACTOR * CPRPR * (CLWIPR ** 2)
72.      55 CONTINUE
73.  C
```

TABLE 1

SUMMARY OF THE CONSTANTS OF MODELS I, II AND III

Constant	Value	Basis of Choice
C_1	1.44	Computer optimization
C_2	1.92	By reference to decay of turbulence behind a grid
C_μ	0.09	By reference to the properties of the "constant-stress" wall region
C'	0.0035	Computer optimization; to achieve predictions in close agreement with the experimental data
C''	0.21	Computer optimization; to achieve predictions in close agreement with the experimental data
C'''	0.0110	Computer optimization; to achieve predictions in close agreement with the experimental data
σ_ε	1.167	By reference to "Constant-Stress" wall region; $\sigma_\varepsilon = (\kappa^2/\sqrt{C_\mu})/(C_2 - C_1)$
σ_k	1.0	
κ	0.41	Von-Karman Constant
A	2.44	Well-established constant of 'Law of the wall'
B	5.0	Well-established constant of 'Law of the wall'.

TABLE 2

COMPARISON OF THE k - ε MODEL CONSTANTS OF THE PRESENT WORK WITH OTHERS

Investigator(s)	C_1	C_2	C_μ	C'	C'''	σ_ε	σ_k	κ	C''
Present Work	1.44	1.92	0.09	0.0035	0.011	1.167	1.0	0.41	0.21
Seale [4], 1982	-	-	-	-	0.045	-	-	-	-
Said [52], 1981	1.44	1.92	0.09	0.003	-	1.167	1.0	0.41	-
Gosman et al [53], 1980	1.44	1.92	0.09	-	-	1.220	1.0	0.42	-
Gosman & Rapley [54], 1978	1.55	2.0	0.09	0.0185	-	1.185	1.0	0.40	-
Tatchell [35], 1975	1.47	1.92	0.09	-	-	1.30	1.0	0.42	-
Launder & Spalding [49], 1974	1.44	1.92	0.09	-	-	1.30	1.0	-	-
Date [66], 1974	1.55	2.0	0.09	-	-	1.30	1.0	0.40	-
Jones & Launder [51], 1973	1.45	2.0	0.09	-	-	1.30	1.0	0.42	-
Jones & Launder [50], 1972	1.55	2.0	0.09	-	-	1.30	1.0	-	-

TABLE 3

THE FUNCTIONS INVOLVED IN THE GENERAL ELLIPTIC EQUATIONS FOR SQUARE DUCTS

Equation	ϕ	a_ϕ	$b_{\phi,y}$	$b_{\phi,z}$	S_ϕ
	$\bar{U}$	1	$\mu + \mu_t$	$\mu + \mu_t$	$\frac{\partial P}{\partial x} = -4\,\bar{\tau}_w/D_h$
	ω	1	μ	μ	$-\rho\{[\frac{\partial^2}{\partial y \partial z}(\bar{v}^2 - \bar{w}^2)] + [\frac{\partial^2}{\partial z^2} - \frac{\partial^2}{\partial y^2}]\,\overline{vw}\}$ for Model I
					$-\rho\,[\frac{\partial^2}{\partial y \partial z}(\bar{v}^2 - \bar{w}^2)]$ for Model II and Model III
	Ψ	0	1	1	$-\rho\,\omega$
	k	1	$\mu + \frac{\mu_t}{\sigma_k}$	$\mu + \frac{\mu_t}{\sigma_k}$	$-\mu_t\,[(\frac{\partial \bar{U}}{\partial y})^2 + (\frac{\partial \bar{U}}{\partial z})^2] + \rho\varepsilon$
	ε	1	$\mu + \frac{\mu_t}{\sigma_\varepsilon}$	$\mu + \frac{\mu_t}{\sigma_\varepsilon}$	$-C_1\,\frac{\mu_t}{k}\,\varepsilon\,[(\frac{\partial \bar{U}}{\partial y})^2 + (\frac{\partial \bar{U}}{\partial z})^2] + C_2\,\frac{\rho\varepsilon^2}{k}$

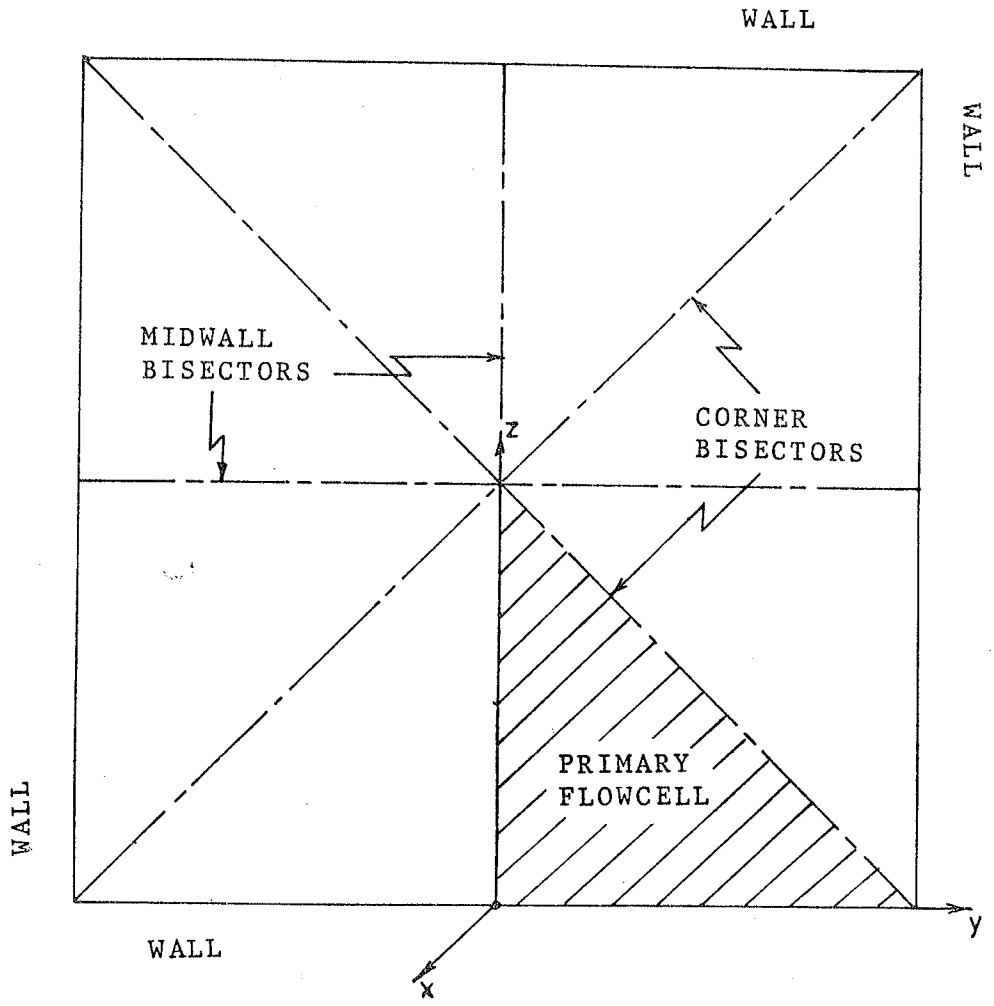

Fig. 1. The domain and coordinate system considered for the analytical models I, II and III

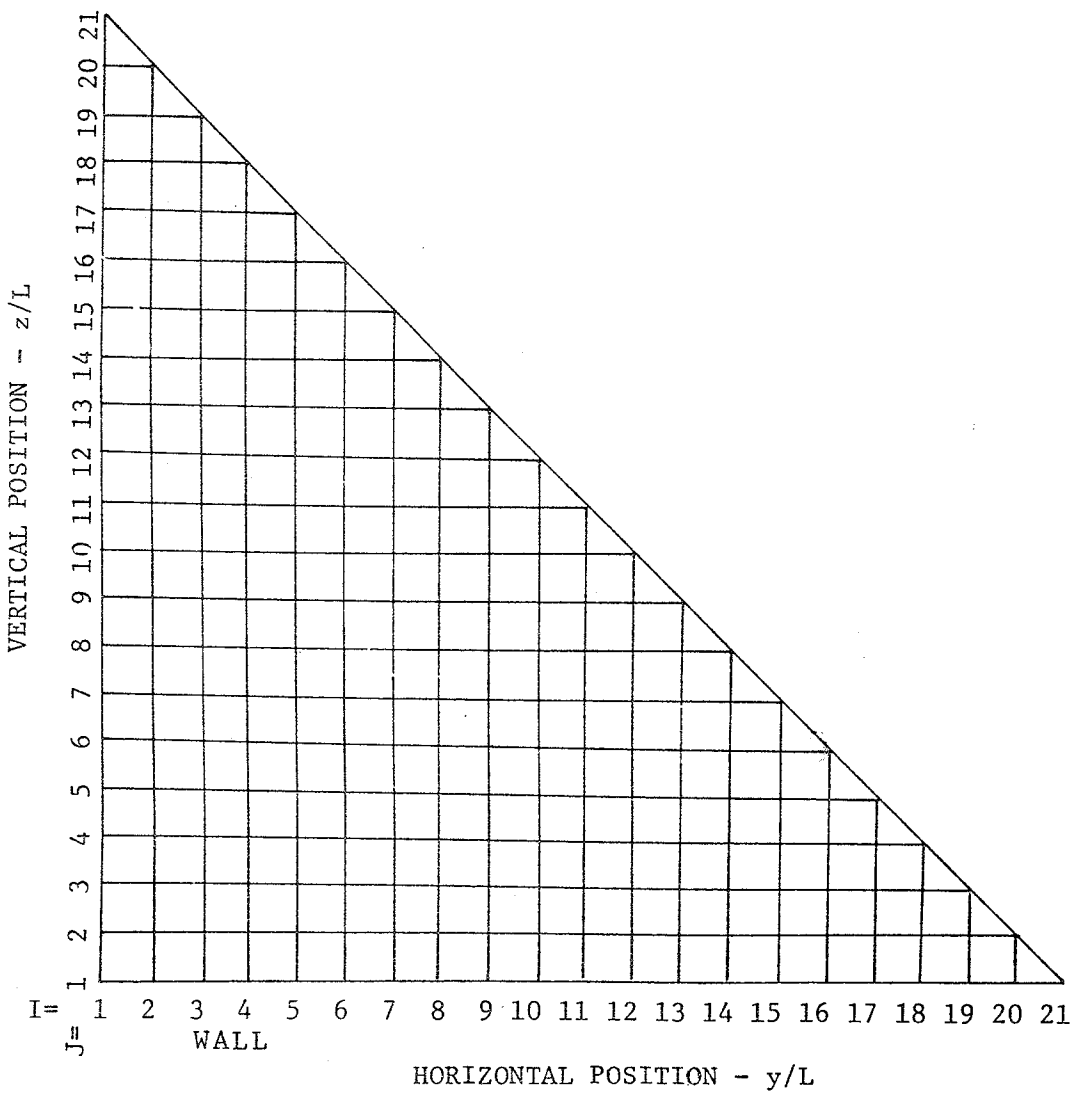

I,J	y/L,z/L
1	0.00
2	0.05
3	0.10
4	0.15
5	0.20
6	0.25
7	0.30
8	0.35
9	0.40
10	0.45
11	0.50
12	0.55
13	0.60
14	0.65
15	0.70
16	0.75
17	0.80
18	0.85
19	0.90
20	0.95
21	1.00

Fig. 2. Finite Difference Grid and Grid Notation for the Analytical Models I, II, III.

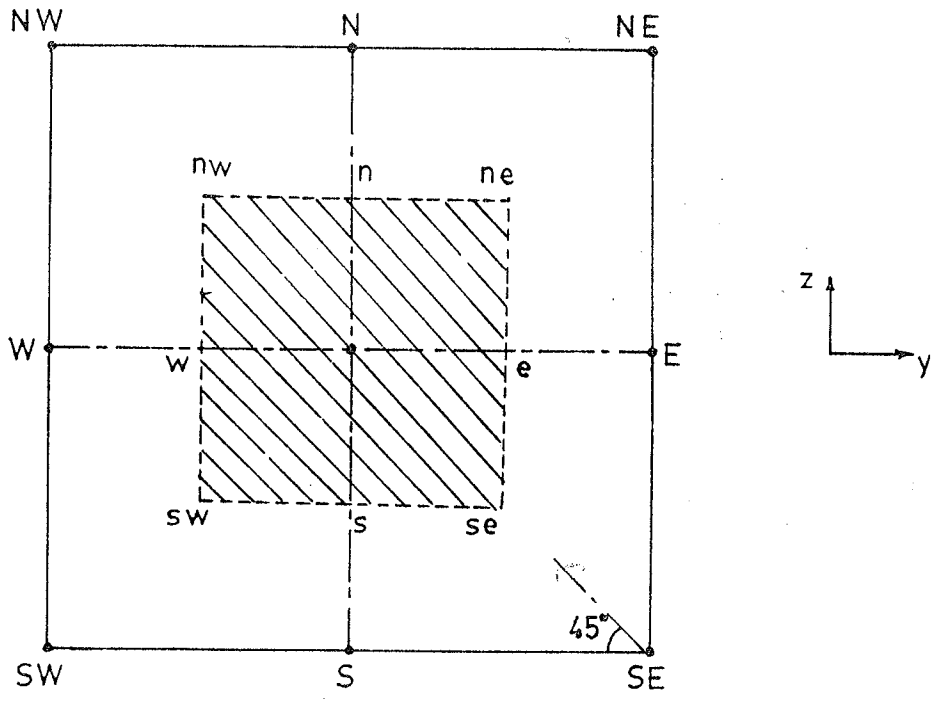

Fig. 3. Portion of the finite difference cartesian grid and the area of integration

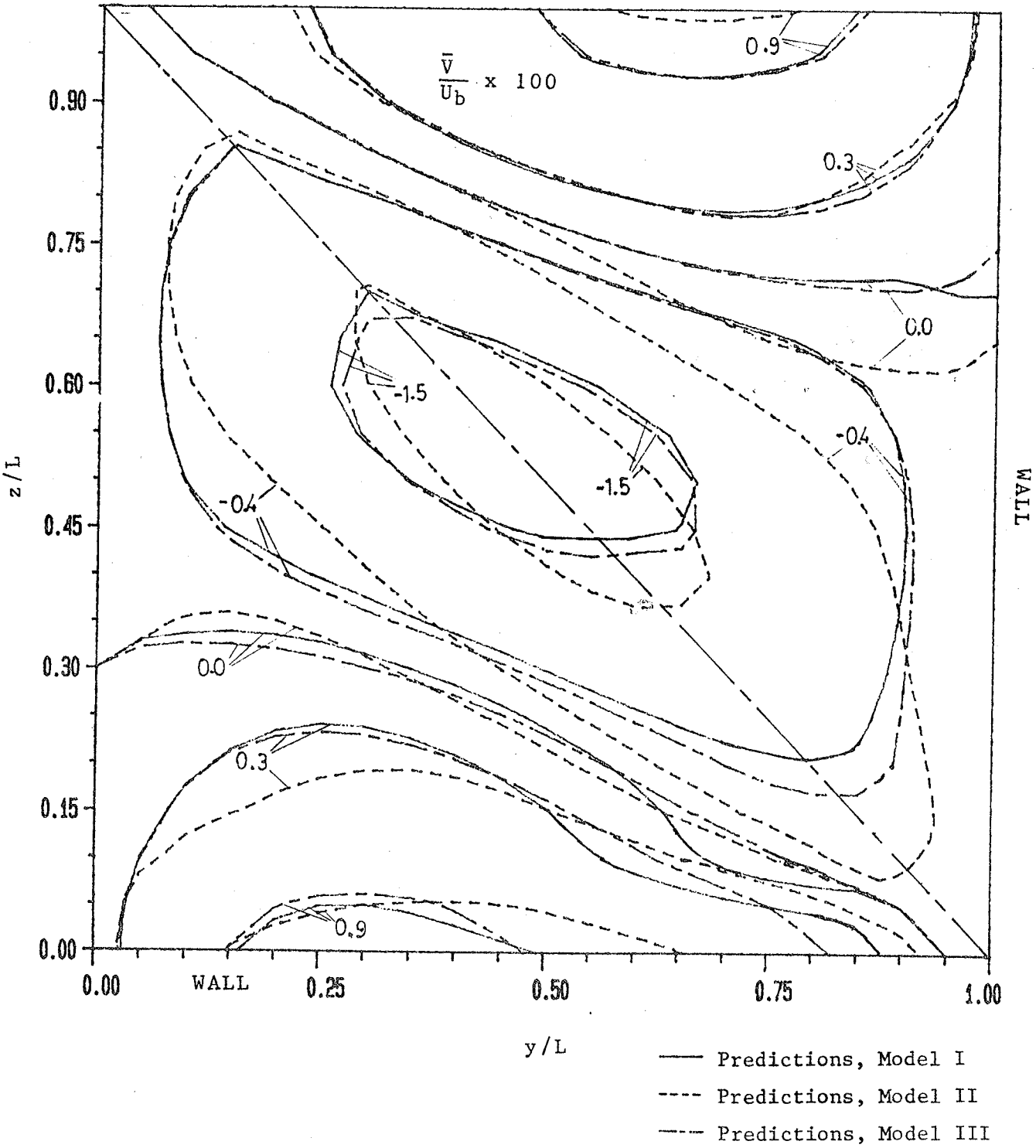

Fig. 4. Comparison of contour plots of predicted secondary velocity, $\bar{V}$ by model I, II and III, Re = 75,000

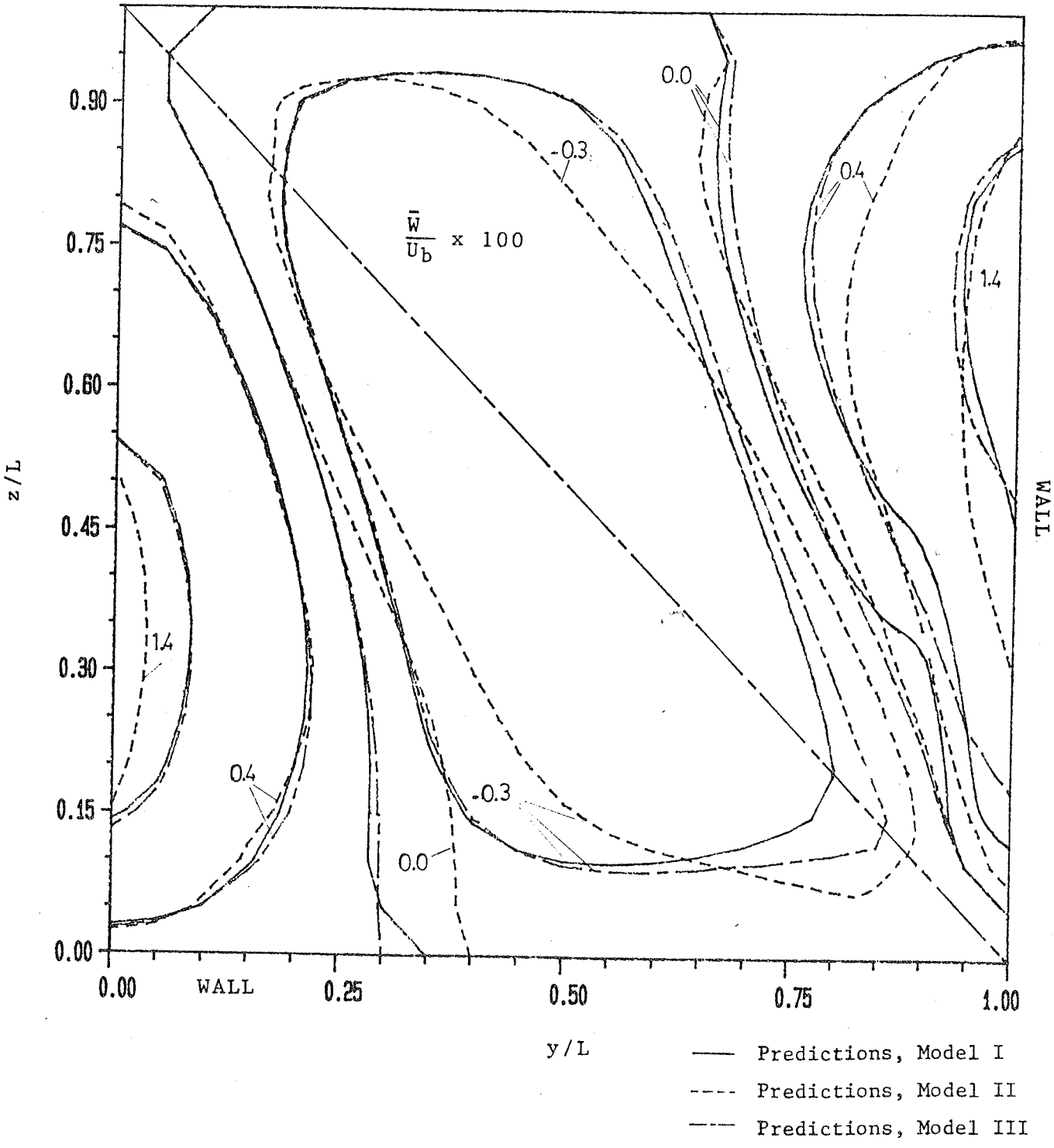

Fig. 5. Comparison of contour plots of predicted secondary velocity, $\bar{W}$ by model I, II and III, Re = 75,000

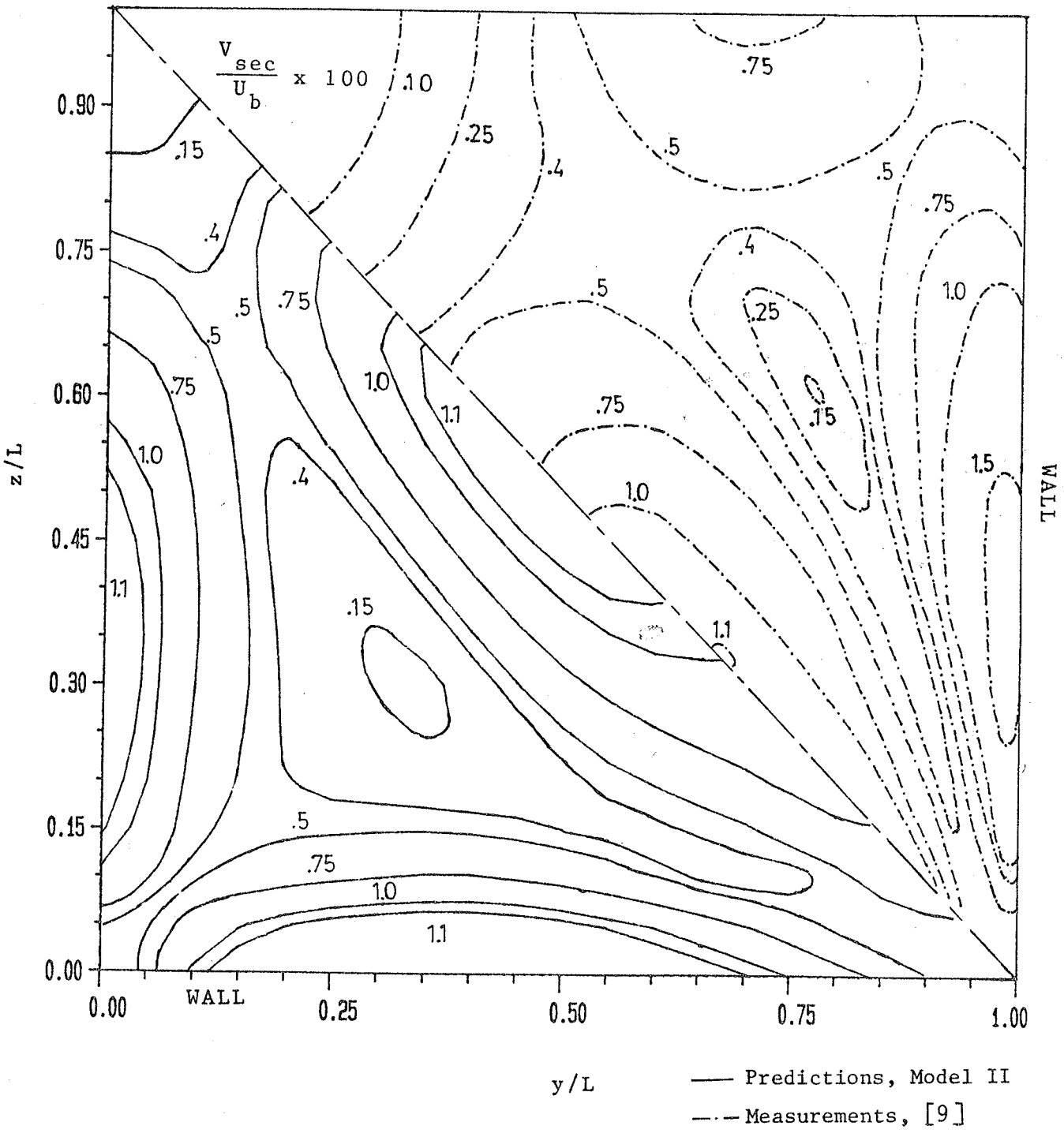

Fig. 6. Comparison of contour plots of predicted resultant secondary velocity, V_{sec} (model II) and measured V_{sec} [9], Re = 75,000

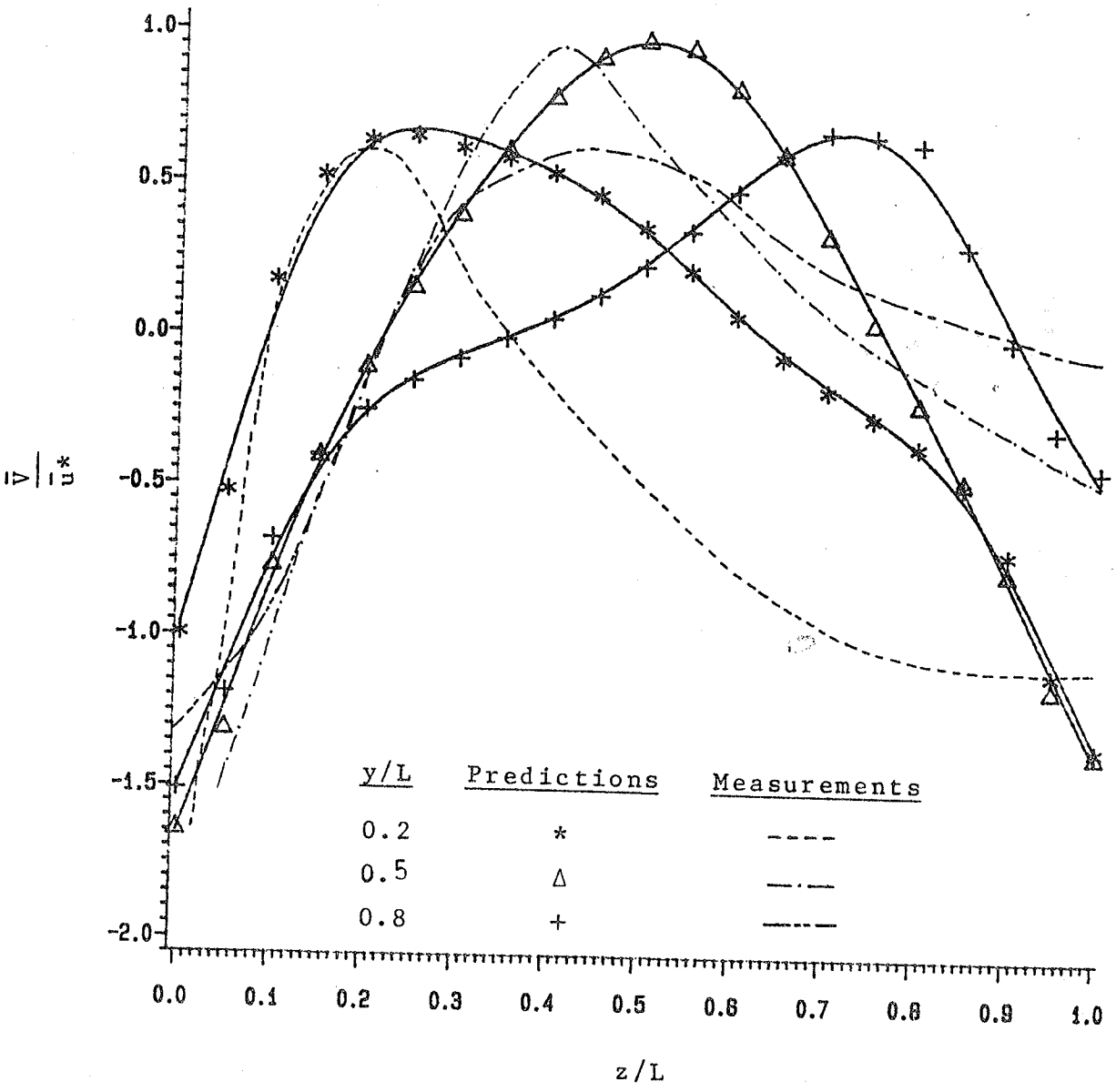

Fig. 7. Comparison of predicted secondary velocity $\bar{V}$ profiles (model II) and measured $\bar{V}$ profiles [14], Re = 215,000

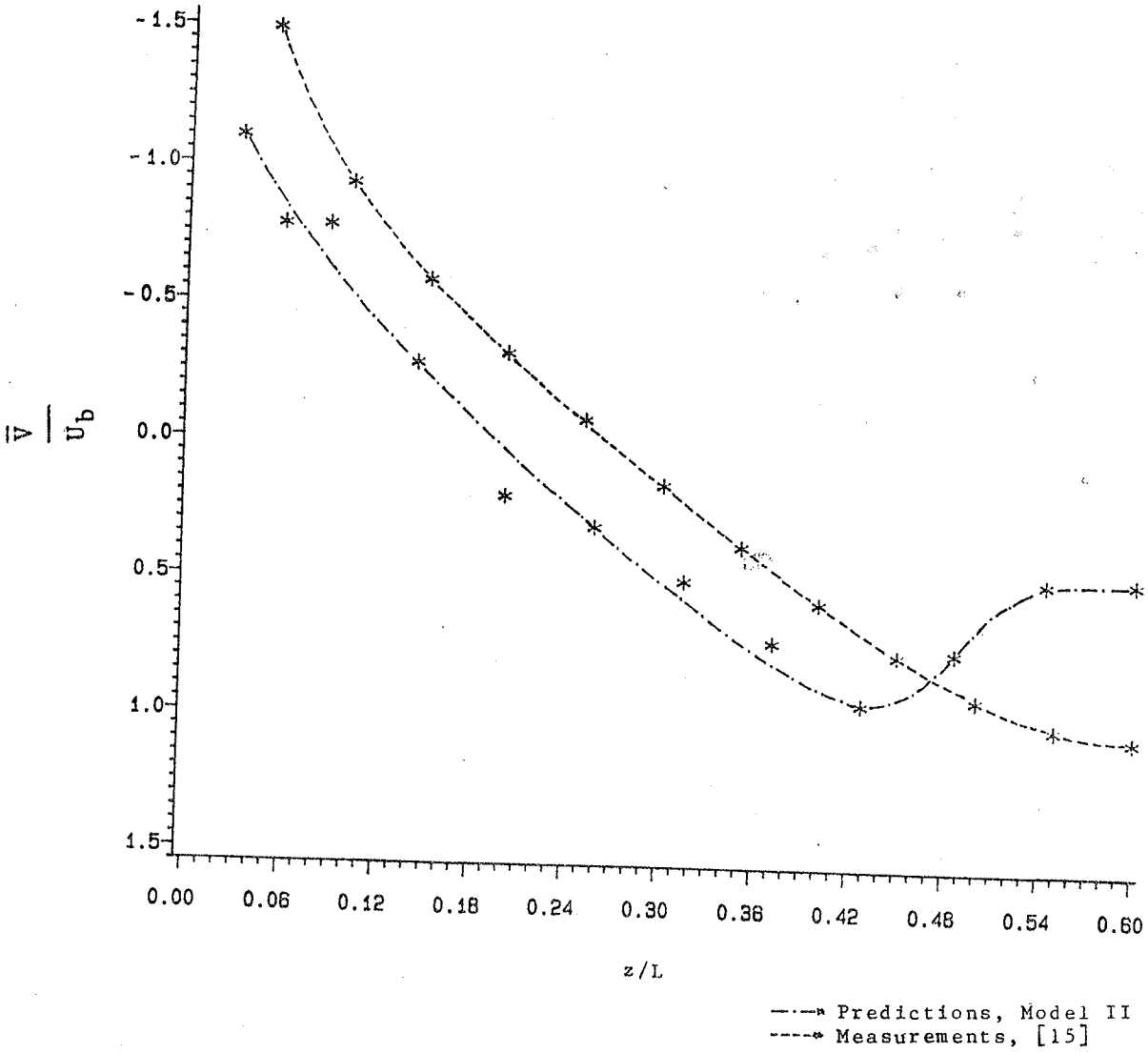

Fig. 8. Comparison of predicted secondary velocity ($\bar{V}$) profiles (model II) and measured $\bar{V}$ profiles [15], Re = 100,000 , y/L= 0.4

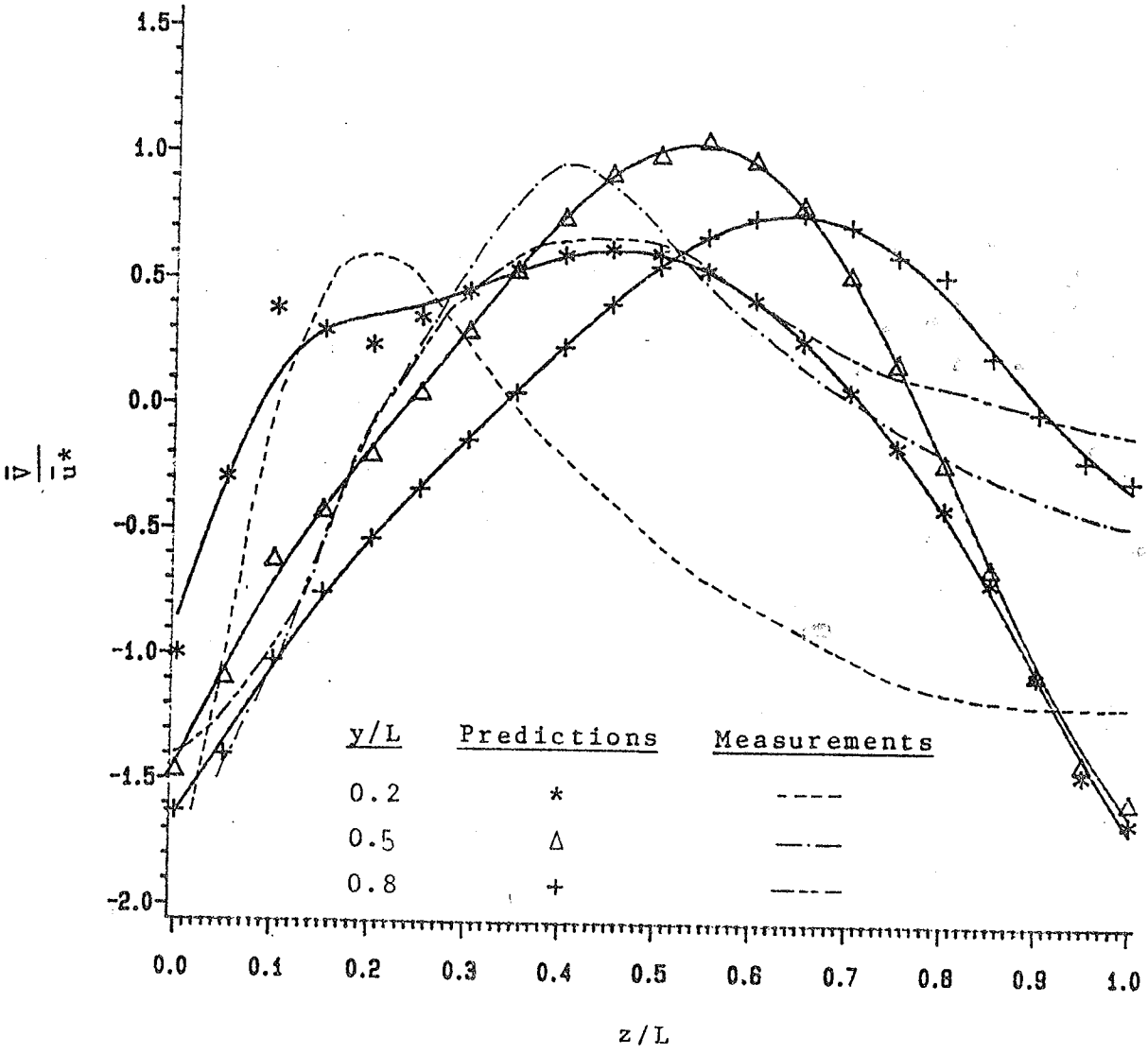

Fig. 9. Comparison of predicted secondary velocity ($\bar{V}$) profiles (model I) and measured $\bar{V}$ profiles [14], Re = 215,000

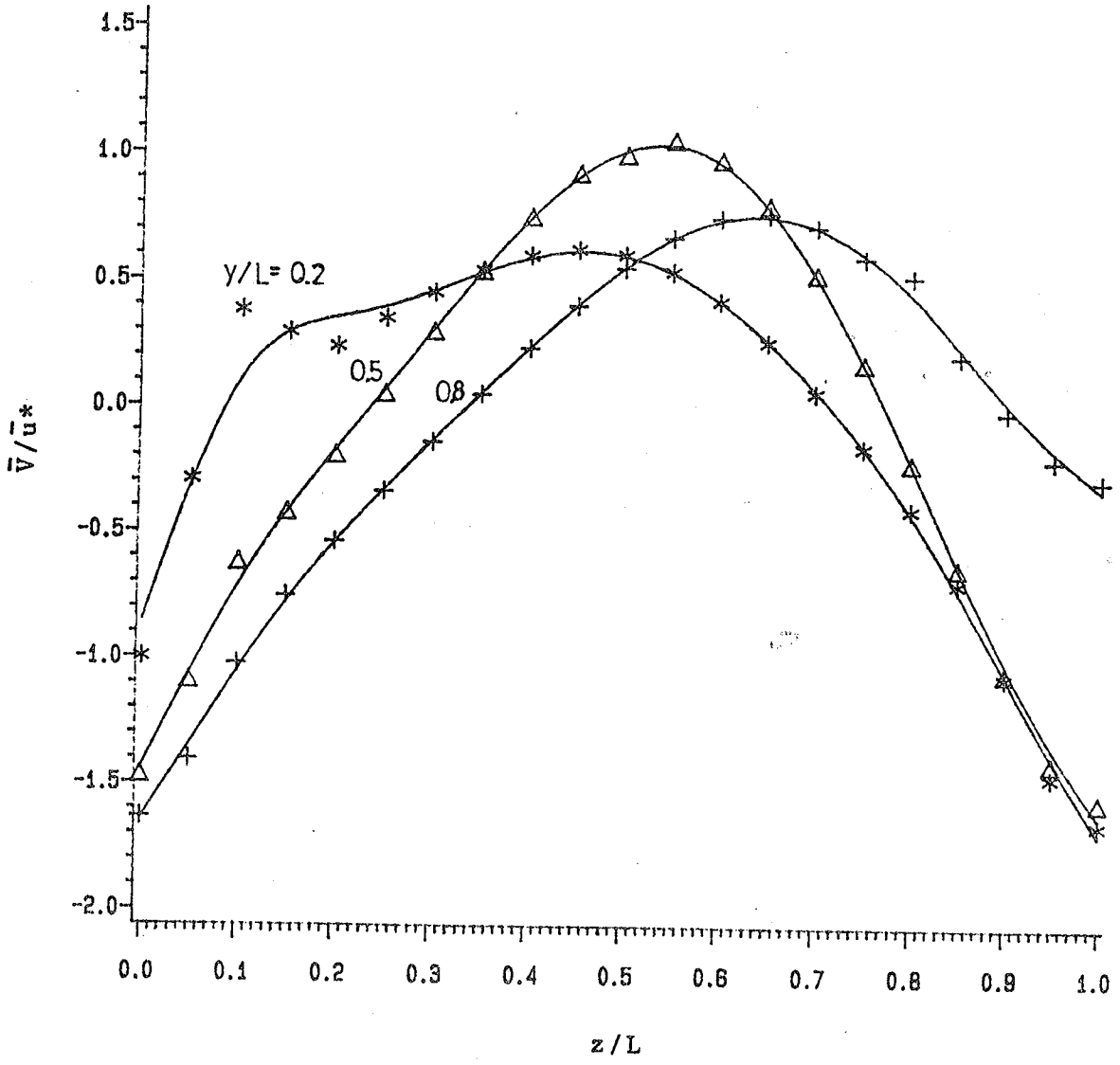

Fig. 10. Predicted secondary velocity ($\bar{V}$) profiles (model I), Re = 83,000

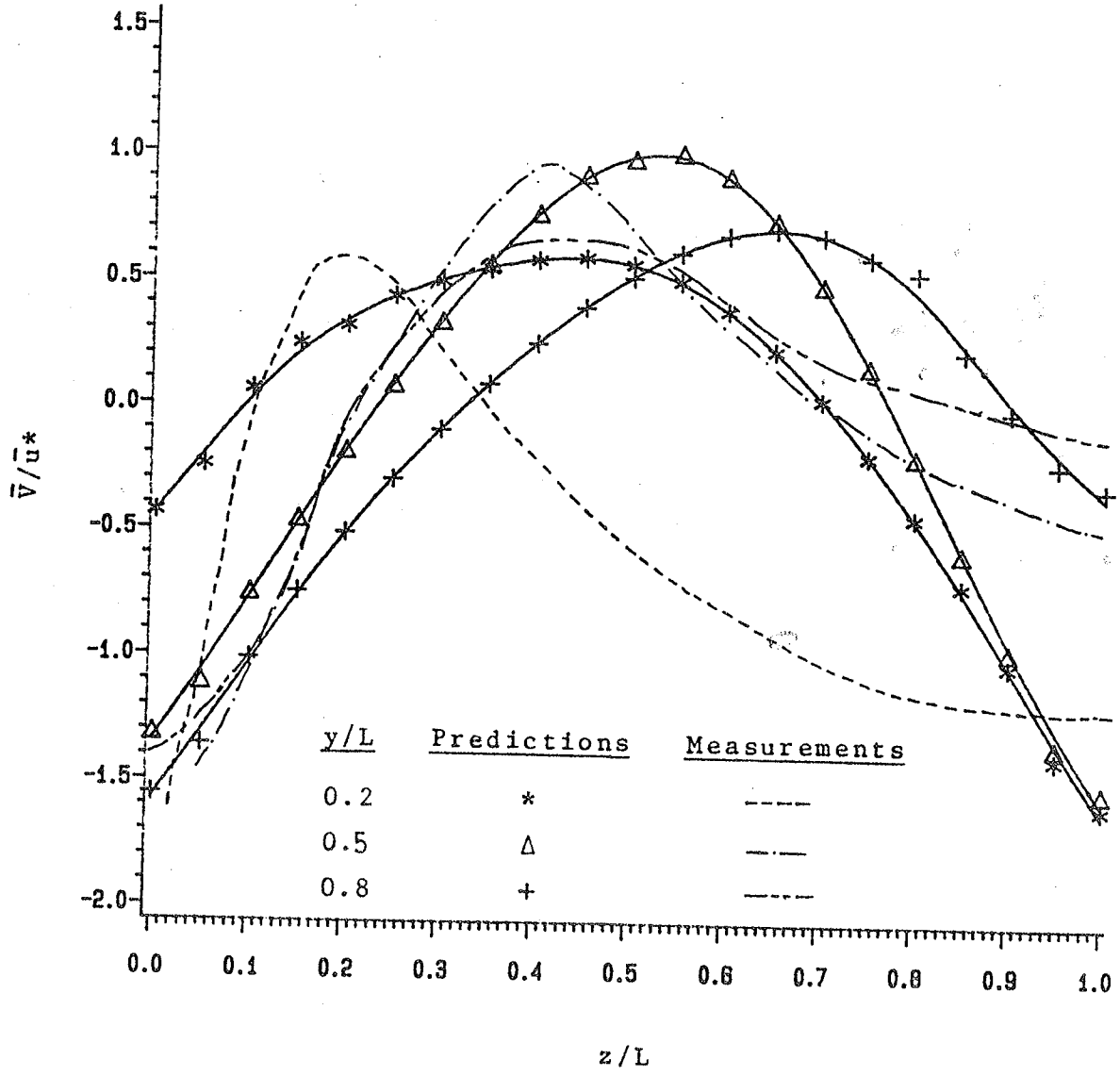

Fig. 11. Comparison of predicted secondary velocity ($\bar{V}$) profiles (model III) and measured $\bar{V}$ profiles [14], Re = 215,000

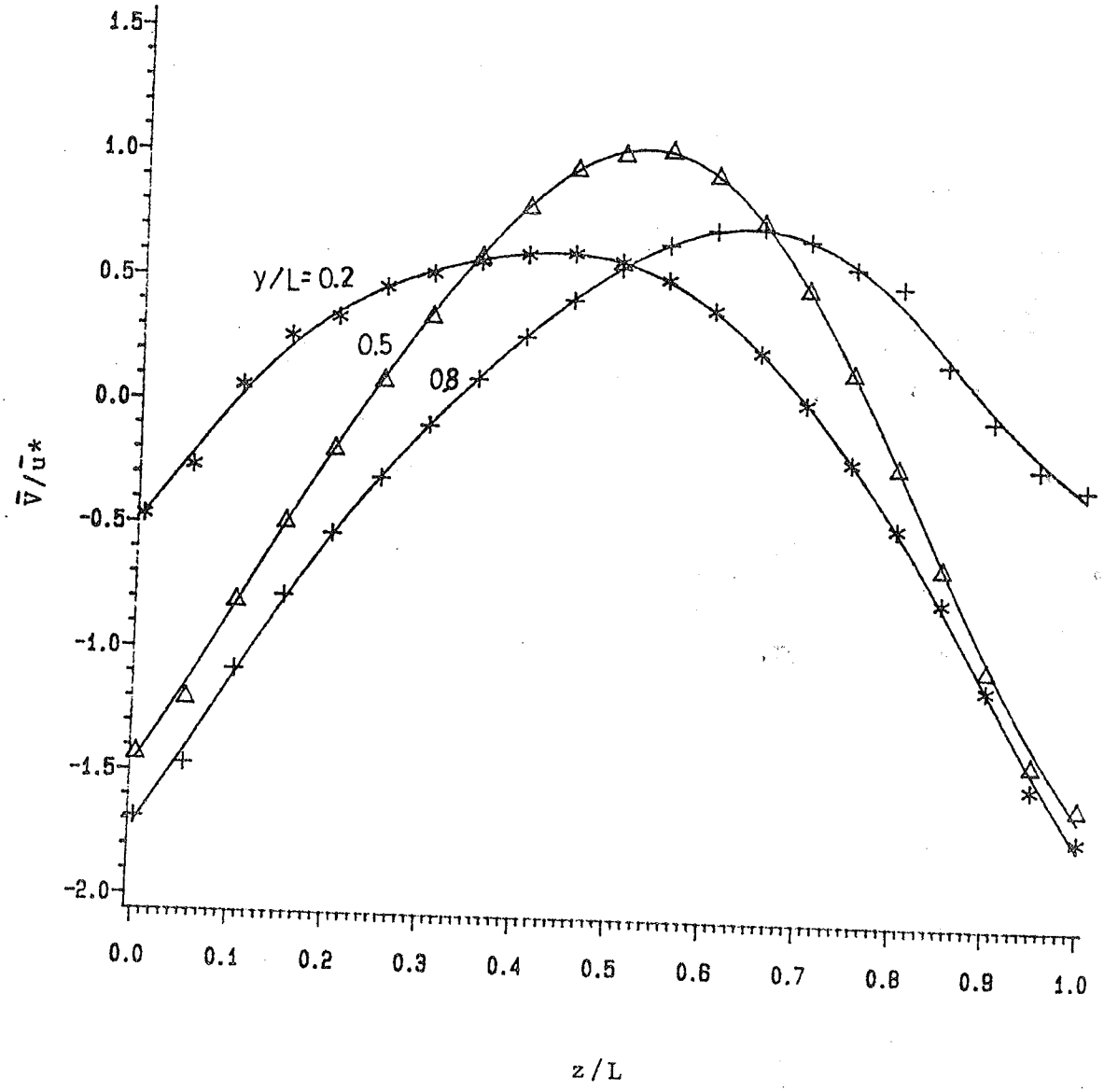

Fig. 12. Predicted secondary velocity ($\bar{V}$) profiles (model III), Re = 83,000

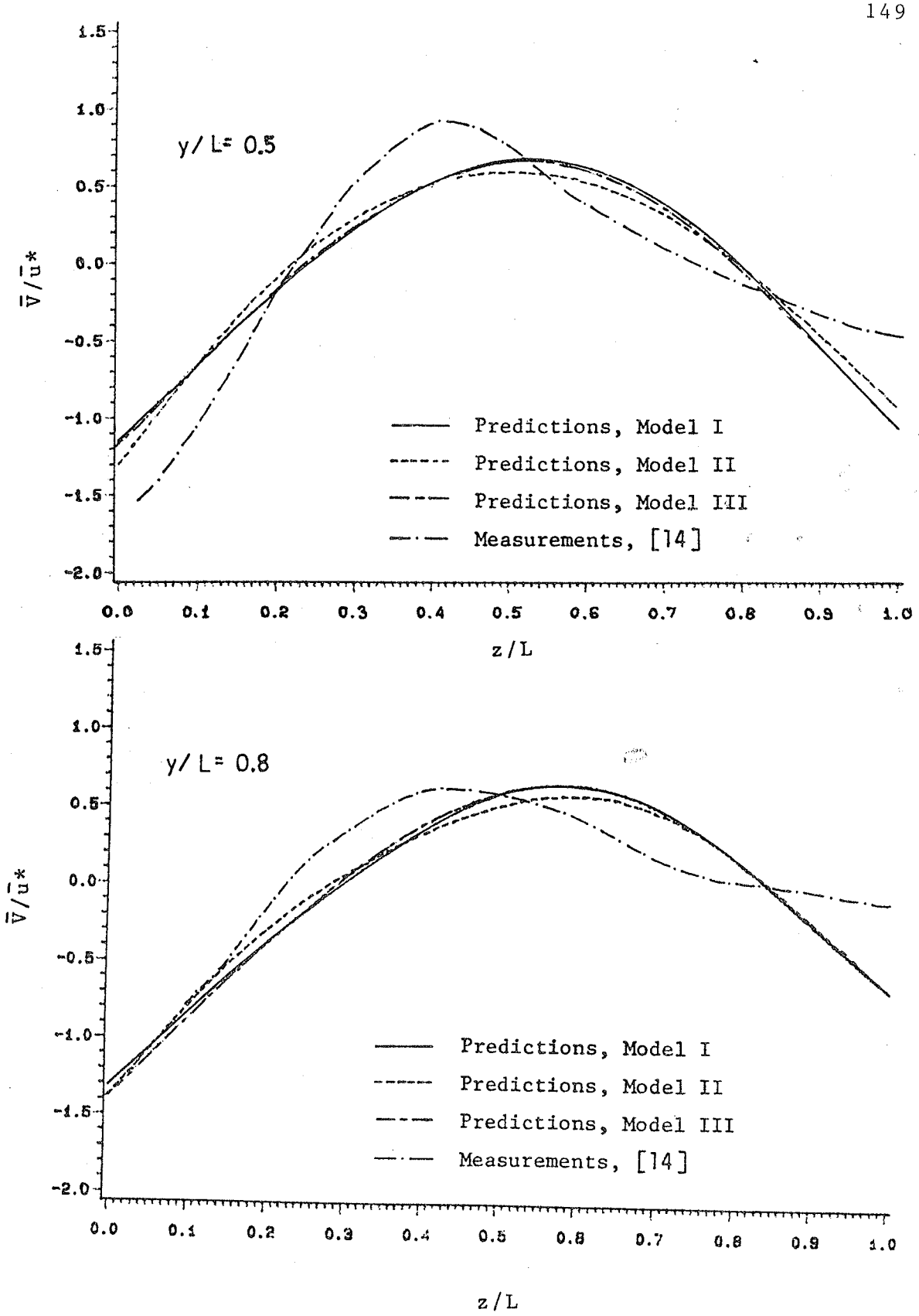

Fig. 13. Comparison of secondary velocity ($\bar{V}$) profiles predicted by model I, II and III, Re = 83,000

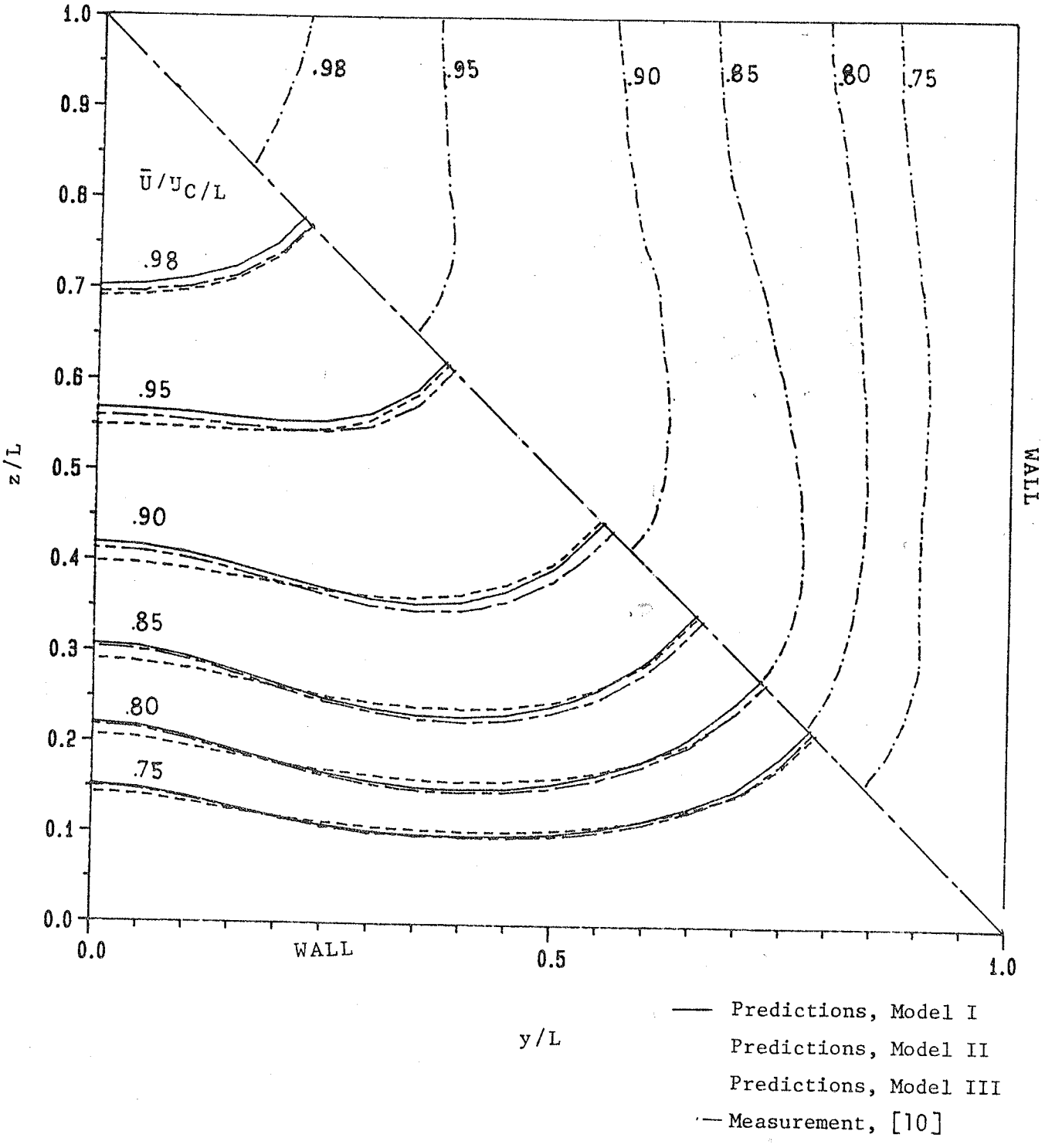

Fig. 14. Comparison of contour plots of predicted $\bar{U}$ (model I, II and III) and measured $\bar{U}$ [10], Re = 83,000

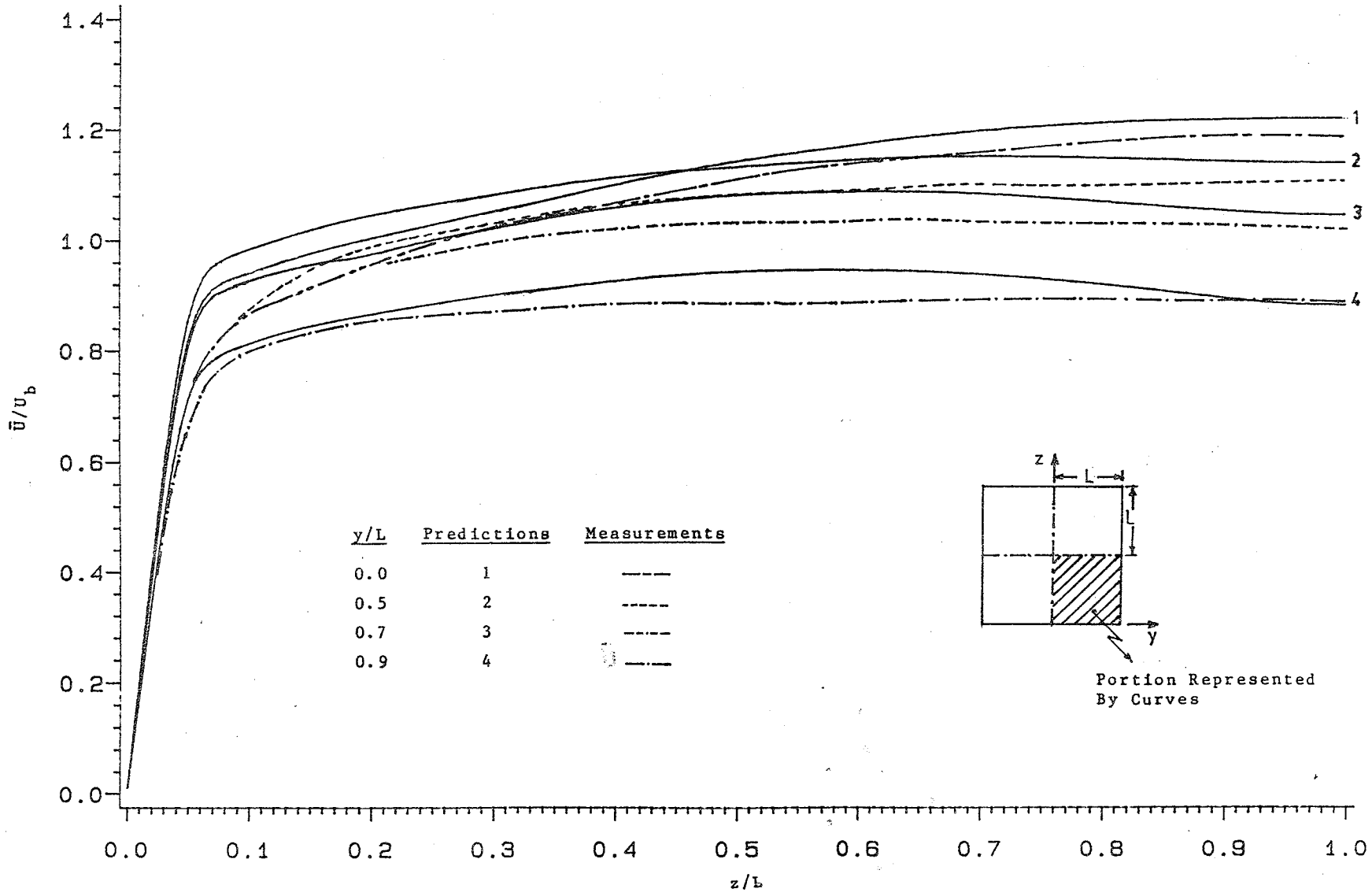

Fig. 15. Comparison of predicted $\bar{U}$ (model I) and measured $\bar{U}$ [14] profiles, Re = 215,000

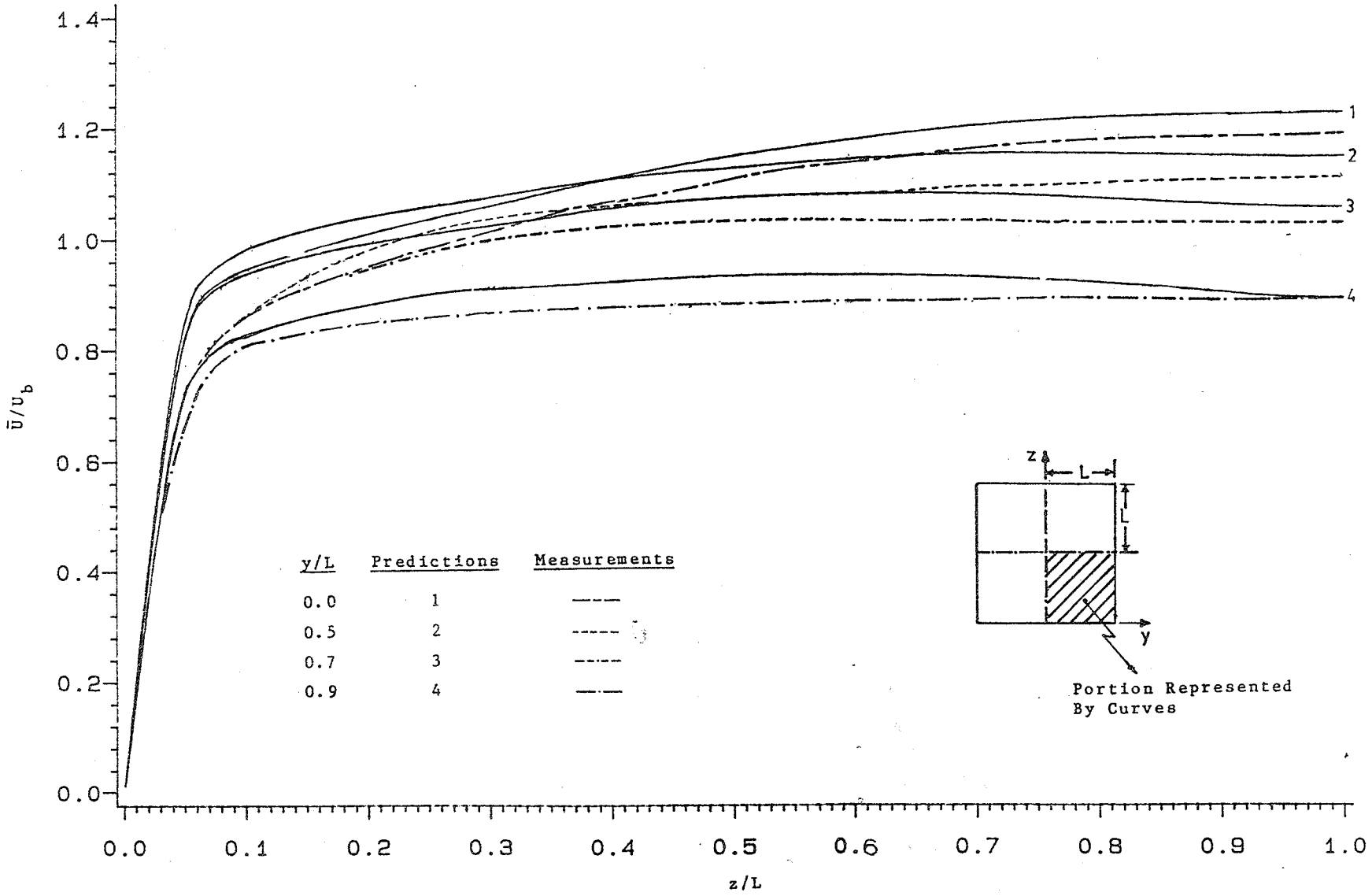

Fig. 16. Comparison of predicted $\bar{U}$ (model II) and measured $\bar{U}$ [14] profiles, Re = 215,000

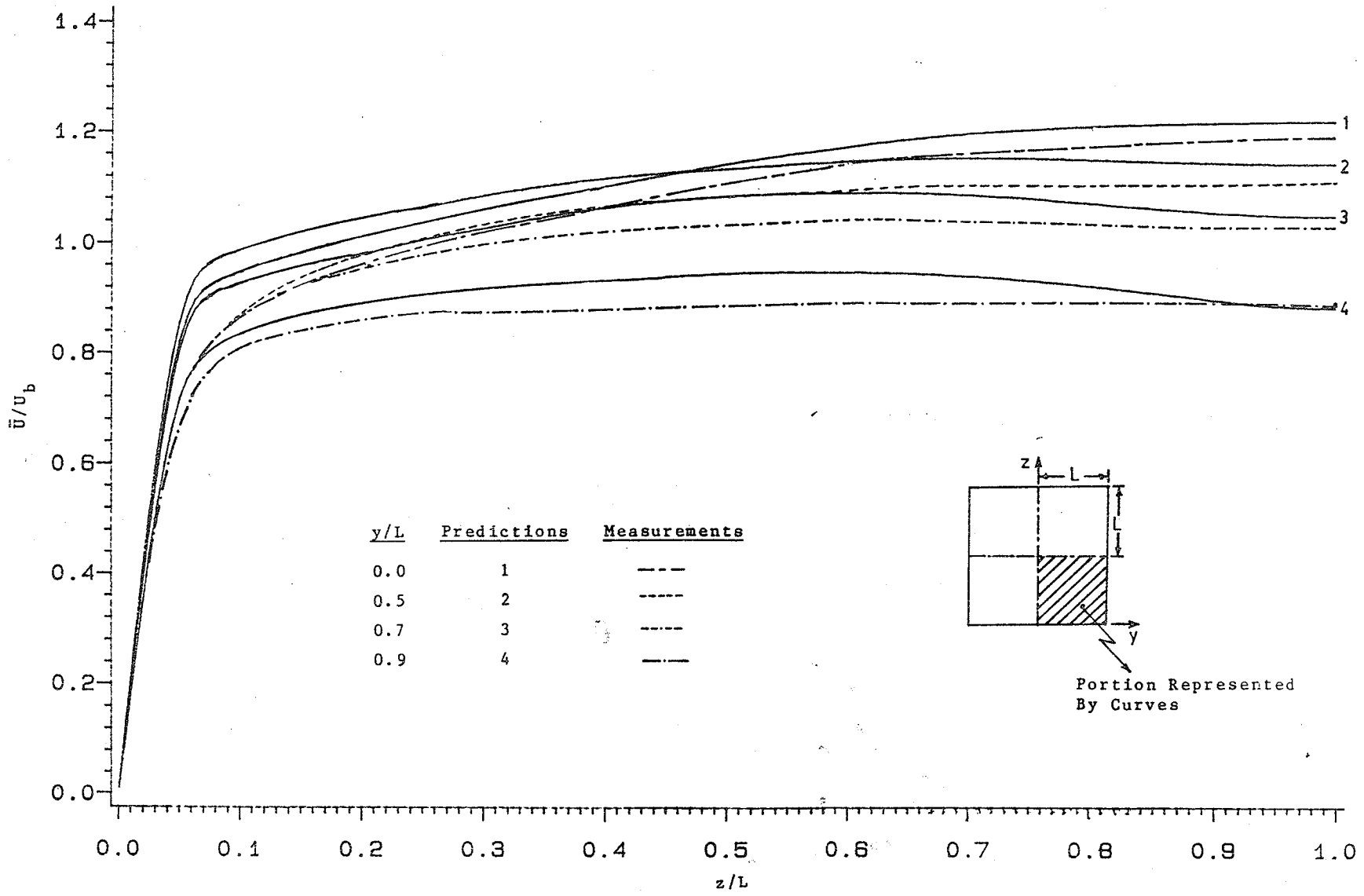

Fig. 17. Comparison of predicted $\bar{U}$ (model III) and measured $\bar{U}$ [14] profiles, Re = 215,000

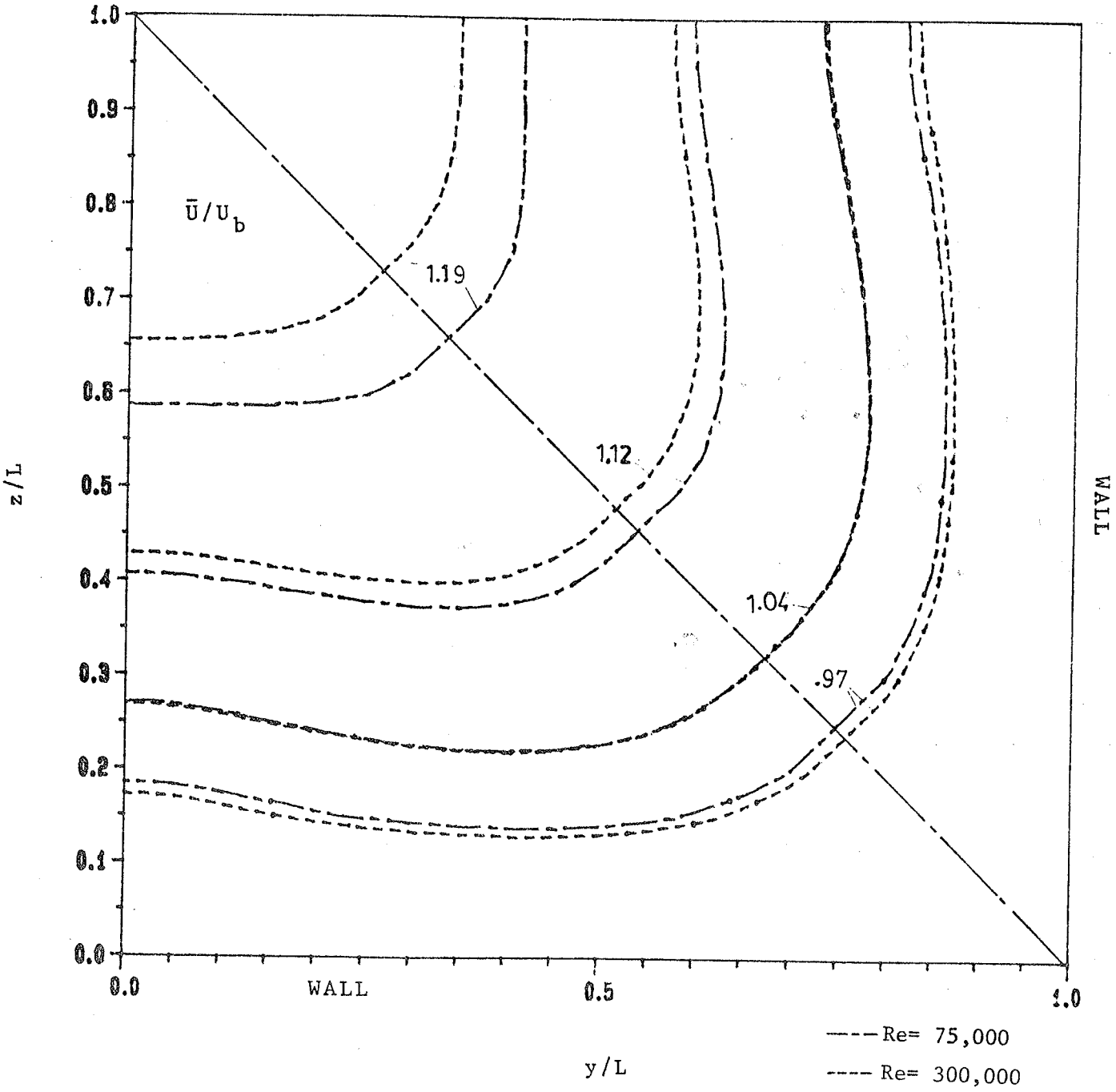

Fig. 18. Comparison of contour plots of predicted $\bar{U}$ (model II) at Re = 75,000 and Re = 300,000

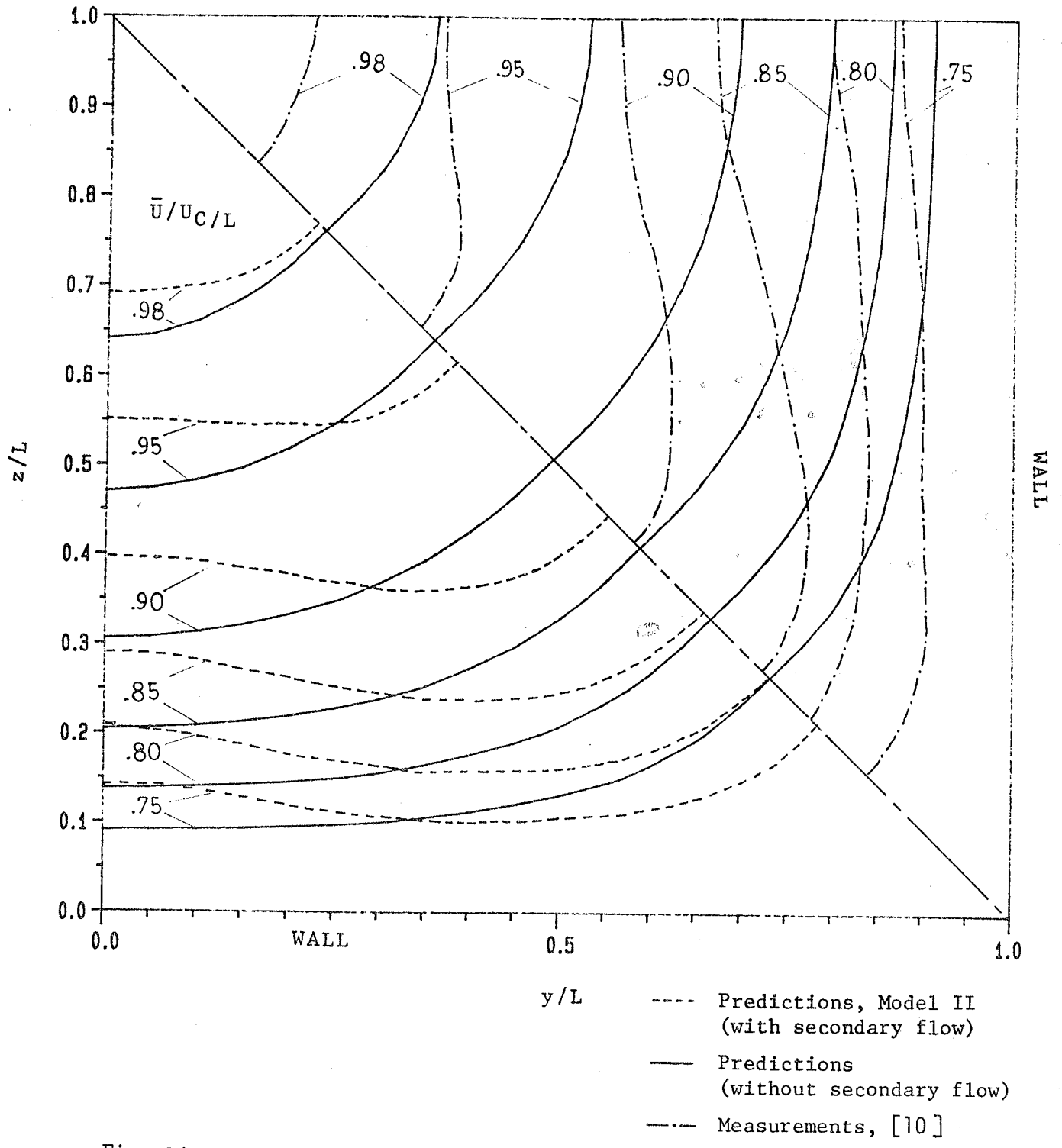

Fig. 19. Comparison of contour plots of predicted $\bar{U}$ (with and without secondary flow), Re = 83,000

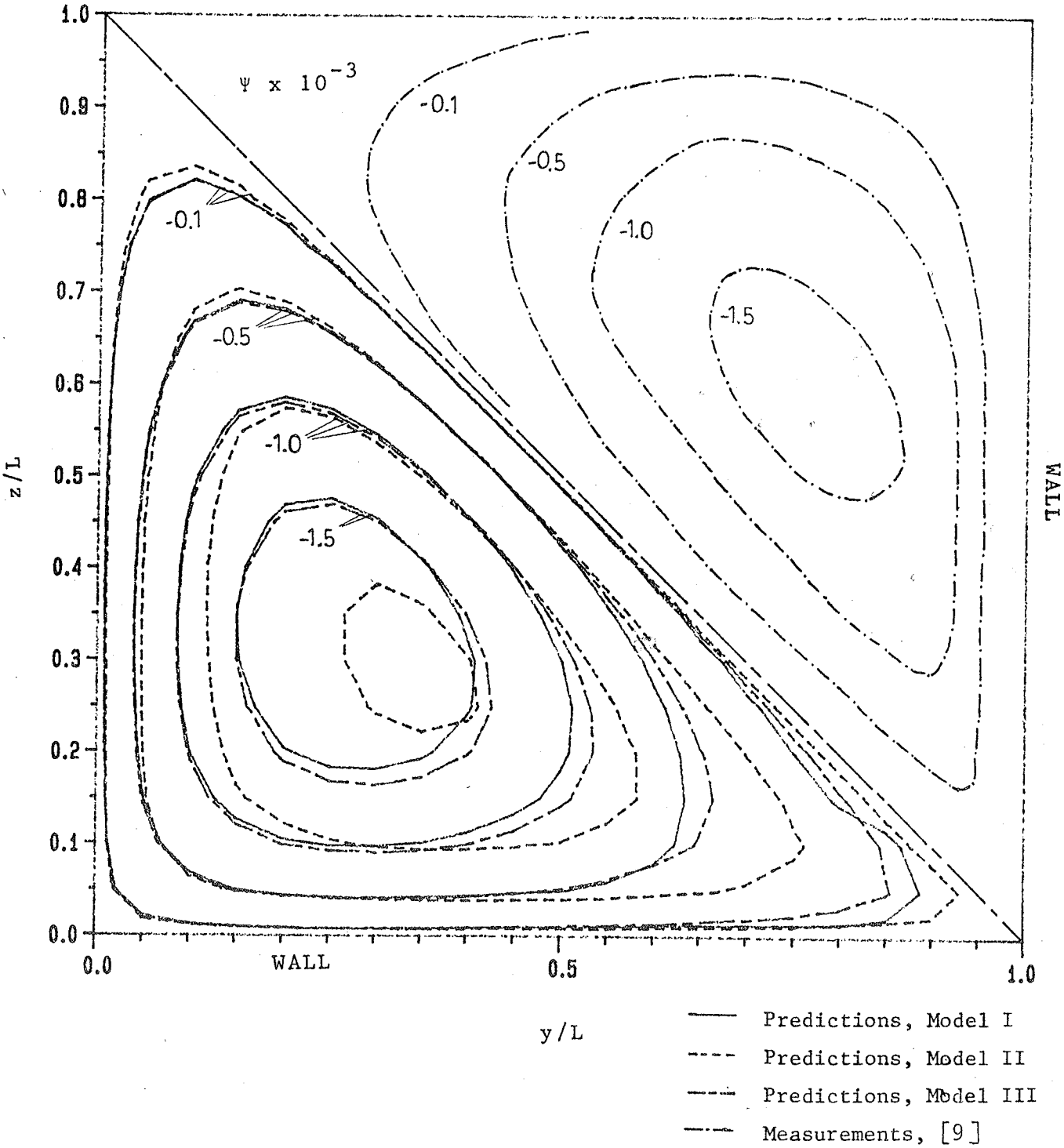

Fig. 20. Comparison of contour plots of predicted Ψ (model I, II and III) and measured Ψ [9], Re = 75,000

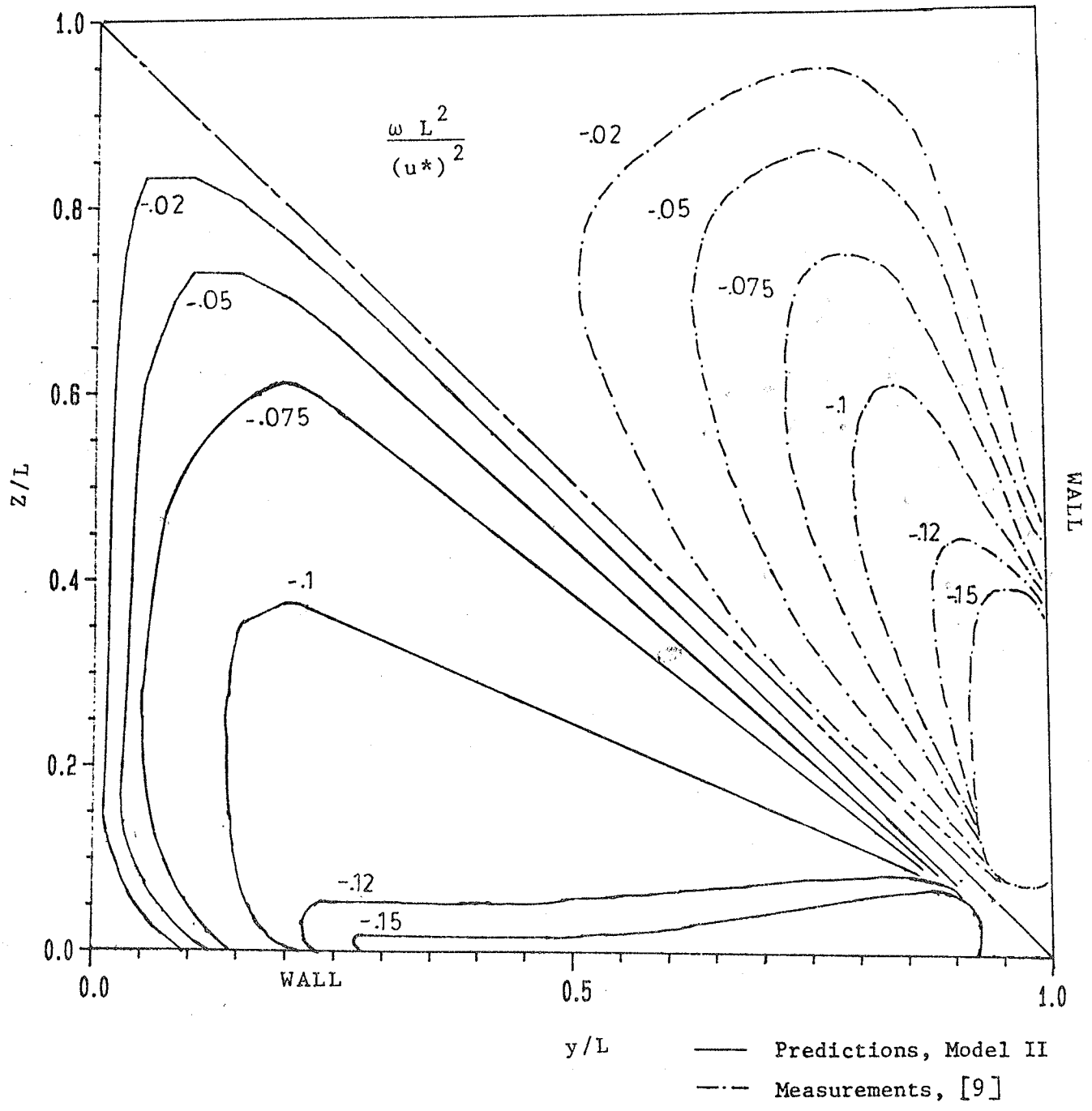

Fig. 21. Comparison of contour plots of predicted ω (model II) and measured ω [9], Re = 60,000

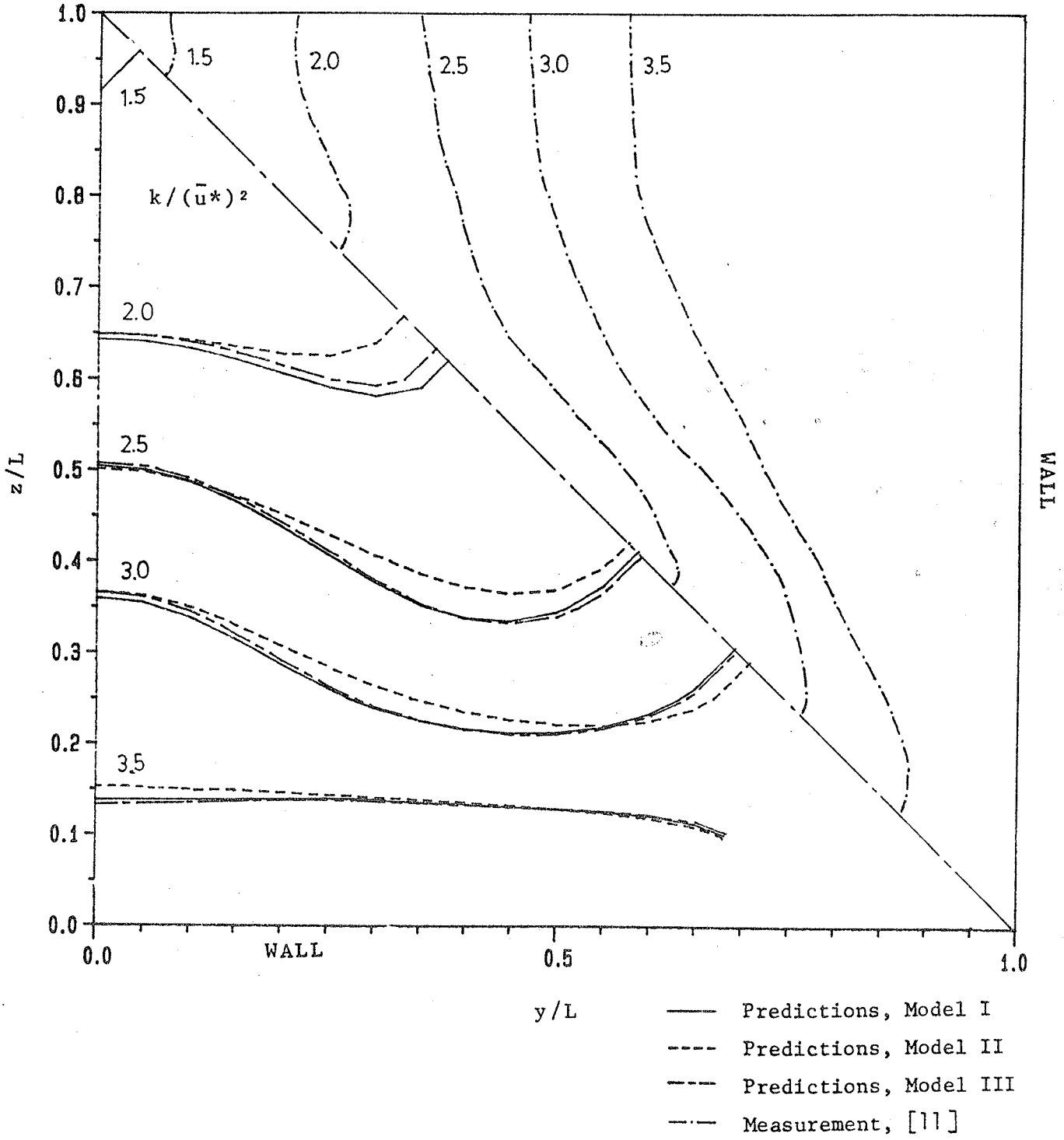

Fig. 22. Comparison of contour plots of predicted k (model I, II and III) and measured k [11], Re = 83,000

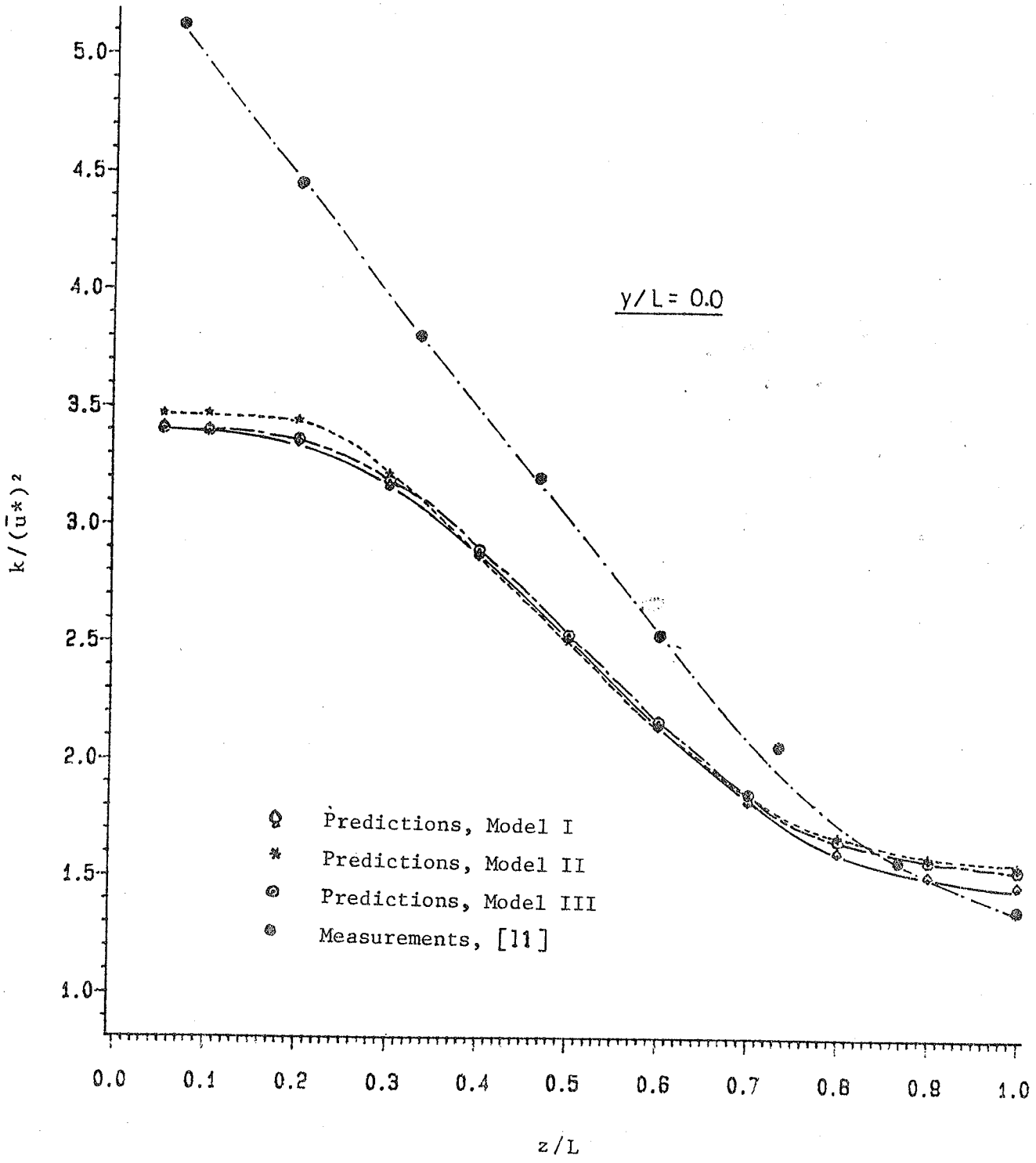

Fig. 23. Distribution of $k/(\bar{u}^*)^2$ normal to wall, Re = 83,000

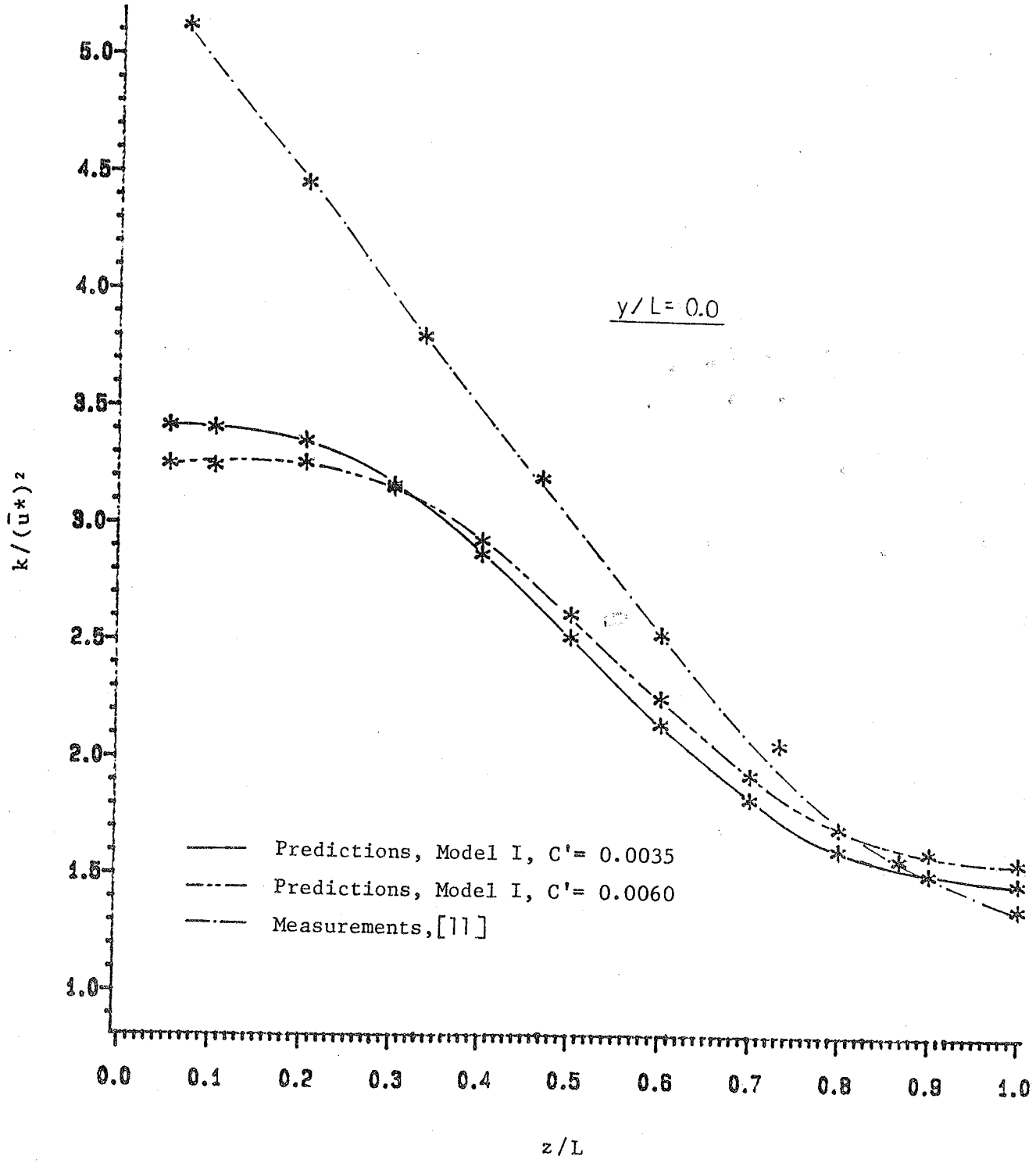

Fig. 24. Distribution of $k/(\bar{u}^*)^2$ normal to wall, Re = 83,000

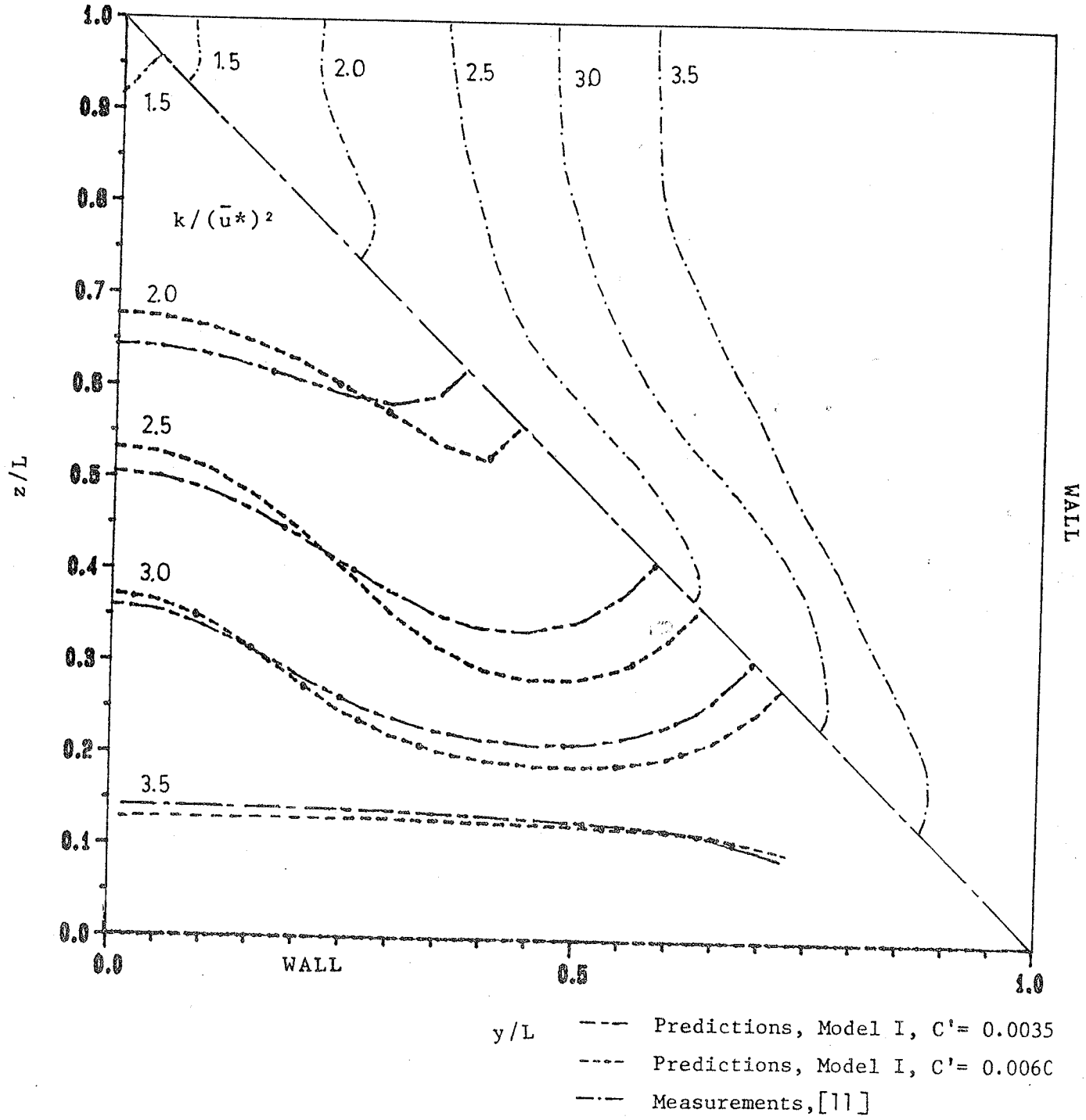

Fig. 25. Comparison of contour plots of predicted k (model I, with C' = 0.0035 and 0.006) and measured k [11], Re = 83,000

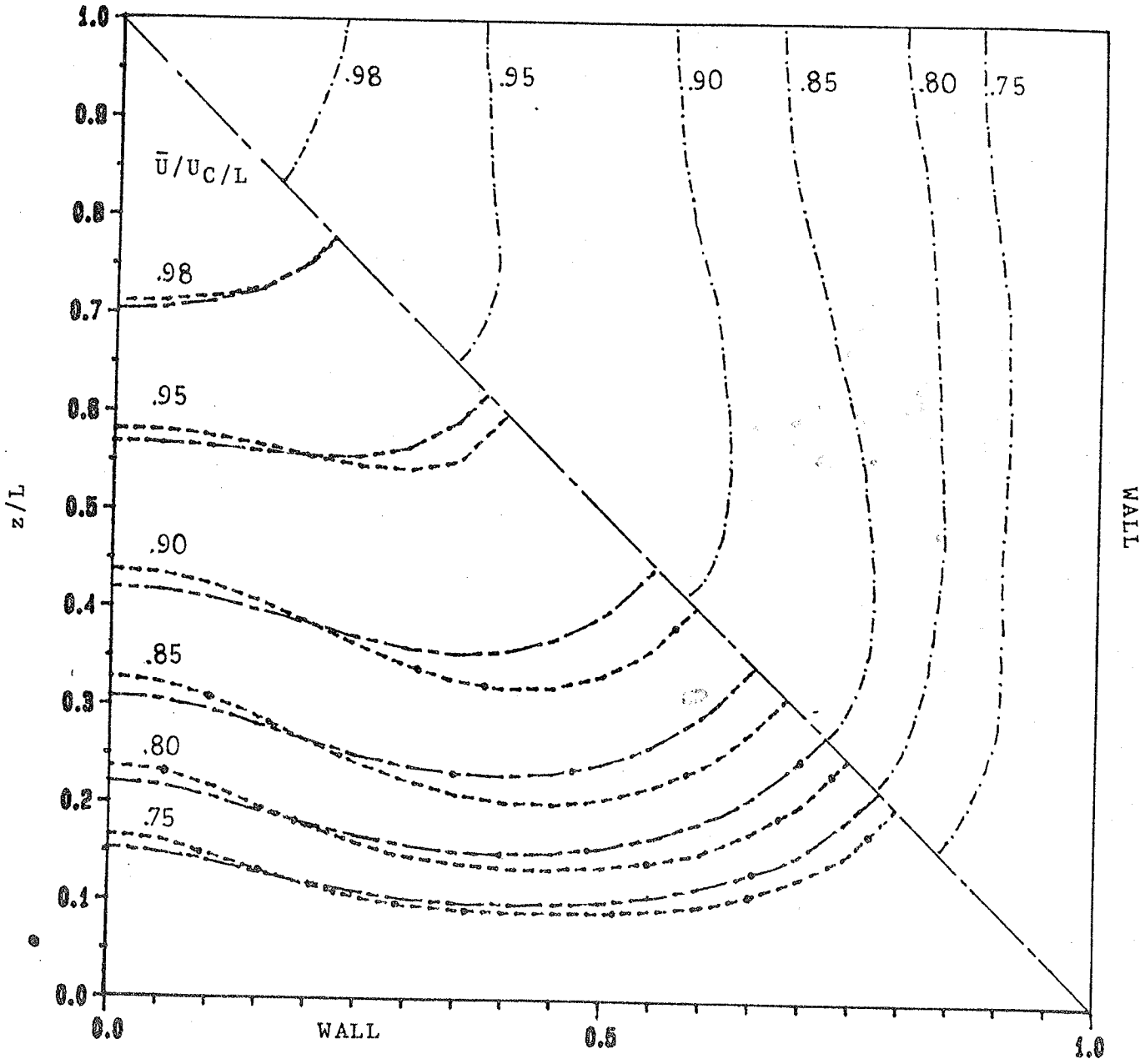

Fig. 26. Comparison of contour plots of predicted $\bar{U}$ (model I, with C'= 0.0035 and 0.0060) and measured k_{11}, Re = 83,000

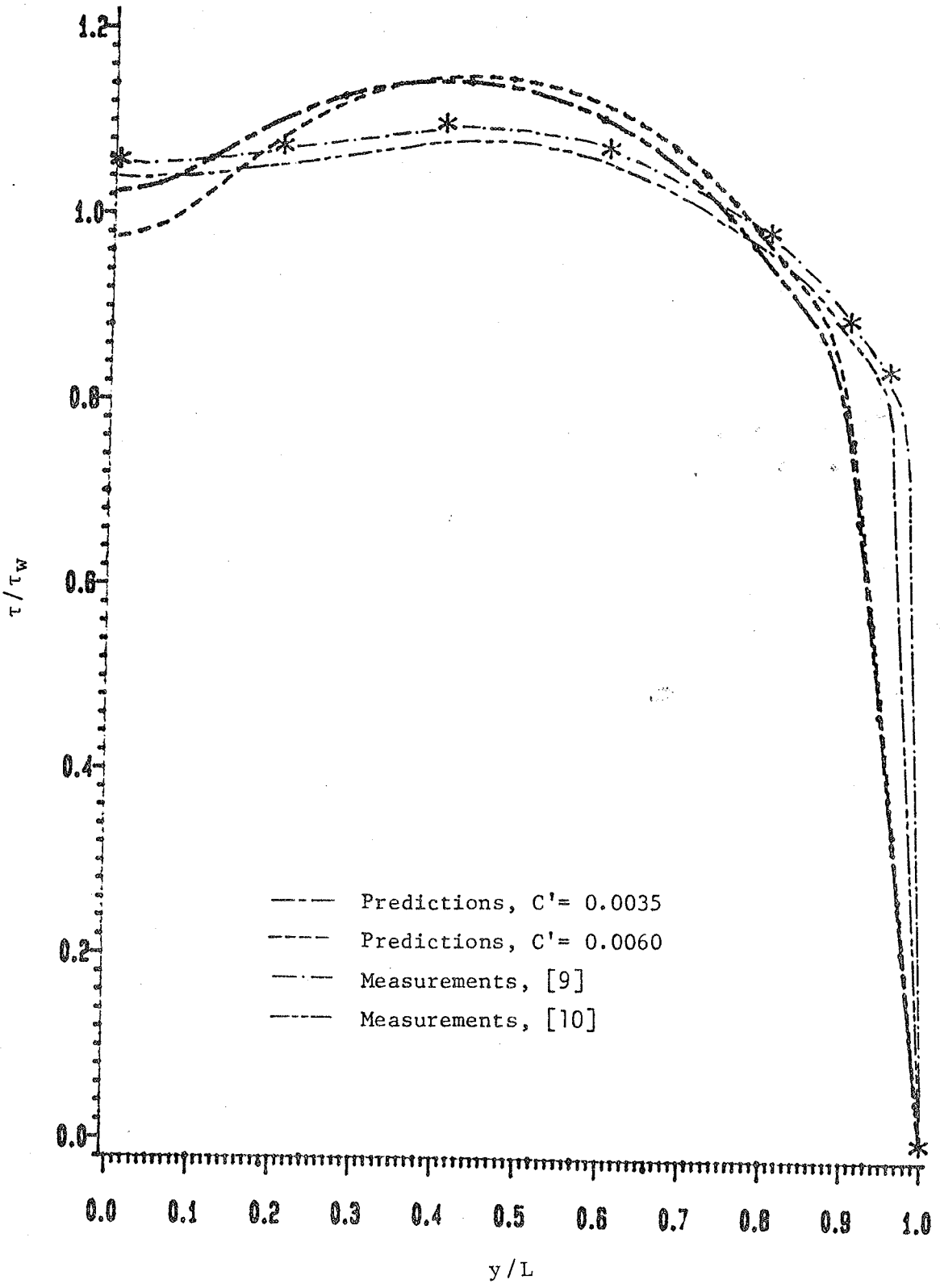

Fig. 27. Comparison of shear stress (τ) distribution (model I, with C' = 0.0035 and 0.006) and measured τ [10], Re = 83,000

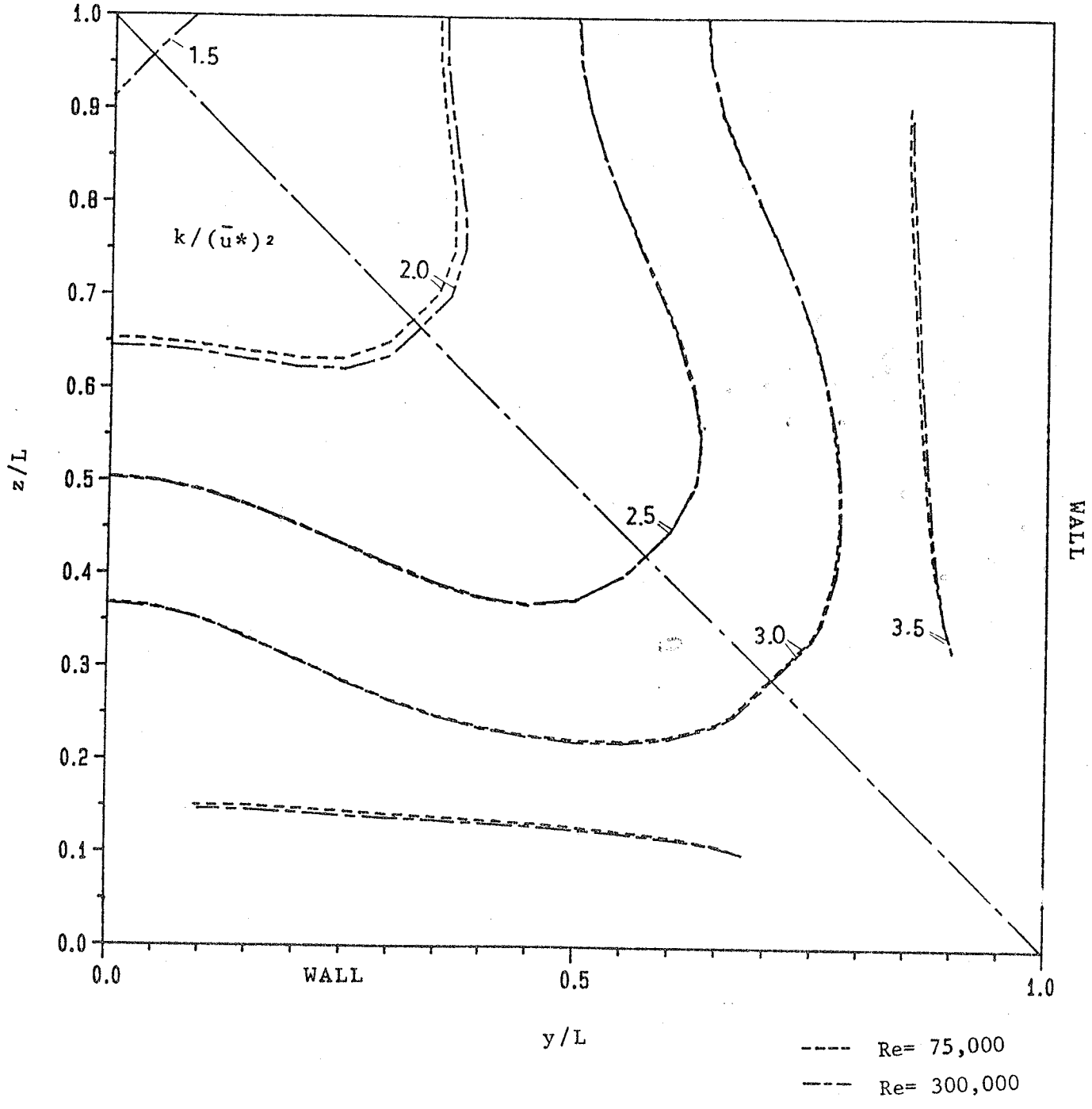

Fig. 28. Comparison of contour plots of predicted k (model II) at Re = 75,000 and Re = 300,000

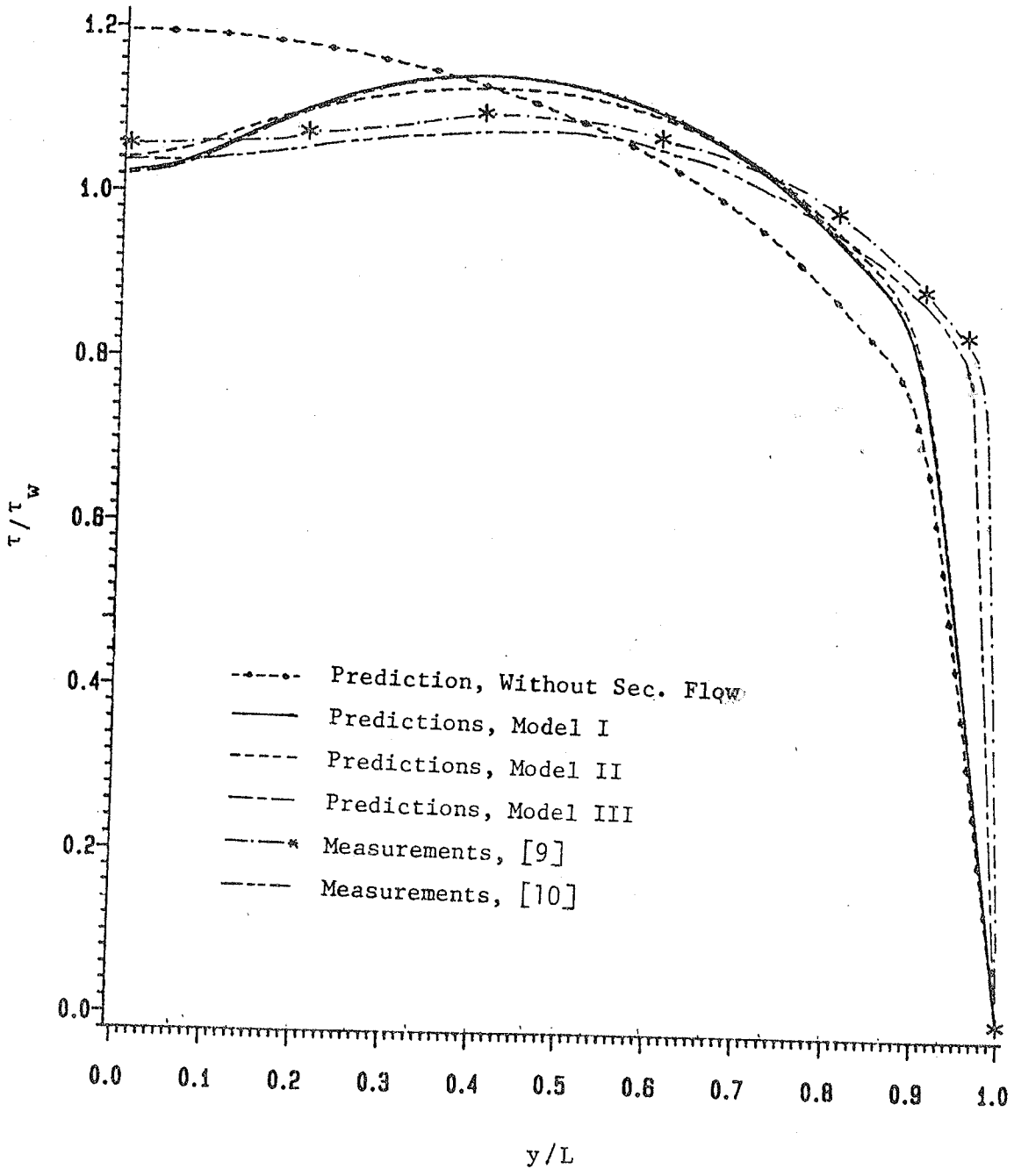

Fig. 29. Wall shear stress distribution (model I, II and III), with and without secondary flow, Re = 83,000 .

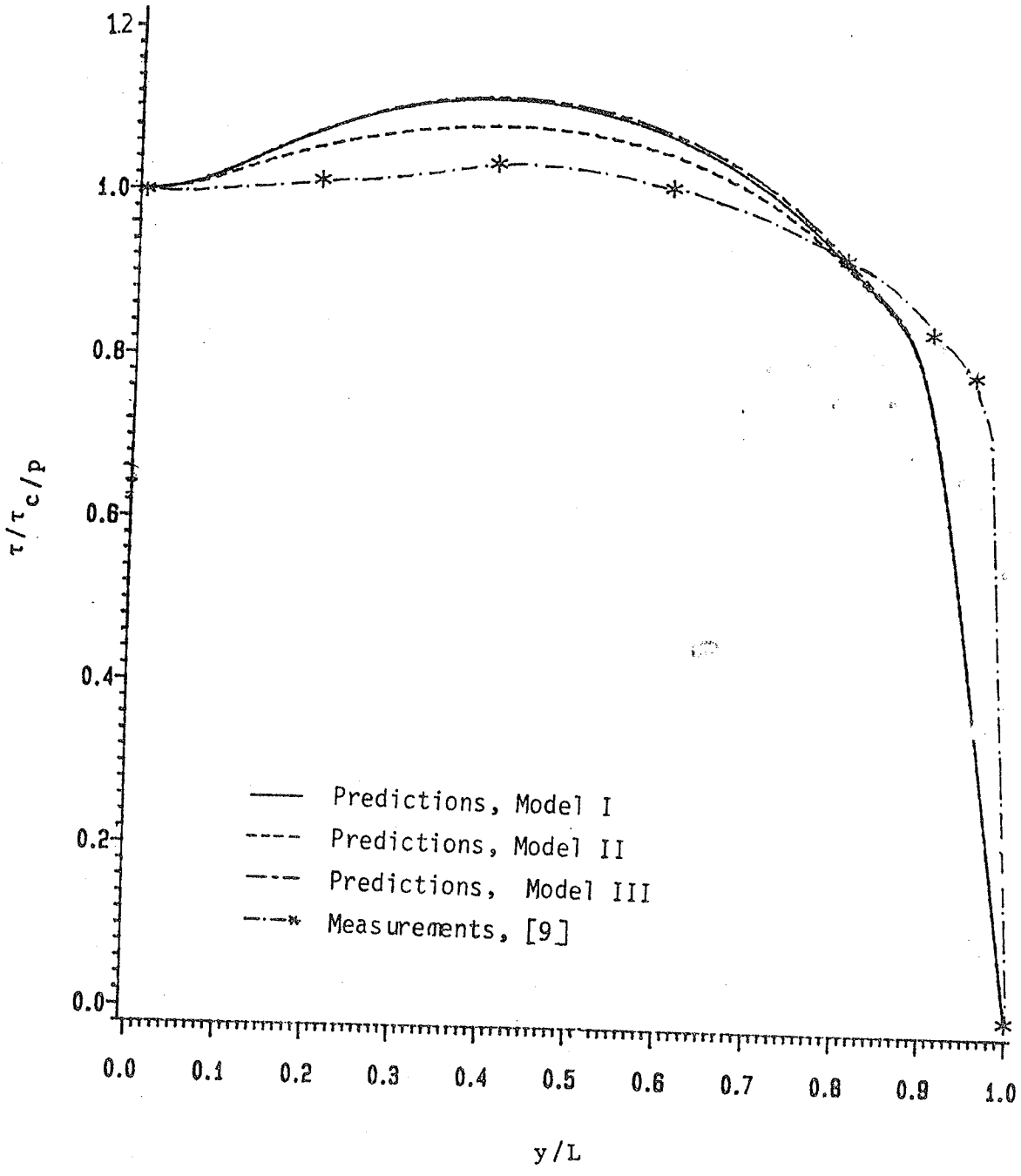

Fig. 30. Comparison of wall shear stress (τ) distribution (model I, II and III) and measured τ [19], Re = 75,000

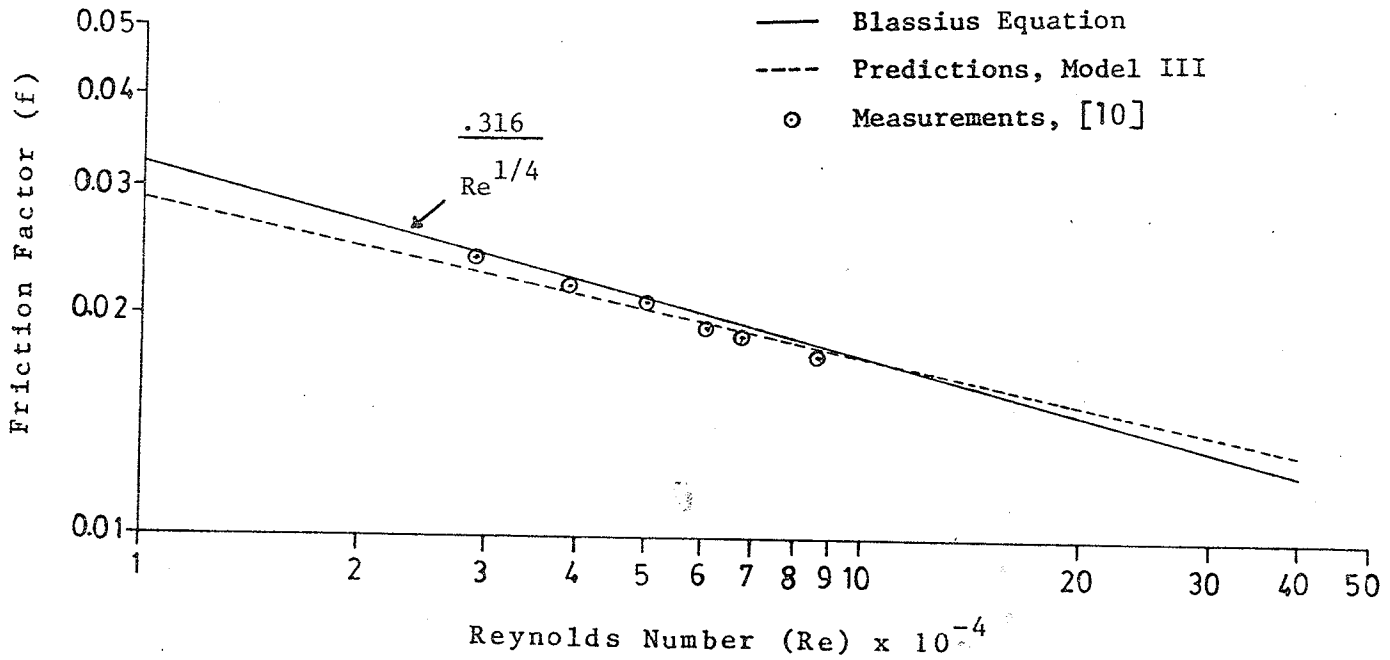

Fig. 31. Friction factor (f) (model III) vs. Reynolds number in square ducts

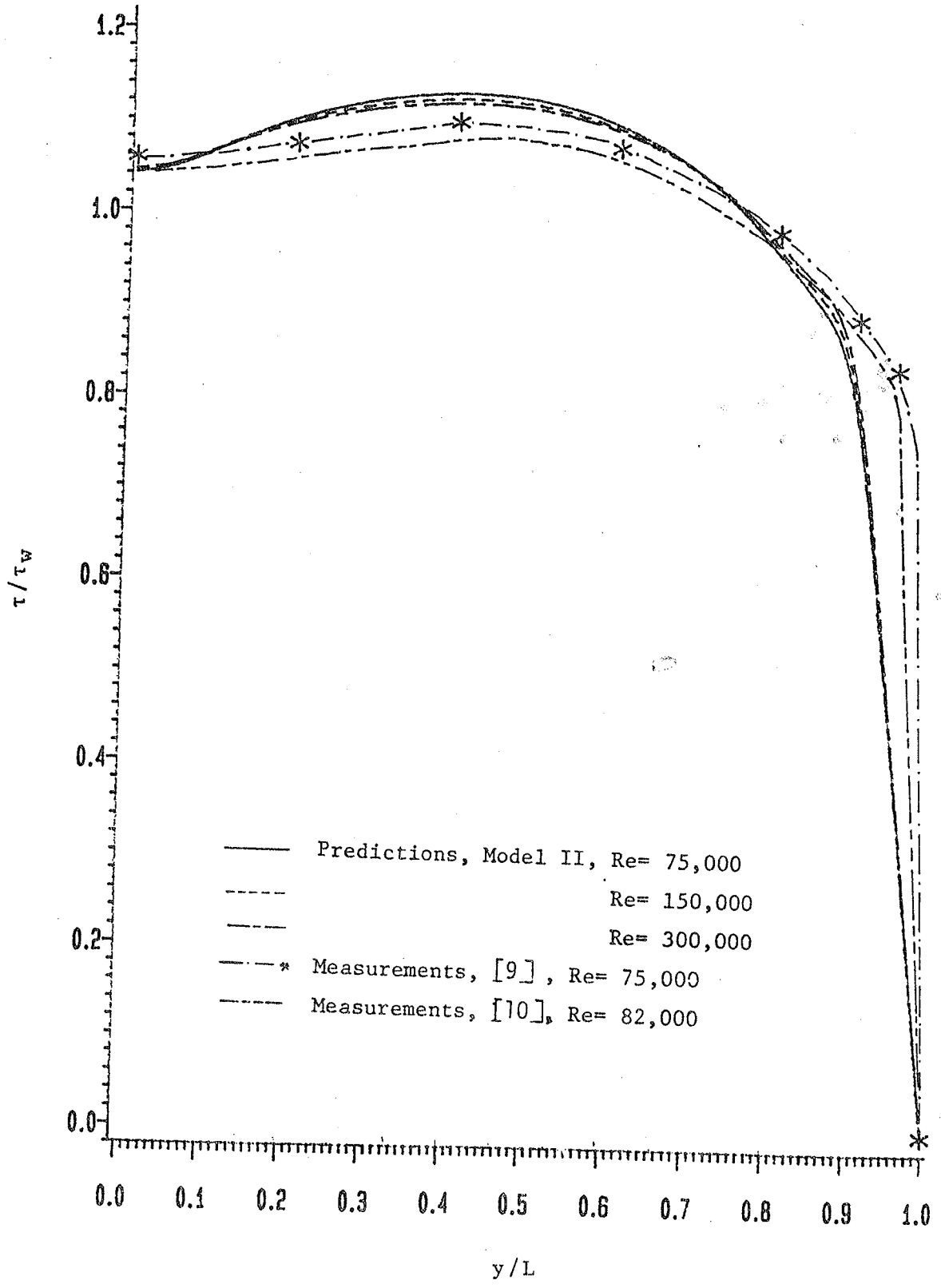

Fig. 32. Comparison of Predicted wall shear stress (model II) at different Reynolds numbers

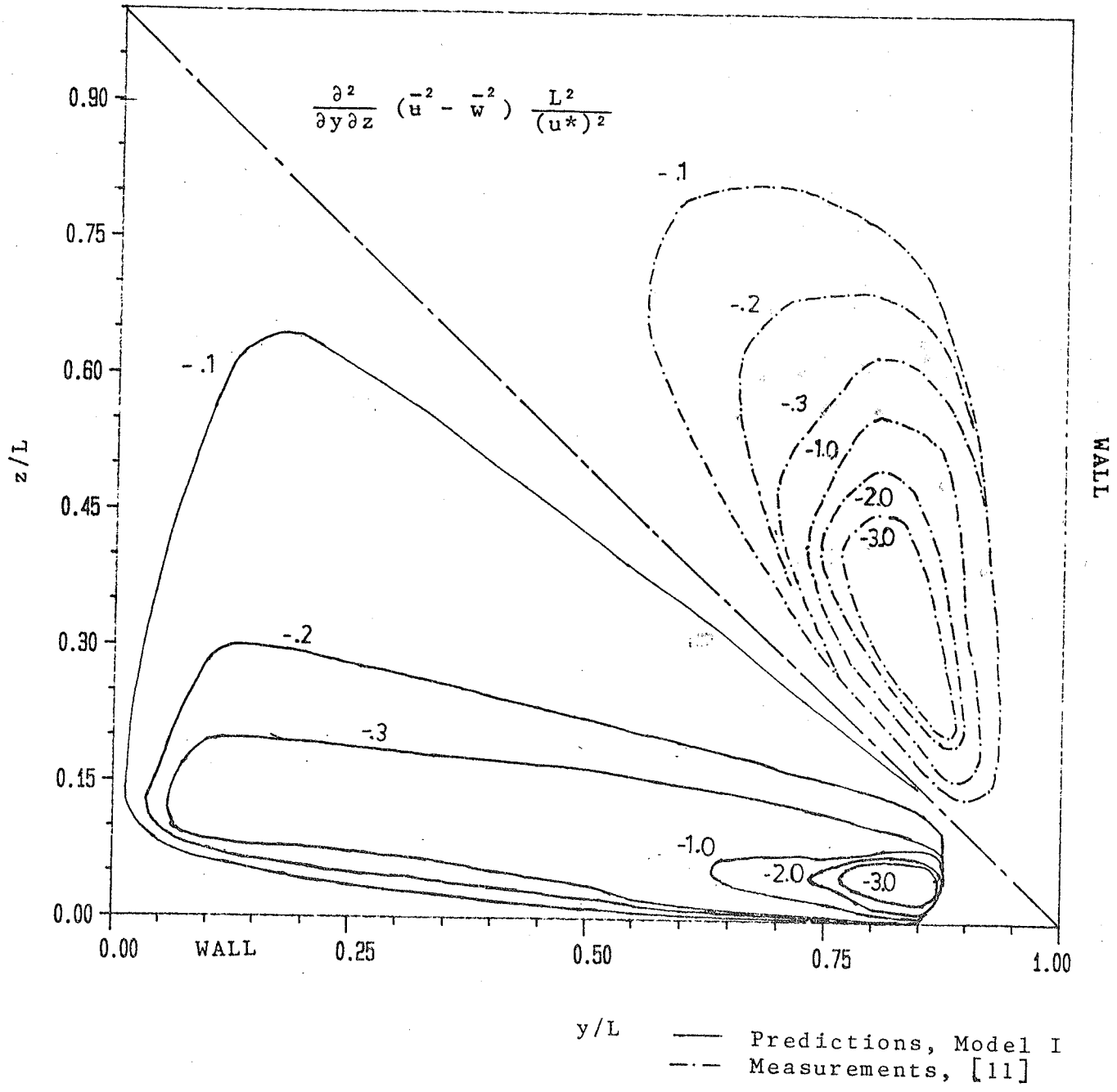

Fig. 33. Comparison of contour plots of predicted (model I) and measured [11] production of vorticity, Re = 83,000

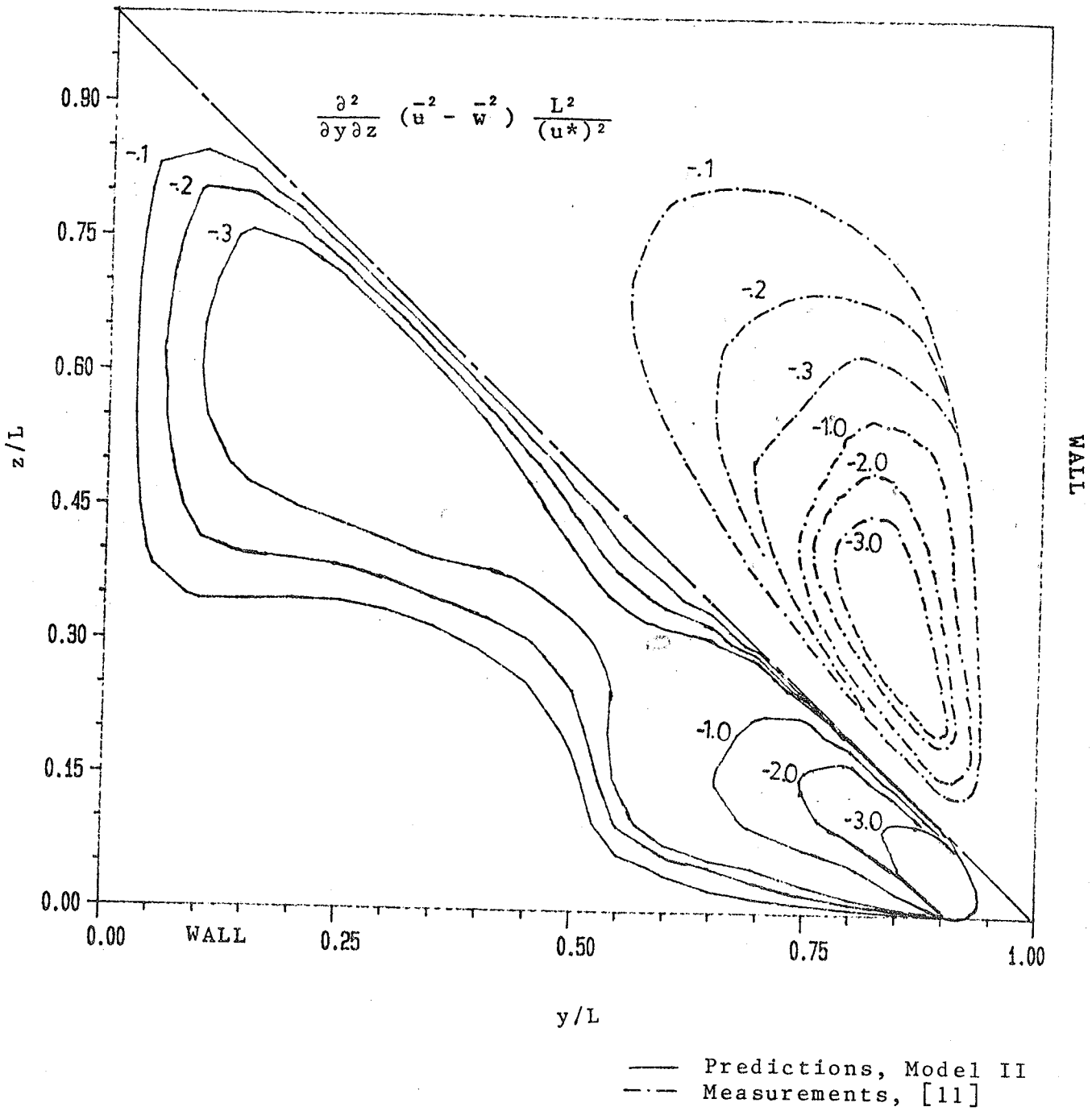

Fig. 34. Comparison of contour plots of predicted (model II) and measured [11] production of vorticity, Re = 83,000

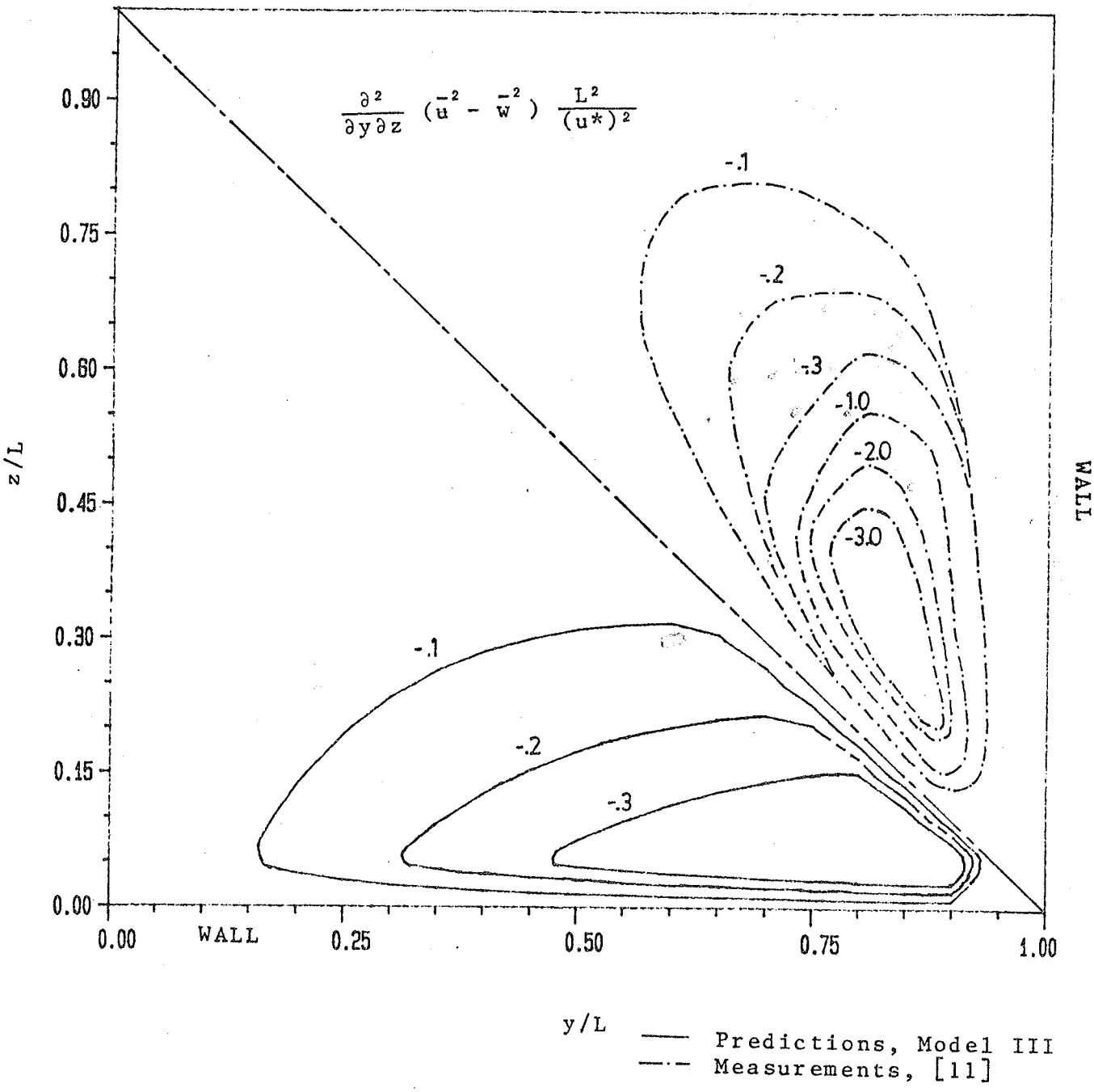

Fig. 35. Comparison of contour plots of predicted (model III) and measured [11] production of vorticity, Re = 83,000

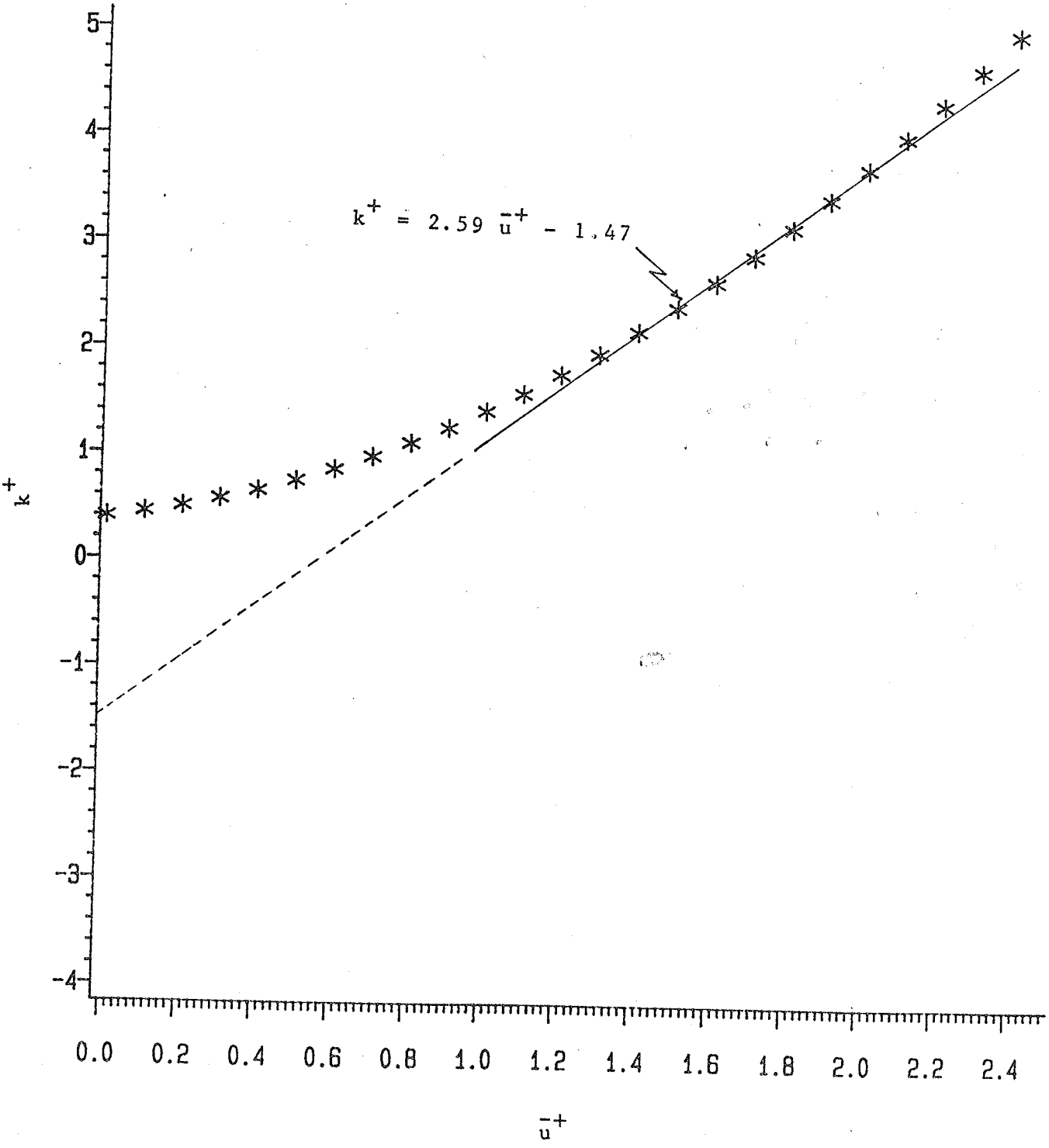

Fig. 36. Variation of k^+ with $\bar{u}^+$ for turbulent flow in square duct